

**PHYSICAL MODEL SIMULATIONS OF SUPER-
CRITICAL SUBSIDENCE UNDER VARIOUS
MINING SEQUENCES AND
EXCAVATION RATES**



**A Thesis Submitted in Partial Fulfillment of the Requirements for the
Degree of Master of Engineering in Geotechnology**

Suranaree University of Technology

Academic Year 2015

การจำลองเชิงกายภาพของการทรุดตัวที่เกินกว่าจุดวิกฤต
ภายใต้การผันแปรลำดับและอัตราการขูดเจาะ



วิทยานิพนธ์นี้เป็นส่วนหนึ่งของการศึกษาตามหลักสูตรปริญญาวิศวกรรมศาสตรมหาบัณฑิต
สาขาวิชาเทคโนโลยีธรณี
มหาวิทยาลัยเทคโนโลยีสุรนารี
ปีการศึกษา 2558

**PHYSICAL MODEL SIMULATIONS OF SUPER-CRITICAL
SUBSIDENCE UNDER VARIOUS MINING SEQUENCES
AND EXCAVATION RATES**

Suranaree University of Technology has approved this thesis submitted in partial fulfillment of the requirements for a Master's Degree.

Thesis Examining Committee

(Asst. Prof. Dr. Decho Phueakphum)

Chairperson

(Dr. Prachya Tepnarong)

Member (Thesis Advisor)

(Prof. Dr. Kittitep Fuenkajorn)

Member

(Prof. Dr. Sukit Limpijumnong)

Vice Rector for Academic Affairs
and Innovation

(Assoc. Prof. Flt. Lt. Dr. Kontorn Chamniprasart)

Dean of Institute of Engineering

นฤมล เสาวนิตย์ : การจำลองเชิงกายภาพของการทรุดตัวที่เกินกว่าจุดวิกฤตภายใต้การผันแปรลำดับและอัตราการขุดเจาะ (PHYSICAL MODEL SIMULATIONS OF SUPER-CRITICAL SUBSIDENCE UNDER VARIOUS MINING SEQUENCES AND EXCAVATION RATES) อาจารย์ที่ปรึกษา : อาจารย์ ดร.ปรัชญา เทพณรงค์, 94 หน้า.

การศึกษามุ่งเน้นในด้านผลกระทบของลำดับขุดเจาะเหมือง อัตราการขุดเจาะ และความเอียงของชั้นหินปิดทับภายใต้สภาวะที่มีการทรุดตัวเกินกว่าจุดวิกฤตโดยใช้โครงจำลองทางกายภาพ (trap door apparatus) ผลการทดสอบระบุว่ามุมการไหลและอัตราส่วนระหว่างการทรุดตัวสูงสุดต่อความสูงของช่องเหมืองลดลงด้วยการเพิ่มขึ้นของอัตราส่วนระหว่างความลึกต่อความสูงของช่องเหมืองเมื่อความสูงของช่องเหมืองถูกกำหนดให้มีค่าคงที่เป็น 50 มิลลิเมตร และความลึกของช่องเหมืองผันแปรจาก 50 ถึง 200 มิลลิเมตร ความต่อเนื่องของลำดับการขุดเจาะจากตรงกลางช่องเหมืองให้ค่ามุมการไหลน้อยที่สุดและค่าการทรุดตัวมากที่สุด ขณะที่การขุดเจาะจากขอบไปยังตรงกลางของช่องเหมืองส่งผลให้ค่าของมุมการไหลมีค่ามากที่สุด และการทรุดตัวบนผิวดินน้อยที่สุด ภายใต้การผันแปรความเอียงของชั้นหินปิดทับ พบว่ามุมการไหลที่ส่วนบน (up-slope) และล่าง (down-slope) ของชั้นหินปิดทับที่มีความเอียง มีค่าเพิ่มขึ้นด้วยการเพิ่มมุมของความเอียงของชั้นหินปิดทับ และอัตราส่วนระหว่างการทรุดตัวสูงสุดต่อความสูงของช่องเหมืองมีค่าลดลงด้วยการเพิ่มขึ้นของอัตราส่วนระหว่างความลึกต่อความสูงของช่องเหมืองและความเอียงของชั้นหินปิดทับ ผลการทดสอบที่ได้จากแบบจำลอง PFC^{2D} มีค่ามากกว่าผลที่ได้จากการทดสอบทางกายภาพในทุกกรณี วิธีการเชิงประจักษ์ที่ดูน่าเสนอโดย Rankin มีความสอดคล้องกันดีกับแบบจำลองเชิงกายภาพภายใต้อัตราการขุดเจาะแบบเร็ว วิธีการเชิงประจักษ์ไม่เหมาะสำหรับการคำนวณลักษณะการทรุดตัวของลำดับการทำเหมืองที่แตกต่างกันและชั้นหินปิดทับลาดเอียง การค้นพบอาจถูกใช้ในการประเมินลักษณะการทรุดตัวสำหรับการผันแปรวิธีการขุดเจาะเหมืองใต้ดินที่ได้รับผลกระทบจากลำดับการขุดเจาะ อัตราการขุดเจาะและชั้นหินปิดทับที่มีความลาดเอียงในมวลหินที่มีรอยแตกจำนวนมาก

สาขาวิชา เทคโนโลยีธรณี

ปีการศึกษา 2559

ลายมือชื่อนักศึกษา _____

ลายมือชื่ออาจารย์ที่ปรึกษา _____

NARUEMOL SAOANUNT : PHYSICAL MODEL SIMULATIONS OF
SUPER-CRITICAL SUBSIDENCE UNDER VARIOUS MINING
SEQUENCES AND EXCAVATION RATES. THESIS ADVISOR :
PRACHYA TEPNARONG, Ph.D., 94 PP.

MINING SEQUENCE/ EXCAVATION RATE/ OVERBURDEN SLOPE/ MODEL

The study is focused on the effects of the mining sequences, excavation rates and overburden slope under super-critical condition by using trap door apparatus. The results indicate that the angle of draw and S_{\max}/H ratio decrease with increasing Z/H ratio when the opening height (H) is maintained constant at 50 mm and the opening depth (Z) varies from 50 mm to 200 mm. Consecutive mining sequence from center of panel gives the lowest angle of draw and highest subsidence while excavation from the edge to center of panel causing the highest angle of draw and lowest subsidence. Under various overburden slopes, the angle of draw on up-slope and down-slope increases with increasing slope angle. The S_{\max}/H ratio decreases with increasing Z/H ratio and slope angle. The results obtained from PFC^{2D} simulations are higher in value than those of the physical model, for all cases. The empirical solution provided by Rankin (1998) fits well to the physical model under high excavation rate. The empirical solution does not allow for subsidence profile calculation of different mining sequences and overburden slopes. The findings may be used to evaluate the subsidence profile for various underground excavation methods as affected by excavation sequence, extraction rate and overburden slope in a heavily fractured rock mass.

School of Geotechnology

Academic Year 2015

Student's Signature_____

Advisor's Signature_____

ACKNOWLEDGMENTS

The author wishes to acknowledge the support from the Suranaree University of Technology who has provided funding for this research.

Grateful thanks and appreciation are given to Prof. Dr. Kittitep Fuenkajorn for his valuable guidance and gave a critical review of this study. I appreciate his strong support, encouragement, suggestions and comments during the research period. Many thanks to Dr. Prachaya Tepnarong, thesis advisor, and Asst. Prof. Dr. Decho Phueakphum for their constructive advice, valuable suggestions and comments on my study. Grateful thanks are given to all staffs of Geomechanics Research Unit, Institute of Engineering who supported my work.

Finally, I would like to thank my parents for their support and encouragement.

Naruemol Saoanunt



TABLE OF CONTENTS

	Page
ABSTRACT (THAI)	I
ABSTRACT (ENGLISH).....	II
ACKNOWLEDGEMENTS	III
TABLE OF CONTENTS.....	IV
LIST OF TABLES	VII
LIST OF FIGURES	VIII
SYMBOLS AND ABBREVIATIONS.....	XIII
CHAPTER	
I INTRODUCTION.....	1
1.1 Background and rationale	1
1.2 Research objectives.....	2
1.3 Scope and limitations	2
1.4 Research methodology	3
1.4.1 Literature review.....	3
1.4.2 Material preparation.....	3
1.4.3 Physical model simulations	5
1.4.4 Computer simulation	5
1.4.5 Analysis and comparisons	5
1.4.6 Discussion and conclusion.....	6

TABLE OF CONTENTS (Continued)

	Page
1.4.7 Thesis writing	6
1.5 Thesis contents	6
II LITERATURE REVIEW	7
2.1 Introduction.....	7
2.2 The prediction of mining subsidence.....	7
2.3 Physical modeling.....	12
2.4 Numerical simulations	21
2.5 Previous relevant researches	25
III PHYSICAL MODEL SIMULATIONS.....	30
3.1 Introduction.....	30
3.2 Material property	30
3.3 Physical model testing	32
3.3.1 Mining sequences.....	34
3.3.2 Excavations rates.....	39
3.3.3 Overburden slope	44
IV COMPUTER SIMULATIONS	48
4.1 Introduction.....	48
4.2 Computer model simulations	48
4.2.1 Mining Sequences	49
4.2.2 Excavation Rates.....	54

TABLE OF CONTENTS (Continued)

	Page
4.2.3 Overburden slopes.....	60
V COMPARISON OF NUMERICAL AND PHYSICAL MODELS	66
5.1 Objectives	66
5.2 Comparison of PFC ^{2D} simulation and physical modeling	66
VI SUBSIDENCE TROUGH VOLUME.....	77
6.1 Introduction.....	77
6.2 Previous studies on subsidence trough	77
6.3 Comparisons of subsidence trough profiles.....	79
6.4 Volume of surface settlement	81
VII DISCUSSIONS AND CONCLUSTIONS.....	84
7.1 Discussions and conclusions.....	84
7.2 Conclusions.....	87
7.3 Recommendations for future studies	88
REFERENCES	89
BIOGRAPHY	94

LIST OF TABLES

Table	Page
3.1 Mechanical properties of granular material (Clean and uniform sand with nominal size of 2 mm) (Thongprapha, 2015).....	31
4.1 PFC ^{2D} simulations results of mining sequences when constant H = 50 mm....	52
4.2 PFC ^{2D} simulations results of excavation rates	57
4.3 Results of overburden slope simulations.....	63
4.4 Depth at angle of draw and maximum subsidence in overburden slope simulations.....	64

LIST OF FIGURES

Figure	Page
1.1 Research methodology.....	4
2.1 Properties of error function curve to represent cross-section settlement trough above tunnel (Peck 1969).....	11
2.2 Physical Model subsidence curve after both extractions (Ghabraie et al.,2014).....	13
2.3 Characteristics of slope movement response to underground mining (Zhang et al., 2011).....	14
2.4 Variables used in physical model simulations and analysis (Thongprapa et al.,2015).....	16
2.5 Small-scale experimental model (Caudron et al., 2006).....	17
2.6 Observed subsidence profiles in Indian coal fields (Singh and Yadav, 1995).....	20
2.7 The generated 3D rock mass illustrating fracture defined particle clusters (Hadjigeorgiou et al.,2009).....	24
2.8 Variables used by Aracheeploha et al. (2009).....	27
2.9 Effect of different overburden properties on the angle of draw (Yao et al., 1991).....	29
3.1 Clean and uniform sand with nominal size of 2 mm used to simulate overburden.....	31

LIST OF FIGURES (Continued)

Figure	Page
3.2	Trap door apparatus used in this study (Thongprapha et al., 2015). 33
3.3	Variables used in physical model simulations and analysis 34
3.4	Mining sequences simulated in the physical models. The numbers indicate for each case of mining excavation sequence model. 36
3.5	Examples of cross-section (A-A') of surface subsidence profiles for different mining sequences. 37
3.6	Maximum subsidence-to-height (S_{max}/H) ratio as a function of opening depth-to-height (Z/H) ratio. 38
3.7	Angle of draw (γ) as a function of opening depth-to- height (Z/H) ratio. 38
3.8	Effects of excavation rate assessed by using different areas of excavation. 40
3.9	Subsidence profiles under various excavation rates. 41
3.10	S_{max}/H ratio as a function of Z/H ratio under high excavation rate and under low excavation rate 42
3.11	γ as a function of Z/H ratio under high excavation rate (a) and low excavation rate 43
3.12	Variables used in physical model simulations of overburden slope. 45
3.13	Subsidence profiles of surface subsidence under various surface slopes. 46
3.14	S_{max}/H ratio as a function of Z/H ratio for each ground surface slope. 47
3.15	γ as a function of Z/H ratio under various slope face angles. 47

LIST OF FIGURES (Continued)

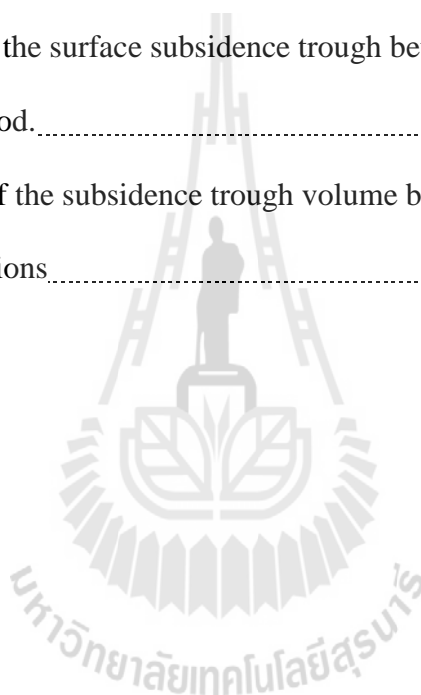
Figure	Page
4.1	Surface subsidence before the opening simulation of mining sequences.....50
4.2	PFC ^{2D} model simulations of surface subsidence after the opening are excavated 51
4.3	S_{\max}/H ratio as a function of Z/H ratio, and γ as a function of Z/H ratio.....53
4.4	Surface subsidence before the opening simulation with predefine overburden thickness of high excavation rate and low excavation rate55
4.5	Surface subsidence of PFC ^{2D} model after the opening simulation of high excavation rate and low excavation rate56
4.6	Maximum subsidence to height ratio (S_{\max}/H) as a function of overburden thickness to height ratio (Z/H) and angle of draw (γ) as a function of overburden thickness to height ratio in case high excavation rate.....58
4.7	Maximum subsidence to height ratio (S_{\max}) as a function of overburden thickness to height ratio (Z/H) and angle of draw (γ) as a function of overburden thickness to height ratio in case high excavation rate (5 mm increment).....59
4.8	Examples of surface subsidence before the opening simulation.....61
4.9	Examples of surface subsidence after the opening simulation.....62
4.10	S_{\max}/H as a function of Z/H ratio (a) and γ as a function of Z/H ratio (b).....65

LIST OF FIGURES (Continued)

Figure	Page	
5.1	Comparison of mining sequences of S_{max}/H ratio as a function of Z/H ratio as a function of Z/H ratio of four mining sequence cases.....	68
5.2	Comparisons of angle of draw (γ) as a function of Z/H ratio of mining sequence in four cases obtained from physical simulation and PFC ^{2D} model simulation.....	69
5.3	Comparisons of the maximum subsidence to height ratio (S_{max}/H) of high excavation rates (50 mm increments) obtained from physical simulation and PFC ^{2D} model simulation.....	70
5.4	Comparisons of the angle of draw (γ) of high excavation rates obtained from PFC ^{2D} and physical simulation.....	71
5.5	Comparisons of the maximum subsidence to height ratio (S_{max}/H) of low excavation rates (5mm increments) obtained from physical simulation and PFC ^{2D} model simulation.....	69
5.6	Comparisons of angle of draw (γ) of low excavation rates (5mm increments) obtained from physical simulation and PFC ^{2D} model simulation.....	70
5.7	Comparisons of S_{max}/H ratio of overburden slope obtained from physical simulation and PFC ^{2D} model simulation.....	74
5.8	The comparisons γ at up-slope are obtained from physical simulation with PFC ^{2D} model simulation of overburden slope.....	75

LIST OF FIGURES (Continued)

Figure	Page
5.9	The comparisons obtained from physical simulation with PFC ^{2D} model simulation of γ at down-slope of overburden slope.....76
6.1	Comparison of the surface subsidence trough between physical model and empirical method.....80
6.2	Comparisons of the subsidence trough volume between physical models and empirical solutions.....83



SYMBOLS AND ABBREVIATIONS

S_{\max}	=	Maximum magnitude of subsidence
γ	=	Angle of draw
γ_{down}	=	Angle of draw on down-slope side
γ_{up}	=	Angle of draw on up-slope side
$S(x)$	=	Vertical displacement
$G(x)$	=	Slope (or tilt)
$\rho(x)$	=	Vertical curvature
$u(x)$	=	Horizontal displacement (lateral movement)
$\varepsilon(x)$	=	Horizontal strain
b	=	Arbitrary constant
c	=	Arbitrary constant
x	=	Horizontal distance
B	=	Radius of critical area of excavation
i	=	Width of settlement trough, defined as distance from center to point of inflection of curve
C_u	=	Uniformity coefficient
C_c	=	Coefficient of curvature
c	=	Cohesion
ϕ	=	Friction angle
K_s	=	Joint shear stiffness

SYMBOLS AND ABBREVIATIONS (Continued)

K_n	=	Joint normal stiffness
W	=	Underground opening width
L	=	Underground opening length
H	=	Underground opening height
Z	=	Underground opening depth (or overburden thickness)
γ_{down}	=	Angle of draw on down-slope
γ_{up}	=	Angle of draw on up-slope
θ	=	Overburden angle (or slope angle)
B_s	=	Block size (or particle size)

CHAPTER I

INTRODUCTION

1.1 Background and rationale

Surface subsidence is a consequential damage from underground mining which can impact the environment and surface structures within the mine area. The subsidence magnitude must therefore be within acceptable range to reduce such problem. The angle of draw and maximum subsidence magnitude is important parameters for use to predict the surface subsidence profile. Many methods exist for predicting the value of maximum subsidence and volume of trough induced by underground mining, i.e. physical modeling, computer model simulation and analytical method. Even though extensive studies have been carried out in an attempt to predict the surface subsidence behavior under various underground excavation methods, the effects of mining sequence and excavation rate have rarely been addressed. This is primarily because the effects of excavation rate and mining sequence occur in the post failure region, and hence it is difficult, if at all possible, to study them with numerical model simulations. This study is therefore focused on the effects of mining sequence and excavation rate on the angle of draw, maximum subsidence and trough shape under super-critical condition by using scale-down physical models in the laboratory.

1.2 Research objectives

The objective of this study is to study the effects of mining sequence excavation rate and overburden slope on the angle of draw, maximum subsidence and trough shape induced in post failure region under super-critical condition using scaled-down physical model. Granular materials are used to represent the overburden. The results obtained from the physical model are compared with those of the computer model simulations (PFC^{2D} code). Similarity and discrepancy are identified.

1.3 Scope and limitations

The scope and limitations of the research include as follows.

- a) A trap door apparatus (Thongprapha et al., 2015) is used to simulate the surface subsidence under super-critical condition.
- b) Granular materials are used to simulate the overburden.
- c) The overburden thickness is varied from 50 mm to 250 mm for all cases
- d) Each series of test are simulated at least 3 times to verify the repeatability of the results.
- e) Maximum subsidence values, angle of draw and volume of trough are determined.
- f) Physical model results are compared with numerical simulations (using PFC^{2D} software).
- g) The main focus is on the super-critical subsidence surface behavior under various mining sequences and excavation rate.

1.4 Research methodology

The research methodology shown in Figure 1.1 comprises 6 steps; including literature review, material preparation, physical model simulation, computer simulations, analysis and comparisons, discussions and conclusions and thesis writing.

1.4.1 Literature review

Literature review is carried out to improve an understanding of surface subsidence knowledge and case studies in Thailand and abroad. The sources of information are from journals, technical reports and conference papers. A summary of the literature review is given in the thesis.

1.4.2 Material preparation

Granular materials are used as the test material. The material is subjected to two tests; grain size analysis and direct shear test. The grain size analysis is performed to determine the percentage of different grain sizes contained within a material. The objective of direct shear test is to determine the cohesion and the friction angle.

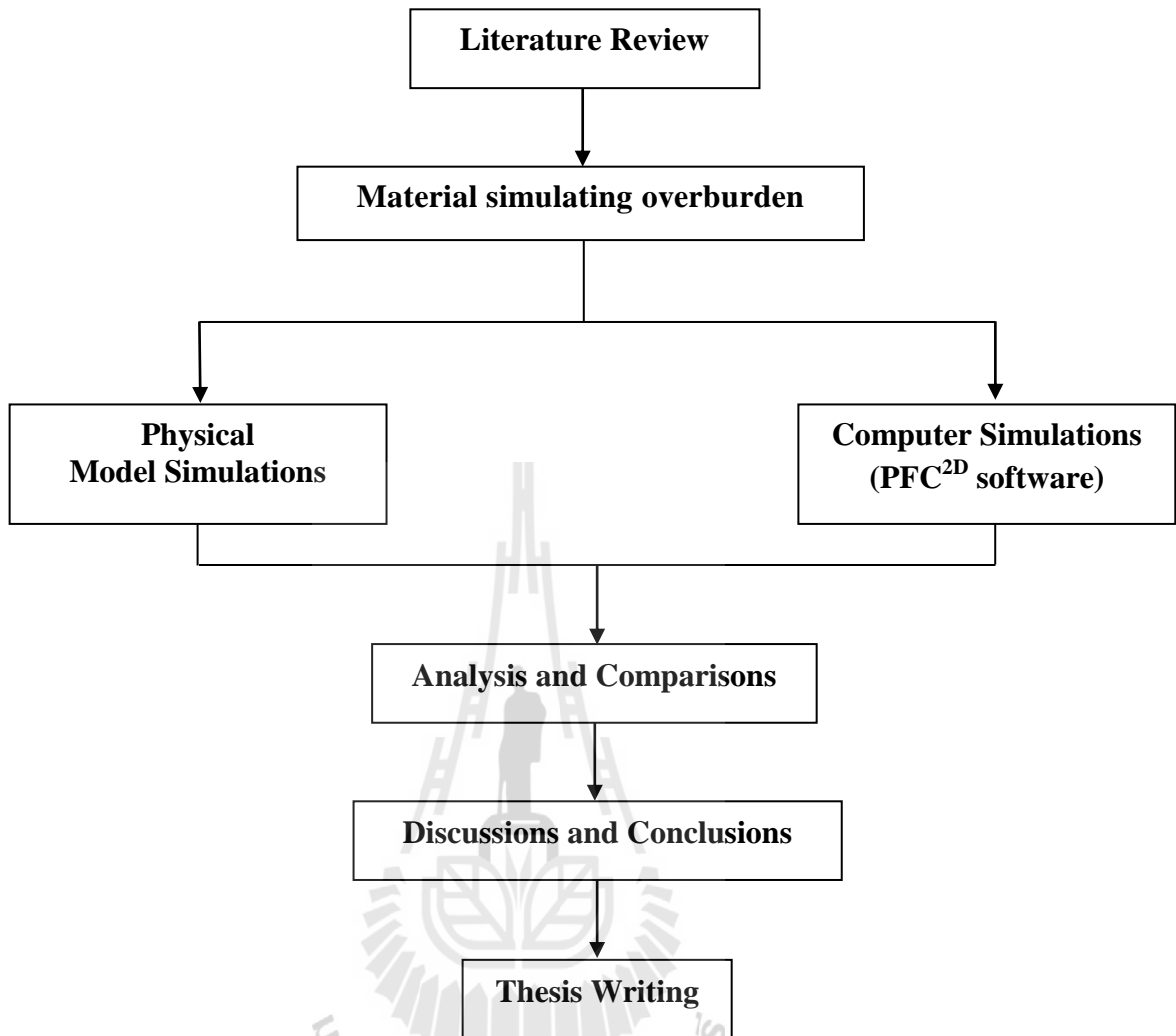


Figure 1.1 Research methodology.

1.4.3 Physical model simulations

A trap door apparatus (Thongrapha et al., 2015) is used to simulate subsidence of overburden in three-dimension. The laboratory testing gives the maximum subsidence (S_{\max}), slope of surface, the angle of draw (γ) and volume of subsidence trough under various mining sequences and excavation rates. The model testing is simulated for the opening width (W) from 50 mm to 250 mm with an increment of 50 mm. The opening length (L) is from 50 mm up to 500 mm, with 50 mm increment. The opening height (H) is from 5 mm to 50 mm, with 5 mm increment. In this study, overburden thickness (Z) is varied from 50 mm to 250 mm. For the incline overburden, the surface angle is varied from 5 degrees to 20 degrees. A laser scanner measures the surface profile of the granular material before and after the subsidence is induced.

1.4.4 Computer simulation

The computer code is used to calculate the subsidence characteristics of the test model by considering the effects of underground excavation methods. Calculation uses PCF^{2D} code. The results are compared with the physical model testing.

1.4.5 Analysis and comparisons

Results obtained from the physical model and numerical simulations are compared to determine the effect of the underground excavation methods, mining sequence and excavation rate the results can be used to minimize the subsidence impacts.

1.4.6 Discussion and conclusion

Discussions are on the reliability and adequacies of the approaches used here. Future research needs are identified. All research activities, methods, and results are documented and compiled in the thesis. The research or findings are published in the conference proceedings or journals.

1.4.7 Thesis writing

All study activities, methods, and results are documented and compiled in the thesis.

1.5 Thesis contents

This research thesis is divided into nine chapters. The first chapter includes background and rationale, research objectives, scope and limitations and research methodology. The second chapter presents results of the literature review to improve an understanding of surface subsidence knowledge. The Chapter three describes materials simulating overburden. Physical model simulations are explicated in chapter four. Computer Simulations by PFC^{2D} software described in chapter five. Comparison and analysis between the results obtained from physical model computer simulation describes in chapter six. Chapter seven presents discussions, conclusions and recommendation for future studies.

CHAPTER II

LITERATURE REVIEW

2.1 Introduction

Relevant topics and previous research results are reviewed to improve an understanding of surface subsidence. These include the surface subsidence prediction, physical modeling and numerical simulations. The review results are summarized below.

2.2 The prediction of mining subsidence

Singh (1992) states that the subsidence is an inevitable consequence of underground mining. The profile function method used to calculate the angle of draw from depth of the excavated opening and the boundary of the subsided area for sub-critical and critical subsidence.

The major objectives of subsidence engineering are

- 1) Prediction of ground movement.
- 2) Determining the effects of such movements on structures and renewable resource.
- 3) Minimizing damage due to subsidence.

Whenever a cavity is created underground, due to the mining of minerals or for any other reason, the stress field in the surrounding strata is disturbed. These stress changes produce deformations and displacements of the strata, the extent of

which depends on the magnitude of the stresses and the cavity dimensions. With time, supporting structures deteriorate and the cavity enlarges, resulting in instability. This induces the superjacent strata to move into the void. Gradually, these movements work up to the surface, manifesting themselves as a depression. This is commonly referred to as subsidence. Thus mine subsidence may be defined as ground movements that occur due to the collapse of overlying strata into mine voids. Surface subsidence generally entails both vertical and lateral movements.

Subsidence consists of five major components, which influence damage to surface structures and renewable resources are vertical displacement, horizontal displacement, slope, vertical strain, and vertical curvature.

Calculation by profile function;

Vertical displacement:

$$S(x) = \frac{1}{2} S_{\max} \left[1 - \tanh\left(\frac{cx}{B}\right) \right] \quad (2.1)$$

Slope (or tilt):

$$G(x) = S'(x) = -\frac{1}{2} S_{\max} \frac{c}{B} \operatorname{sech}^2\left(\frac{cx}{B}\right) \quad (2.2)$$

Vertical curvature:

$$\rho(x) = S''(x) = S_{\max} \frac{c^2}{B^2} \left[\operatorname{sech}^2\left(\frac{cx}{B}\right) \tanh\left(\frac{cx}{B}\right) \right] \quad (2.3)$$

Horizontal displacement (lateral movement):

$$u(x) = -\frac{1}{2} S_{\max} \frac{bc}{B} \operatorname{sech}^2\left(\frac{cx}{B}\right) \quad (2.4)$$

Horizontal strain:

$$\varepsilon(x) = S_{\max} \frac{bc^2}{B^2} \left[\operatorname{sech}^2\left(\frac{cx}{B}\right) \tanh\left(\frac{cx}{B}\right) \right] \quad (2.5)$$

where S_{\max} is the maximum subsidence,

D is depth of cavern,

x is horizontal distance,

c is arbitrary constant,

b is constant, and

B is maximum radius of cavern area.

Kyu-Seok et al. (2013) perform the empirical investigation and characterization of surface subsidence related to block cave mining. Guidance on relationships between caving depth and surface subsidence, a comprehensive database was developed after an exhaustive search of published data from cave mining operations from around the world. The distribution of data was found to largely focus on caving angles and macro deformations; very little empirical data exists on the extent and magnitudes of smaller surface displacements. The data clearly show that caving-induced surfaced formations tend to be discontinuous and asymmetric due to large movements around the cave controlled by geologic structures rock mass heterogeneity and topographic effects. The data also show that as undercut depth increases for a given extraction volume, the magnitude and extent of the caved zone on surface decreases. The numerical modeling indicates that this is only the case for macro deformation and the extent of smaller displacements actually increases as a function of undercut depth. The results presented caution against relying on existing

empirical design charts for estimates of caving-induced subsidence where small strain subsidence is of concern, as the data being relied upon does not properly extrapolate.

Beyond the macro deformations that make up the majority of the observations. The findings also suggest that the extent and magnitudes of subsidence may be underestimated if the analysis adopted neglects the influence of geological structures and assumes symmetrical surface displacements above the undercut.

Fattah et al. (2013) predicted and compared the shape of settlement trough induced by tunneling in cohesive soil is investigated by different approaches, namely analytical solutions, empirical solutions, and numerical solutions by the finite element method. The width of settlement trough was obtained by the finite element method through establishing the change in the slope of the computed settlement profile. The finite element elastic-plastic analysis gives better predictions than the linear elastic model with satisfactory estimate for the displacement magnitude and slightly overestimated width of the surface settlement trough. The finite element method over predicted the settlement trough width compared with the results of Peck (1969) for soft and stiff clay, but there is an excellent agreement with Rankin's (1988) estimation. The results show that there is a good agreement between the complex variable analyses for $Z/D = 1.5$, while using $Z/D = 2$ and 3 , the curve diverges in the region far away from the center of the tunnel.

Peck (1969) described that shape of subsidence examples for more than 20 cases by use the Gaussian curve, shown in Figure 2.1. He presents equation to find shape of trough using subsidence maximum (S_{max}), distance from middle of opening (x) and width of trough (i).

Rankin (1988) presents an equation to calculate the opening width by defining the dimensionless (k) as constant $k=0$ for clay and $k=2.5$ for cohesionless soil. Part of opening width or tunnel is measurement from middle to surface before subsidence (Z_0) show in the Figure 2.1.

$$\text{Surface subsidence: } S = S_{\max} \exp(-x^2/2i^2) \quad (2.6)$$

$$\text{Width of trough: } i = k \cdot Z_0 \quad (2.7)$$

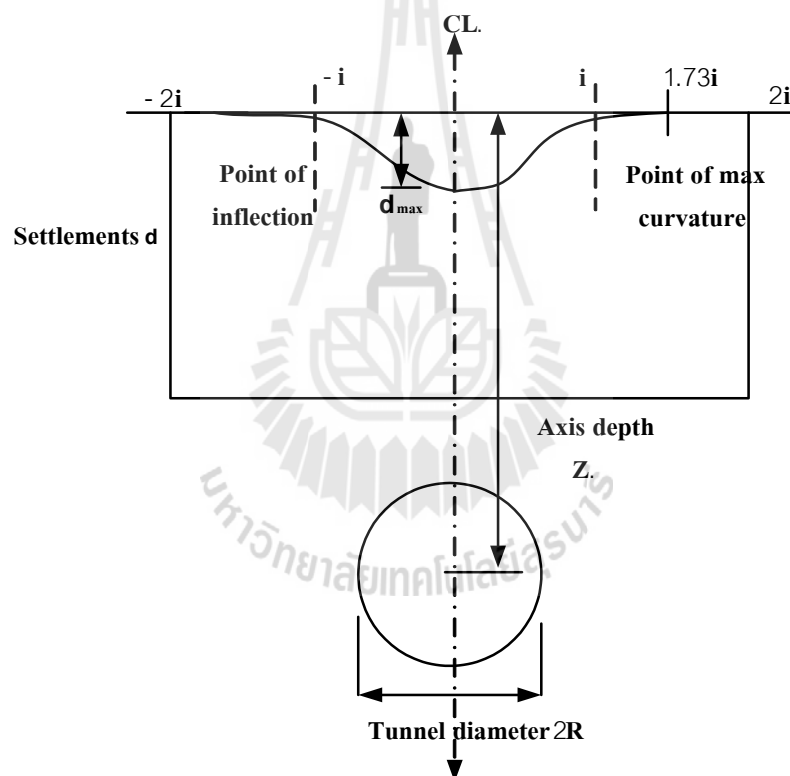
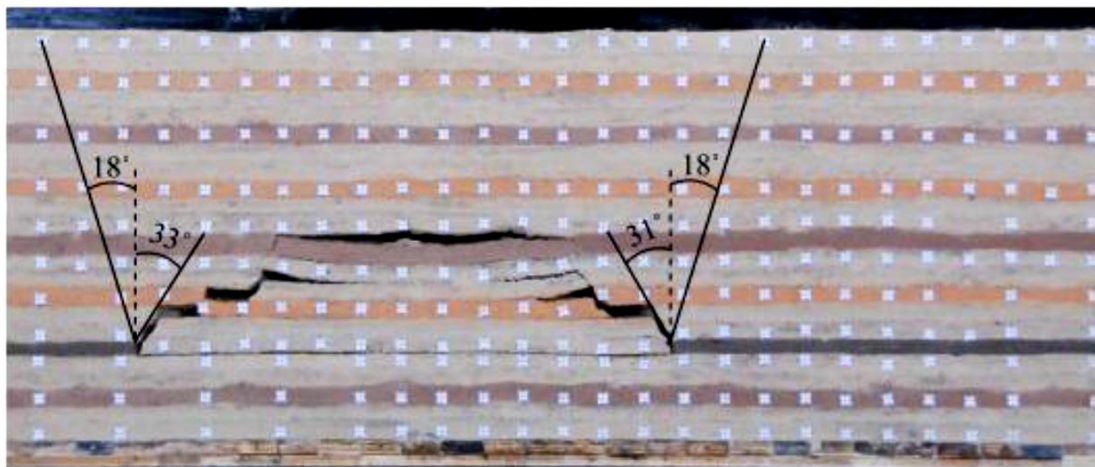


Figure 2.1 Properties of error function curve to represent cross-section settlement trough above tunnel (Peck 1969).

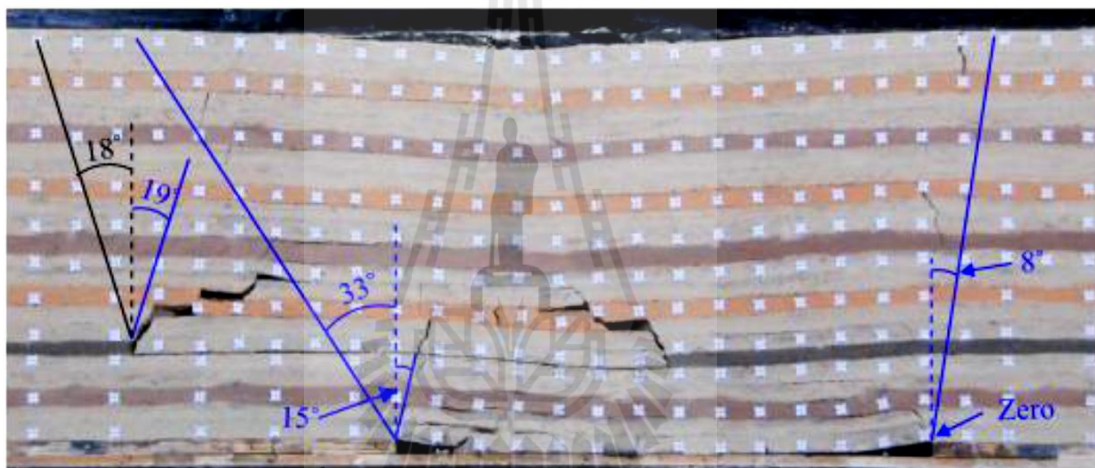
2.3 Physical Modeling

Physical modeling is one of the most effective techniques in studying the rock strata behavior affected by longwall mining (Whittaker and Reddish, 1989). It has been used by many researchers to simulate longwall mining-induced subsidence and other related problems (Whittaker et al., 1989; Wold, 1985; Huayang et al., 2010; Liu et al., 2011). Processes such as surface movement, crack propagation, caving, substrata movements and the overburden movement after sequential multiple-seam mining can be investigated by physical modeling (Liu et al., 2011). Ghabraie et al. (2014) investigate the subsidence mechanisms from sequential extraction of overlapping coal longwall panels (Figure 2.2), and find that the zone of the two long wall panels under goes greater total subsidence compared to a single seam of equivalent thickness.

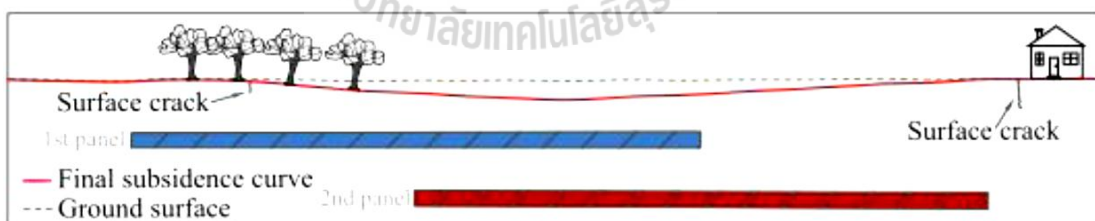
Zhang et al. (2011) studied gully slope movements, subject to underground mining, with physical model simulation and theoretical analysis. The rules disclose that the slope rock slides horizontally in response to mining in the direction of gullies. They simulated a mechanical model in term of a polygon block hinged structure and investigated the variation of horizontal and shear force at the hinged point in the relation to the rotation angle (Figure. 2.3). The gully slope angle model is 15 degree, the overburden thickness is only 600 cm, the opening length is 160 cm and the excavation interval 5 cm. They indicate that the horizontal force decrease with the increase of the rotation angle, the shear force will increase with increase in the rotation angle and the rotation instability increase with an increase the slope angle.



(a)



(b)

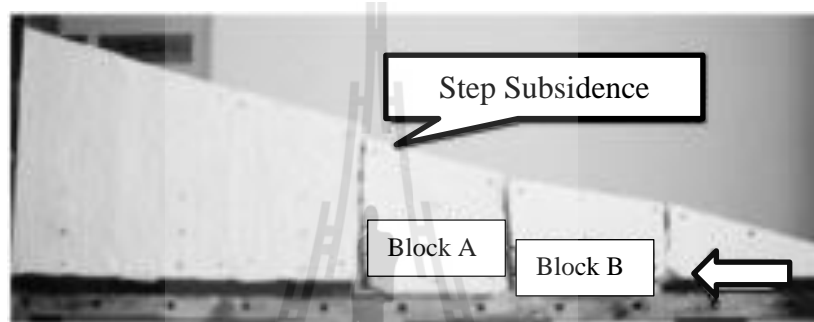


(c)

Figure 2.2 Physical Model subsidence (a) angle of draw and angle of break after extraction of single extraction, (b) multiple extraction and (c) ground subsidence curve after both extractions (Ghabraie et al.,2014).



(a) Mining in the direction of a gully.



(b) Hinged status of polygon block.

Figure 2.3 Characteristics of slope movement response to underground mining (Zhang et al., 2011).

Shu and Bhattacharyya (1992) study the subsidence movements on a overburden slope above a completely mined panel using a combination of an equivalent horizontal surface and a ray projection method. The ray projection method provides the subsidence components on a overburden slope. The overburden slope or ground inclination affects the distribution of surface subsidence. Compare with the subsidence on the equivalent horizontal surface, the magnitude of subsidence increases on the down-slope side and decreases on the up-slope side of the extraction.

Thongprapa et al. (2015) present the physical model simulations to determine the effects of underground opening configurations on surface subsidence under super-critical conditions. This study indicates the importance of the main factors that control the extent of subsidence produced on the surface and determines the effects of geometry of underground openings on the angle of draw, the maximum subsidence and the volume of the subsidence trough. A trap door apparatus with the test area of $95 \times 95 \text{ cm}^2$ has been fabricated to perform the scaled-down simulations of surface subsidence. Gravel is used to represent the overburden in order to exhibit a cohesionless frictional behavior. In plan view the excavation dimensions are sufficient to induce maximum possible subsidence. The findings can be used to evaluate the subsidence profile for tunnels and caverns in soft ground. The results show that the angle of draw and the maximum subsidence are controlled by the width (W), length (L), height (H) and depth (Z) of the underground openings show in Figure 2.4. The angle of draw and maximum subsidence increase with increasing L/W ratio and tends to approach a limit when L/W equals 3. For the same L/W ratio and H/W ratio, increasing the Z/W ratio reduces the angle of draw and maximum subsidence. The volume of the subsidence trough increases with increasing H/W ratio and L/W ratio. The width of the subsidence trough can be represented by sets of empirical relations. The relation between opening depth and subsidence trough developed by Rankin (for cohesionless soils) is in good agreement with most physical model results for deep openings ($Z/W = 2-4$), while for $Z/W = 1$, the predicted trough width is less than the physical model simulation. The volume of the subsidence trough is largest for $Z/W = 2.5$ and for $H/W = 0.6$, and is about 60% of volume of the underlying opening.

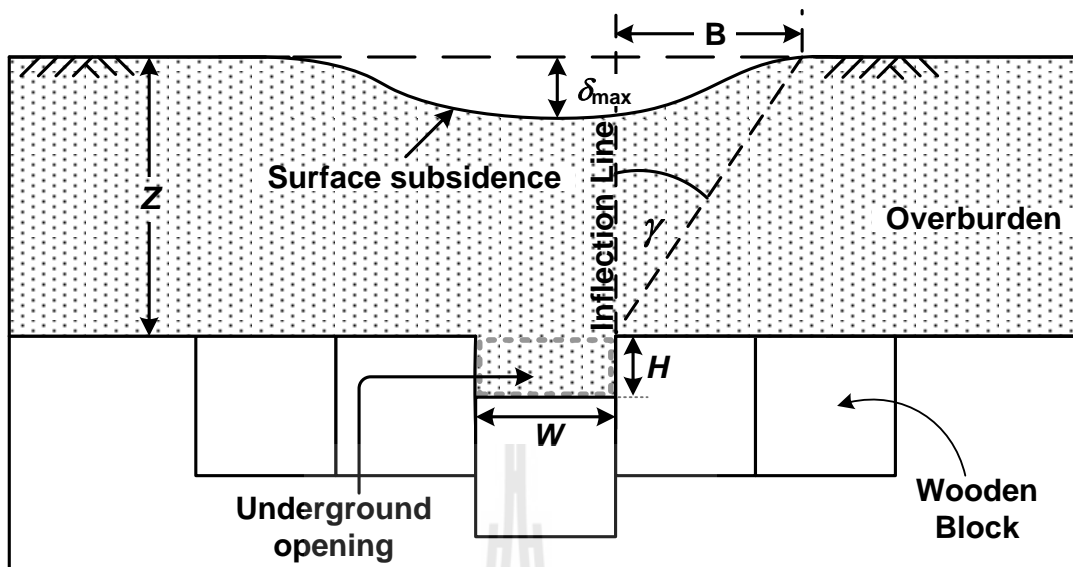


Figure 2.4 Variables used in physical model simulations and analysis: W = opening width, H = opening height, Z = opening depth, γ = angle of draw, δ_{\max} = maximum subsidence and B = half width of subsidence trough (Thongprapa et al., 2015).

Caudron et al. (2006) study the soil-structure interaction during a sinkhole phenomenon using an analog two-dimensional soil and a physical model and a numerical method. They use bidimensional Schneebeli material (Figure 2.5) in a small-scale model allowing fully controlled test conditions. The Schneebeli material is modified in order to exhibit a cohesive frictional behavior. The physical model allows to represent a case of study and to determine it completely with a limited set of parameters.

Cui et al. (2000) predict the subsidence caused by underground mining from theory and those experienced in practice. By using non-linear geometrical field theory, the deformation factors are modified and the limitation of linear elastic theory is established to determine maximum subsidence and angle of draw. They found that the physical models are helpful for understanding the subsidence mechanisms and suitable for rectangular panels. The predicted results are usually smaller than the measured field values.

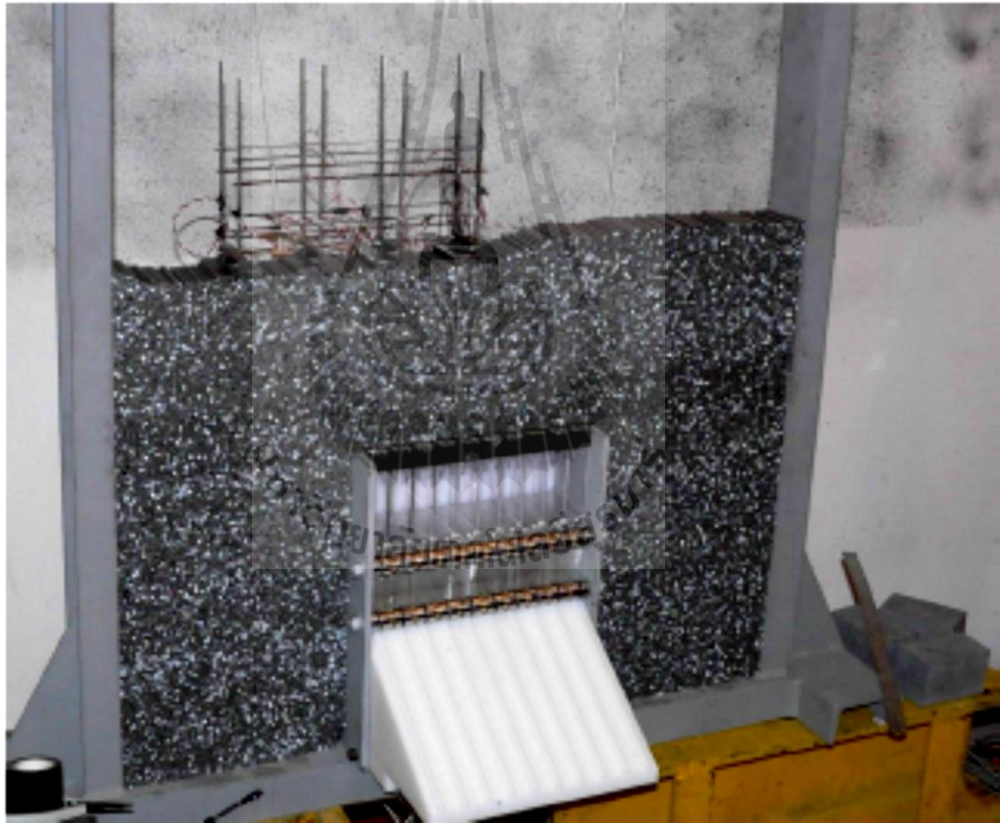
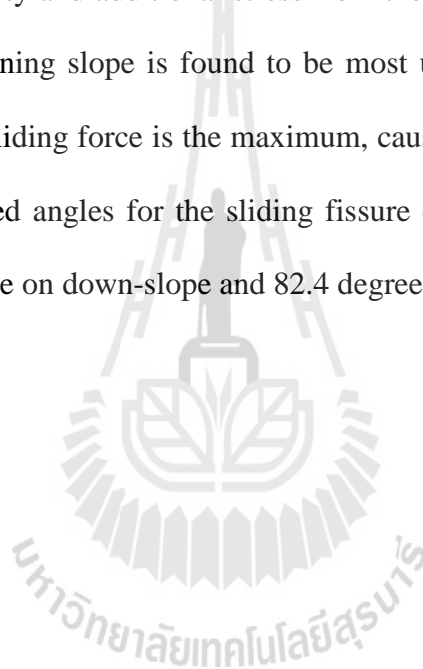


Figure 2.5 Small-scale experimental model(Caudron et al., 2006)

Liu et al. (2015) developed a mechanical model for a mining slope with slope stability analysis, and studied the mechanism of formation and development of a sliding ground fissure by the circular sliding slice method. They established a prediction model of a sliding fissure based on a mechanical mechanism, and verified its reliability, an engineering example, situated at Daliuta coal mine of Shendong mining area in western China. The results show that the stress state of a mining slope is changed by its gravity and additional stress from the shallow-buried coal seam and gully terrain. The mining slope is found to be most unstable when the ratio of the down-sliding to anti-sliding force is the maximum, causing local fractures and sliding fissures. The predicted angles for the sliding fissure on both sides of the slope are found to be 64.2 degree on down-slope and 82.4 degree on up-slope side.



Singh and Yadav (1995) predict the ground surface subsidence by using a visco-elastic modeling. The results indicate that excavation time can affect the surface subsidence and that the subsidence increases continuously during the first two years after excavation. Three types of subsidence profiles (as shown in Figure 2.6) are observed in Indian coalfields under different mining conditions and different geological environments:

- (a) Continuous subsidence profile – observed in deep coal mines.
- (b) Stepped subsidence profile – observed in shallow coal mines with strong (rigid) overburden.
- (c) Continuous subsidence profile with many small steps – observed in coal mines with weak (flexible) overburden. The natures of the overburden (mostly sandstones) are found to be variable in the Raniganj coalfield area.

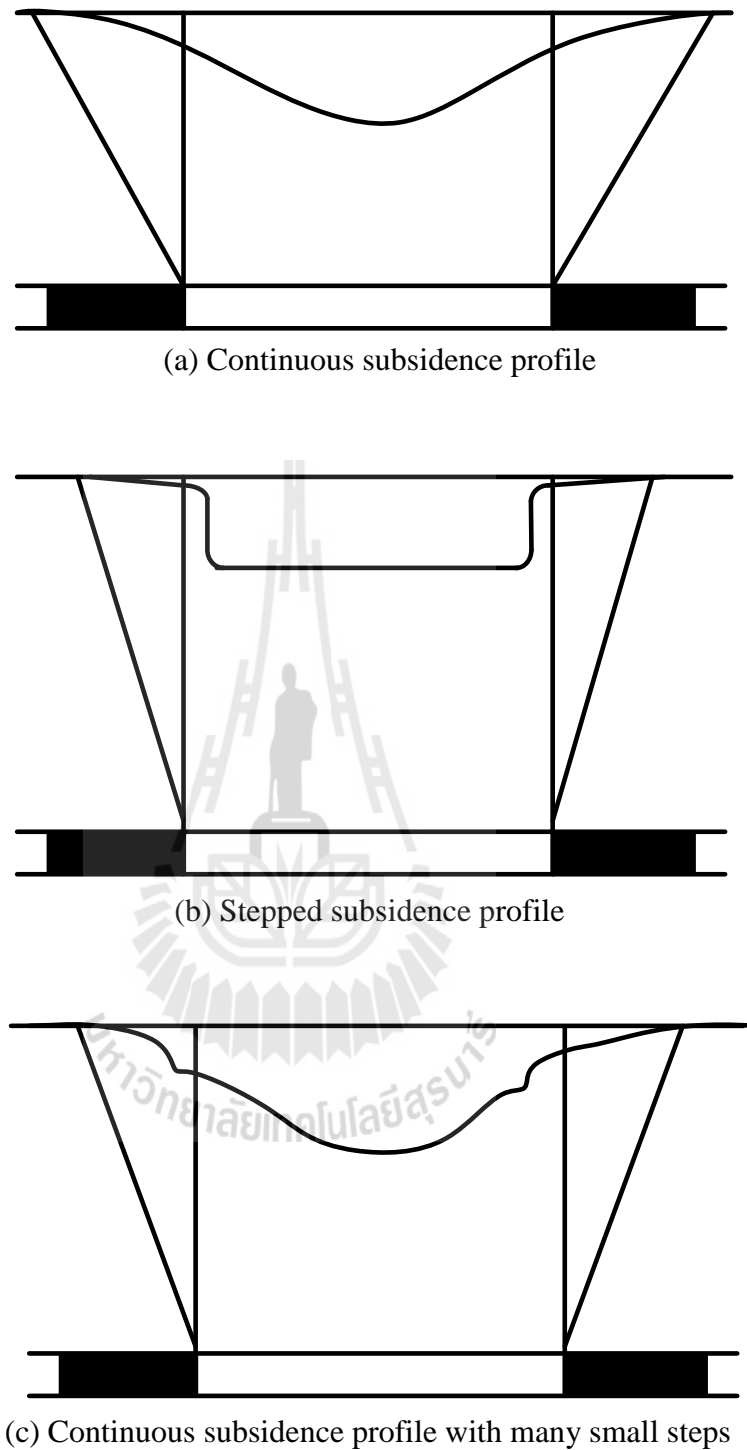


Figure 2.6 Observed subsidence profiles in Indian coal fields (Singh and Yadav, 1995)

2.4 Numerical simulations

PFC^{2D} (Particle Flow Code in 2 Dimensions) developed by Itasca Consulting Group Inc. (2008). PFC^{2D} is a discontinuum code used in analysis, testing, and research in any field where the interaction of many discrete objects exhibiting large-strain and/or fracturing is required. Because PFC^{2D} is not designed to examine a particular type of problem, its range extends to any analysis that examines the dynamic behavior of a particulate system.

In PFC^{2D} materials may be modeled as either bonded (cemented) or unbounded (granular) assemblies of particles. Though the code uses circular particles by default, particle shape may be defined in a PFC^{2D} model through use of the built-in clump logic.

The efficient contact detection scheme and the explicit solution method ensure that a wide variety of simulations from rapid flow to brittle fracture of a stiff solid are modeled accurately and rapidly. All the equations used in PFC^{2D} are documented. The user has access (via the powerful built-in programming language, FISH) to almost all internal variables. The codes are not “black boxes,” but open software that can be used with confidence.

PFC^{2D} uses an explicit solution scheme that gives stable solutions to unstable processes. It can describe non-linear behavior and localization with accuracy that cannot be matched by typical finite element programs. This makes PFC^{2D}, along with its three-dimensional counterpart PFC^{3D}, the only commercially available codes of their kind.

Li and Wang (2011) used Particle Flow Code to simulate the process of subsidence and to calculate the distribution of contact force and displacement of ore particles, which have a good consistency in comparison with the actual survey data in Shandong province. PFC^{2D} well simulates the process of the mine collapse. Particle flow method has unique advantages in the simulation of mechanical behavior of broken ore particles, in the mechanical analysis of collapse process and in the collapse displacement of ores. Discrete element modeling is employed for this study due to its advantages in analyzing large deformations and discontinuous processes.

Hadjigeorgiou et al. (2009) studied the stability analysis of vertical excavations in hard rock by integrating a fracture system into a PFC model indicating that the fracture system is consequently linked into a distinct element stress analysis. The particle flow code was selected as it potentially allows greater flexibility in representing a fracture system. In the first example a 3D fracture system was linked into a PFC^{2D} model (Figure 2.7). Although this has allowed for an improved quantification of stress structure interaction it necessitated important simplifications which may not be necessarily appropriate. These have been overcome by providing a complete integration of a 3D fracture system to a PFC^{3D} model. This is potentially led into a design tool that adequately account for the stress structure interaction on the stability of vertical or near vertical excavations in hard rock. This is demonstrating that it is possible to provide a complete 3D approach in investigating the stability of vertical excavations in hard rock. This has drawn from experience in 3D fracture systems and the use of the particle flow code both in 2D and 3D.

Ren and Li (2008) study the extent of mining subsidence affected area is defined by the limit angles, which is predominantly controlled by geological conditions of the overburden strata and the mining configurations, including seam inclination angle. From observational data worldwide and numerical modeling analysis the following conclusions are drawn: The stiffness, strength and failure of the overburden play an important role in the characteristics of subsidence limit. When overburden rocks are sufficiently strong and no major failure or break up taking place in the roof, the limit angle would tend to be greater in roof rocks with higher stiffness. However, if the roof collapses, stronger strata would produce lower limit angle at the surface and weak roof strata would result in greater limit angle. When there is an adequately strong and stiff rock bed in the overburden, it is possible for a sub-critical subsidence profile to be developed over a panel of super-critical width. The rock strength and stiffness also affect the magnitude of the maximum subsidence. Generally the maximum subsidence over a strong overburden is less than that over a weak overburden. Numerical model has demonstrated that the effect of seam inclination is such that it increases the limit angle at the dip-side of the panel and reduces the limit angle at the rise-side. The values of limit angles over inclined seams may be established from observed data set. Empirical relationship between the limit angles and the seam inclination angle may be derived either using numerical modeling techniques or observed data set in a specific mining field.

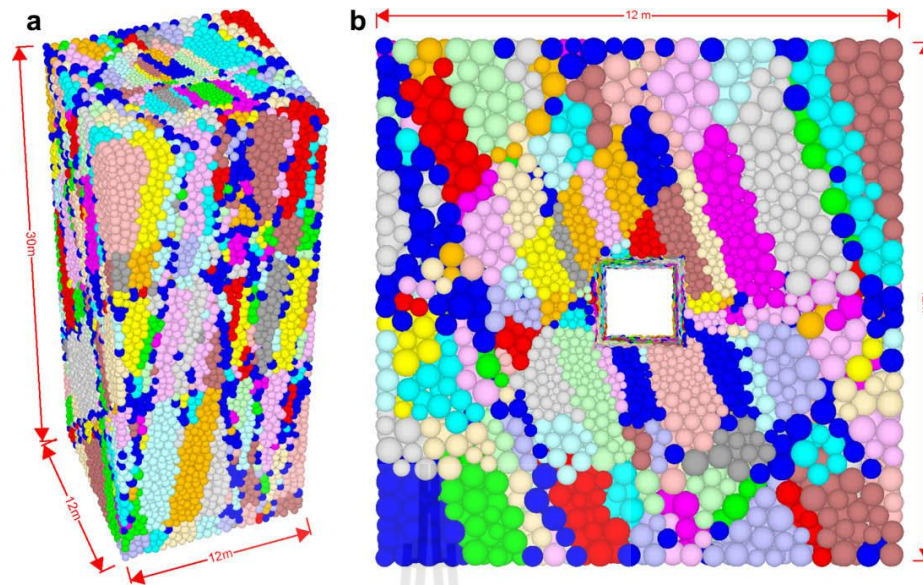


Figure 2.7 The generated 3D rock mass illustrating fracture defined particle clusters:
 (a) 3D,(b) 2D view (Hadjigeorgiou et al.,2009)

Mcneary and Barker (1998) compared physical and numerical models of the block-caving mining methods. PFC^{2D} program was used in an attempt to better understand the deformations and flow within each of the physical models during the draw procedure. Bridging and interlocking of the blocks occurred in approximately the same places and similar times during the draw sequence. The results show that the draw down patterns and the rate of draw generated within the numerical models were very similar in development of the physical models. For the given cases of the physical model, the numerical model simulated the behavior of the physical model quite well. The only constraints that were placed on the numerical models were the initial boundary conditions of the physical models. By inspection, the overall shape and flow lines of both the numerical and physical models were extremely close in area

removed and flow characteristics. The numerical results as reported in this study are the result of the internal algorithms of the PFC^{2D} software.

2.5 Previous relevant researches

Thongprapha et al. (2015) study the surface subsidence above an underground opening using a trap door apparatus to determine the effects of underground opening configurations on surface subsidence under super-critical conditions. They found that the angle of draw and maximum subsidence increase with increasing opening length and tends to approach a limit when opening length-to-width ratio equals 3. For the same opening geometry, increasing the opening depth reduces the angle of draw and maximum subsidence. The volume of the subsidence trough increases with increasing opening height and width.

Aracheeploha et al. (2009) developed an analytical method to predict the location, depth and size of caverns created at the interface between salt and overlying formations. A governing hyperbolic equation is used in a statistical analysis of the ground survey data to determine the cavern location, maximum subsidence, maximum surface slope and surface curvature under the sub-critical and critical conditions. A computer program is developed to perform the regression and produce a set of subsidence components and a representative profile of the surface subsidence under sub-critical and critical conditions.

Finite difference analyses using FLAC code correlate the subsidence components with the cavern size and depth under a variety of strengths and deformation moduli of the overburden. Set of empirical equations correlates these subsidence components with the cavern configurations and overburden properties.

For the super-critical condition a discrete element method (using UDEC code) is used to demonstrate the uncertainties of the ground movement and sinkhole development resulting from the complexity of the post-failure deformation and joint movements in the overburden. The correlations of the subsidence components with the overburden mechanical properties and cavern geometry are applicable to the range of site conditions specifically imposed here (e.g., half oval-shaped cavern created at the overburden-salt interface, horizontal rock units, flat ground surface, and saturated condition). These relations may not be applicable to subsidence induced under different rock characteristics or different configurations of the caverns. The proposed method is not applicable under super-critical conditions where post-failure behavior of the overburden rock mass is not only unpredictable but also complicated by the system of joints, as demonstrated by the results of the discrete element analyses. The proposed method is useful as a predictive tool to identify the configurations of a solution cavern and the corresponding subsidence components induced by the brine pumping practices as shown in Figure 2.8.

Even though extensive study has been carried out in an attempt to understand and predict the surface subsidence behavior induced by underground excavations, the effects of opening geometry under super-critical condition have rarely been addressed. The difficulty in predicting the subsidence under super-critical condition is due to the complexity of the post-failure behavior of the overburden.

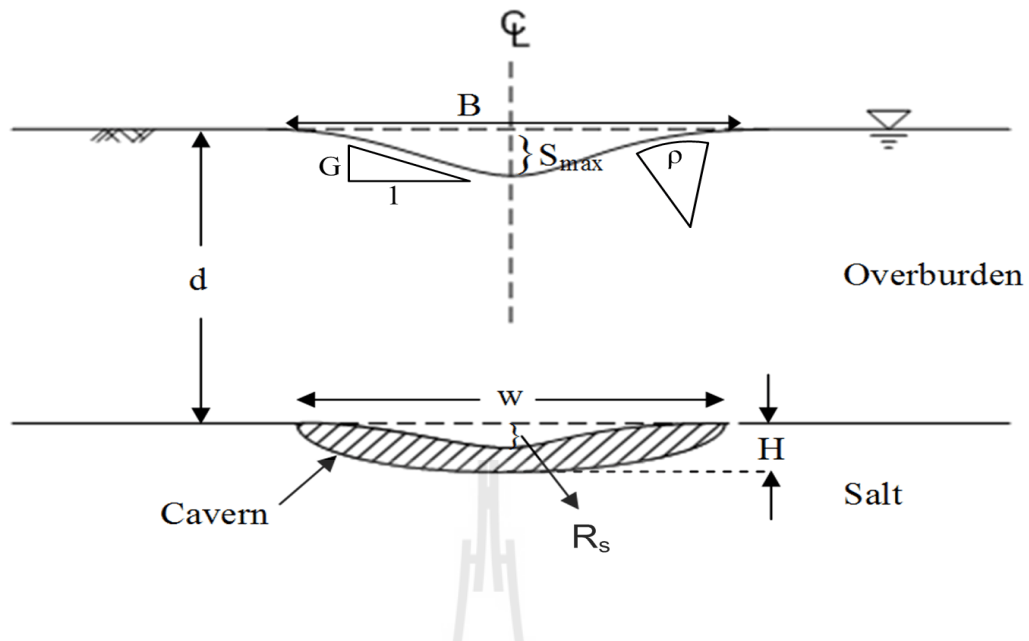


Figure 2.8 Variables used by Aracheeploha et al. (2009)

Park and Li (2004) states that surface subsidence causes damage such as the failure and deterioration of buildings, infrastructures, dams, underground utility lines, ground water regimes, etc., resulting in severe economic loss and environmental hazards. The major cause of subsidence is underground mining activities. In order to minimize or prevent subsidence damage, it is necessary to understand subsidence phenomena. It is difficult to simulate or predict subsidence development because of the complexity in physical characteristics such as rock failure and yield behavior, dimensional variations and time dependent behavior. In this paper a new physical subsidence modeling technique is introduced. The method utilizes laser optical triangulation distance measurement devices, which can scan the surface of any material, including granular or viscous materials, and digitally measure vertical distances with an extremely high accuracy and resolution. With this new technique, the effect of cavity shape and size, depth, and material parameters can be analyzed.

Using this unique technology and method of analysis, significant results were produced. Subsidence profiles, subsidence factors, and angles of draw were analyzed. This research is being continued using the same technique for simulating subsidence with different model materials for various underground cavity dimensions, tunneling, and time dependent subsidence phenomena.

Yao et al. (1991) introduced an analytical calculation model for the angle of draw by the use of a finite element model proposed by Reddish (1989) at the Nottingham University. They studied the influence of overburden strength and different rock mass properties, and the presence of a distinct bed, on subsidence limit characteristics. Their results show that the angle of draw is related to the overburden properties, depth and configurations of the mine openings.

Five cases have been studied in order to investigate the effect of different rock mass properties on the angle of draw. The relationship between the percentage of maximum subsidence and the relevant angle of draw for each case has been examined. The results show that increasing the strength of the cover rock mass reduces the angle of draw (Figure 2.9).

For the effect of strong and weak beds in the overburden on the angle of draw, it can be seen that the weak bed in the overburden increases the angle of draw. Additionally, it is also important to note that a decrease in the uniaxial compressive strength in the weak bed causes a significant increase in the angle of draw. However, it seems that with an increase in the uniaxial compressive strength of the strong bed, the angle of draw decreases only slightly.

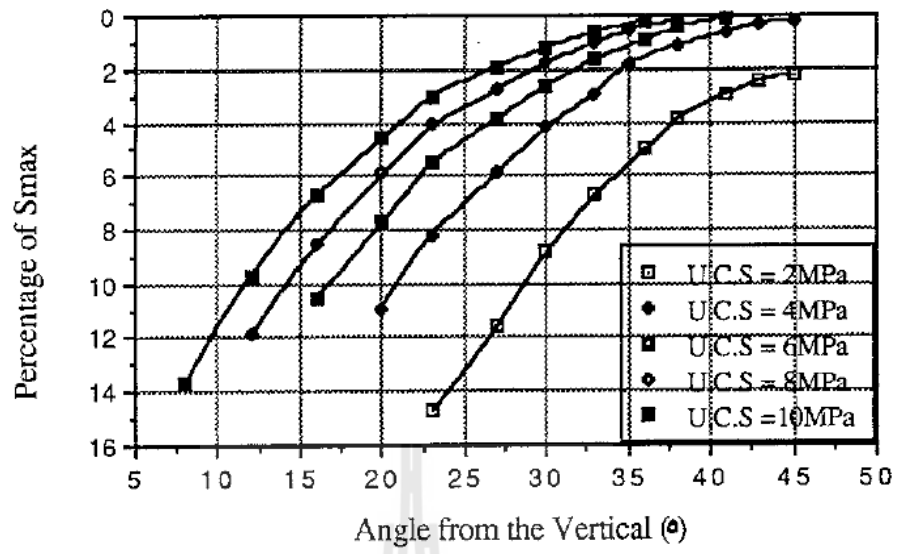


Figure 2.9 Effect of different overburden properties on the angle of draw (Yao et al., 1991)



CHAPTER III

PHYSICAL MODEL SIMULATIONS

3.1 Introduction

The objective of the physical model testing in this study is to assess effect of underground excavation methods (mining sequences and excavation rates) and of overburden slope on the angle of draw, maximum subsidence and subsidence trough shape under super-critical condition. This chapter describes method, equipment and results of the tests.

3.2 Material property

Clean and uniform sand (Figure 3.1) is used as the test material to simulate overburden in the physical model simulations. This is because the effect of the angularity is less for the smaller particles size (Thongprapha, 2015). The mechanical properties (grain size analysis and direct shear test) for the tested granular material are obtained from the testing results obtained by Thongprapha (2015). Table 3.1 shows the mechanical property of granular material with nominal size of 2 mm used in this study.

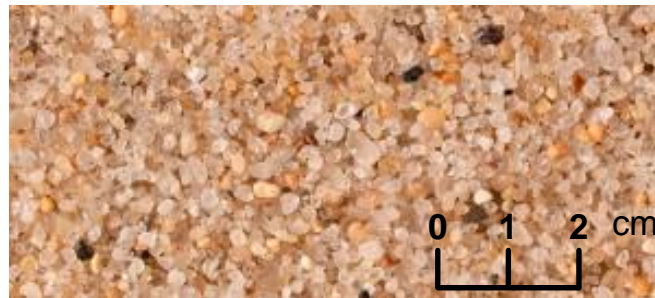


Figure 3.1 Clean and uniform sand with nominal size of 2 mm used to simulate overburden.

Table 3.1 Mechanical properties of granular material (Clean and uniform sand with nominal size of 2 mm) (Thongprapha, 2015).

Test method	Soil properties	Values	
Grain size Analysis	Uniformity coefficient, C_u	1.29	
	Coefficient of curvater, C_c	1.07	
	Type of soil		Poorly-graded sand
	Grain Shape	Sphericity	High sphericity
		Roundness	Subangular
Direct shear test	Bulk density (kN/m^3)	1455	
	Cohesion, c (kPa)	15.61	
	Friction angle, ϕ (degree)	24.7	
	Normal stiffness, K_n (MPa/m)	1590.72	
	Shear stiffness, K_s (MPa/m)	26.07	

3.3 Physical model testing

A trap door apparatus (Thongprapha et al., 2015) is used in the physical model simulations, as shown in Figure 3.2. The sample container is filled with the clean and uniform sand to a pre-defined overburden thickness. The sand is lightly packed and the top surface is flattened before the test. The various underground opening configurations are simulated by systematically pulling down the blocks underneath the sample container. The laser scanner measures the surface profile of the sand before and after the subsidence is induced. Figure 3.3 shows the test parameters and variables defined in the simulations. A trap door apparatus can be simulated the opening width (W) from 50 mm to 250 mm with an increment from 50 mm. The opening height (H) is selected from 5 mm to 50 mm with 5 mm increment. The opening length (L) can be simulated from 50 mm to 500 mm with 50 mm increment. In this study, overburden thickness (Z) is varied from 50 mm to 200 mm with 25 mm increment for all cases. The effect of overburden slope is studied by variations the angle of overburden surface which the angles vary from 5, 10, 15 to 20 degrees.

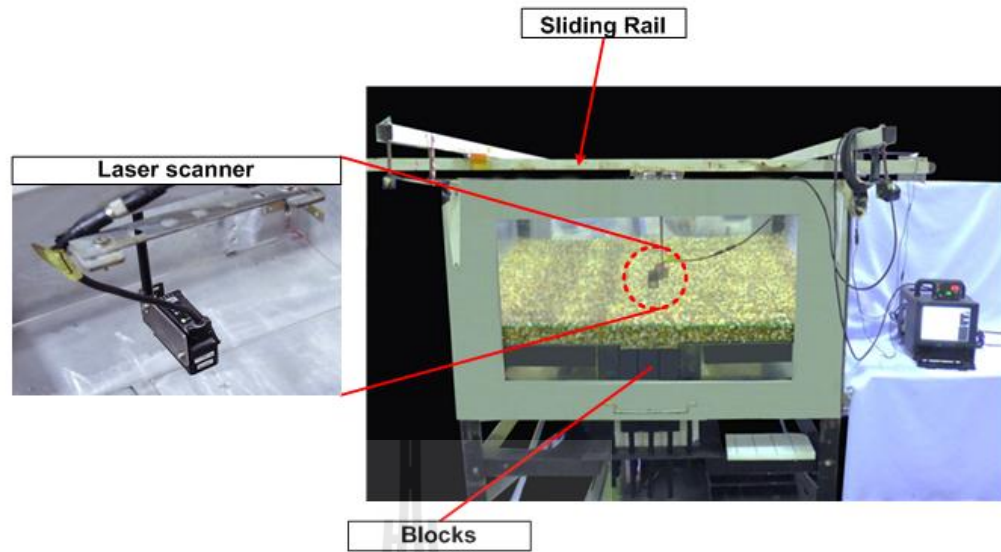


Figure 3.2 Trap door apparatus used in this study (Thonggrapha et al., 2015).



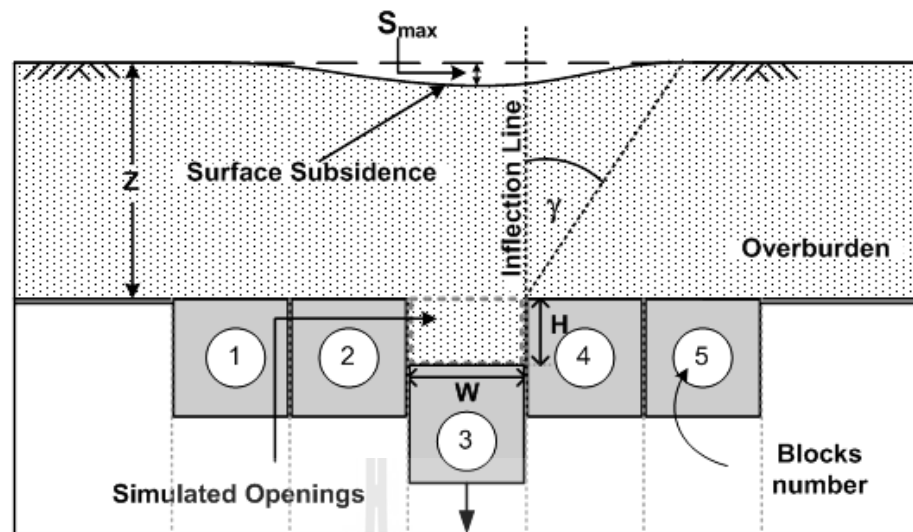


Figure 3.3 Variables used in physical model simulations and analysis: W = opening width, H = opening height, Z = opening depth, γ = angle of draw and S_{\max} = maximum subsidence.

3.3.1 Mining sequences

Four cases of mining sequence are simulated to study the effect of excavation orders of the mine panel, as shown in Figure 3.4. The number on the blocks indicates the order of panel excavation row. Each panel excavation is made by simultaneously moving down of 6 blocks ($L/W=6$, when $L=300$ mm and $W=50$ mm) in the defined location. This is because the effects of the opening ends decrease and eventually disappear when the opening length-to-width ratio beyond 3 (Thongprapha et al., 2015). Figure 3.4(a) shows excavation from one side to the other. Figures 3.4(b) and Figures 3.4(c) show the excavation starting from the center of the panel and from two sides of the center, respectively. Figure 3.4(d) shows excavation from the edge to the center of the panel. In this study the opening width is increasing from 50 mm to 250 mm, the opening length is maintained constant at 300 mm and 50 mm.

The opening depth-to-height (Z/H) ratios are varied from 1, 2, 3 to 4 for all cases. The examples of cross-sections of surface subsidence profile for different mining sequence are shown in Figure 3.5.

The measurement results are presented in terms of the angle of draw (γ) and the maximum subsidence (S_{\max}). The angle of draw is a parameter used for defining the position of the limit of subsidence at the surface. The angle of draw is the angle between a vertical line from the edge of the underground opening and a line from the edge of the opening to the point of zero surface subsidence. The point of maximum surface subsidence is located in the point of the maximum subsidence trough.

The results show that different mine panel excavation sequences can affect the subsidence trough profile. Case (A) shows the trough profile smoother than the trough obtained from other cases (Figure 3.5(a)). The maximum subsidence-to-opening height (S_{\max}/H) ratio tends to decrease with increasing Z/H ratio (Fig. 3.6). Figure 3.7 shows the angle of draw as a function of opening depth-to-opening height ratio for various mining sequences. The angle of draw decreases with increasing Z/H ratio for all cases, particularly for $Z/H = 1$. The effect of mining sequence characteristics becomes larger. Case (B) shows the lowest angle of draw at all depths, while case (D) shows the lowest subsidence for all depths. This is due to that the sequences of excavation affect the particles flow into the opening. For case B, the excavation started from the center of the panel may have an impact on the particles to accumulate combined at the center of panel. It has an impacted on lowest angle of draw and highest surface subsidence while excavation from the edge to the center of the panel (case D) gives the lowest surface subsidence because the particles flow into

the opening at edge of panel before flowing into center of panel causing the highest angle of draw and lowest subsidence.

Case	Mine opening				
(A)	1	2	3	4	5
(B)	2	4	1	5	3
(C)	3	1	5	2	4
(D)	1	2	5	4	3

Figure 3.4 Mining sequences simulated in the physical models. The numbers indicate for each case of mining excavation sequence model.

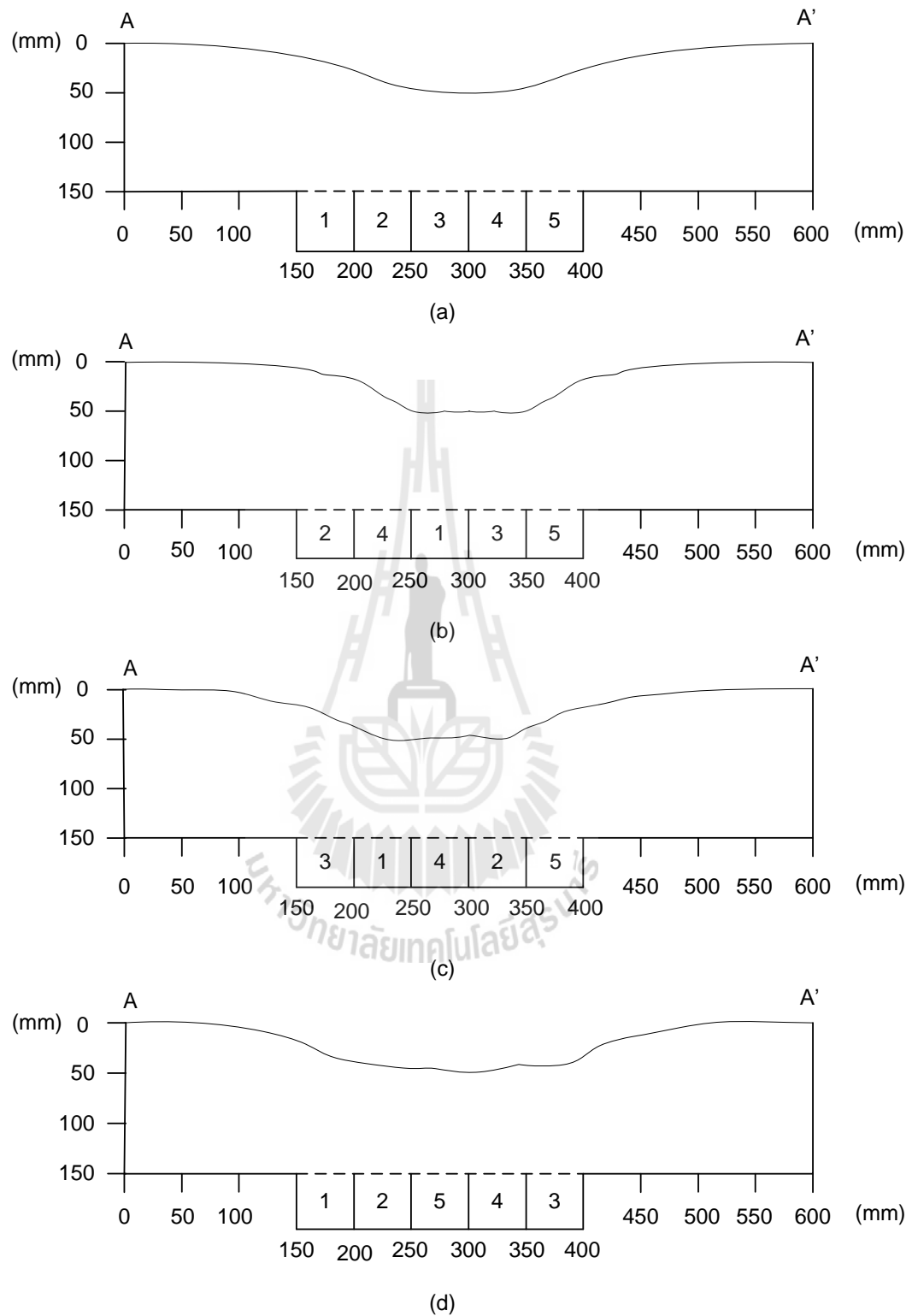


Figure 3.5 Examples of cross-section (A-A') of surface subsidence profiles for different mining sequences.

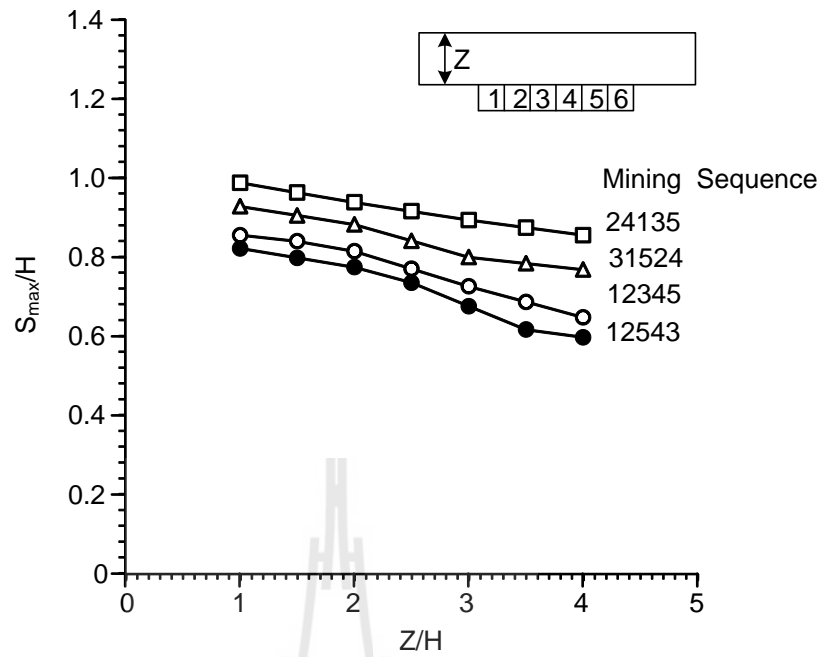


Figure 3.6 Maximum subsidence-to-height (S_{max}/H) ratio as a function of opening depth-to-height (Z/H) ratio.

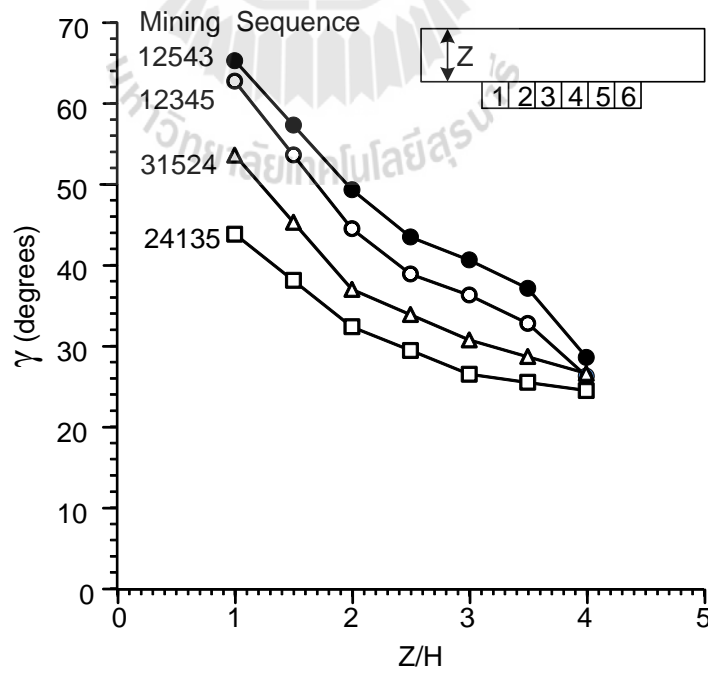


Figure 3.7 Angle of draw (γ) as a function of opening depth-to- height (Z/H) ratio.

3.3.2 Excavations rates

The effect of excavation rate is investigated by systematically moving down of the blocks to simulate the mining excavation with different rates. This study considers two rates: high excavation rate with 50 mm increment of opening height, and low excavation rate with 5 mm increment of opening height. These excavation rates are used to simulate under various excavation areas (Figure 3.8). The excavation areas have width \times length from 50 \times 50, 100 \times 100, 150 \times 150 to 200 \times 200 mm². The opening depth-to-height ratios are varied from 1, 1.5, 2, 2.5, 3, 3.5 to 4. The opening height is 50 mm for all cases. Figure 3.9 shows the subsidence profile for different excavation areas under various excavation rates.

Under low excavation rate, the subsidence trough profile shows small steps of slope. The subsidence trough profile tends to be smoother when excavation rate is greater. Figures 3.10 and 3.11 show the S_{\max}/H and angle of draw as a function of Z/H ratio for various excavation areas. The angle of draw and S_{\max}/H decrease with increasing Z/H ratio. This is due to that the particles have created new voids in the overburden above the opening.

Under the same excavation area, higher excavation rates give the lower angle of draw and maximum subsidence. This is probably because the testing under high excavation rates tends to create the inter-locking of particles above the opening. The overburden slightly subsides if the opening is narrow (Figure 3.8 (a)) and the subsidence profile is more extent, and steps of surface subsidence occurs (Figure 3.9 (d)) when the opening area increases (Figure 3.8 (d)).

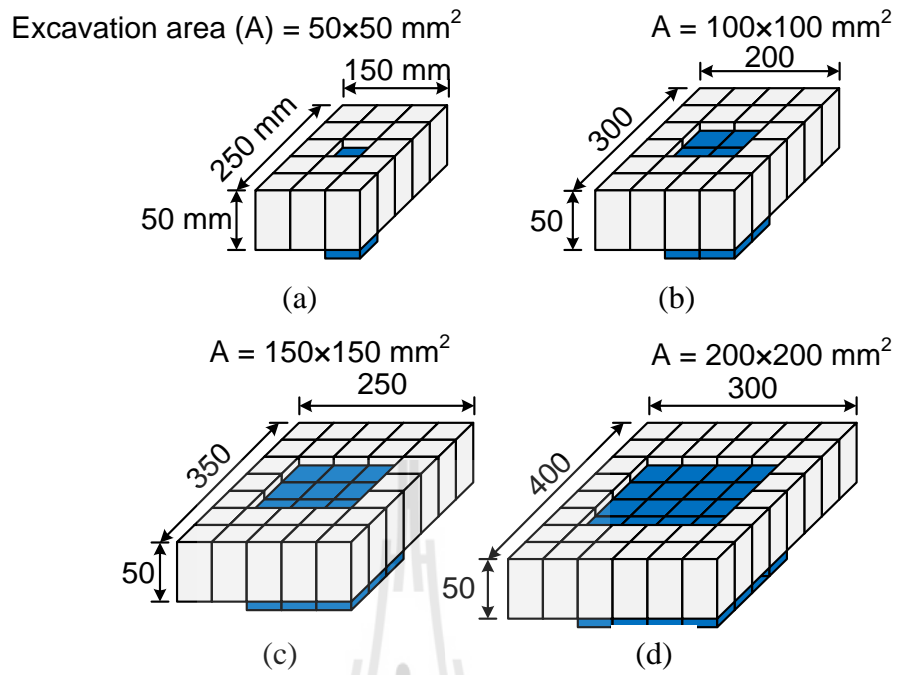


Figure 3.8 Effects of excavation rate assessed by using different areas of excavation.



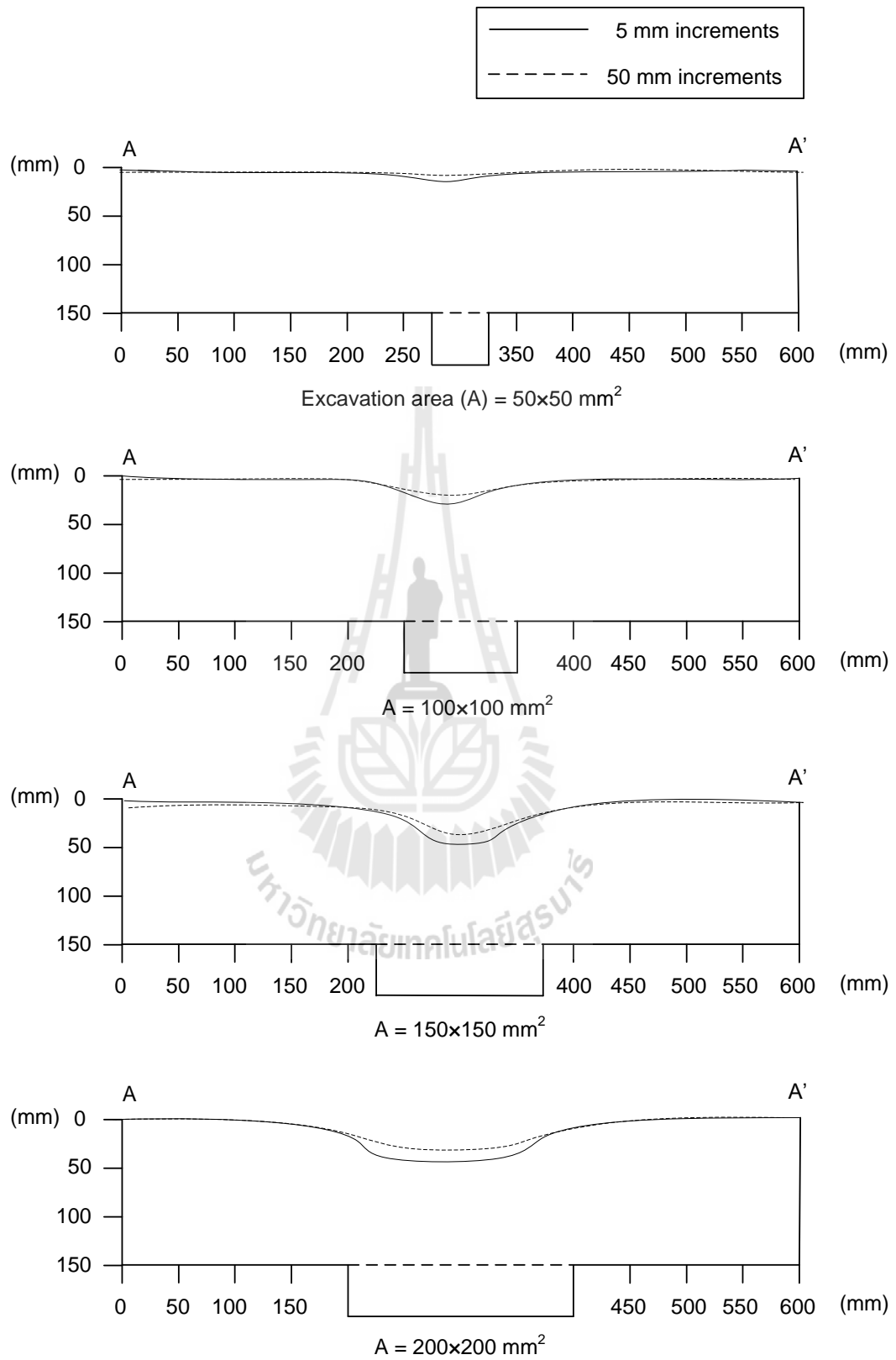


Figure 3.9 Subsidence profiles under various excavation rates.

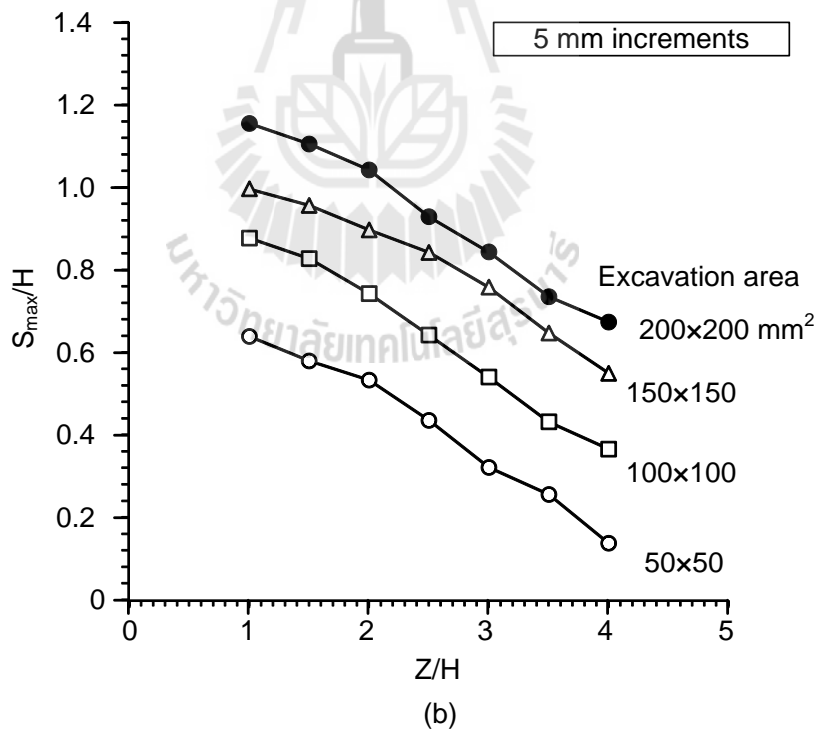
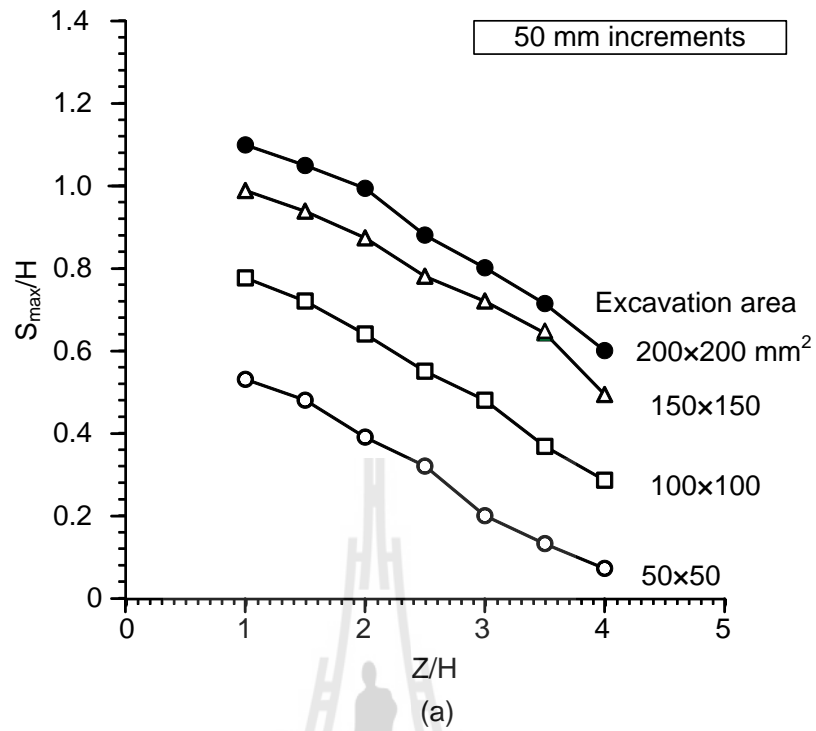


Figure 3.10 S_{\max}/H ratio as a function of Z/H ratio under high excavation rate (a) and under low excavation rate (b).

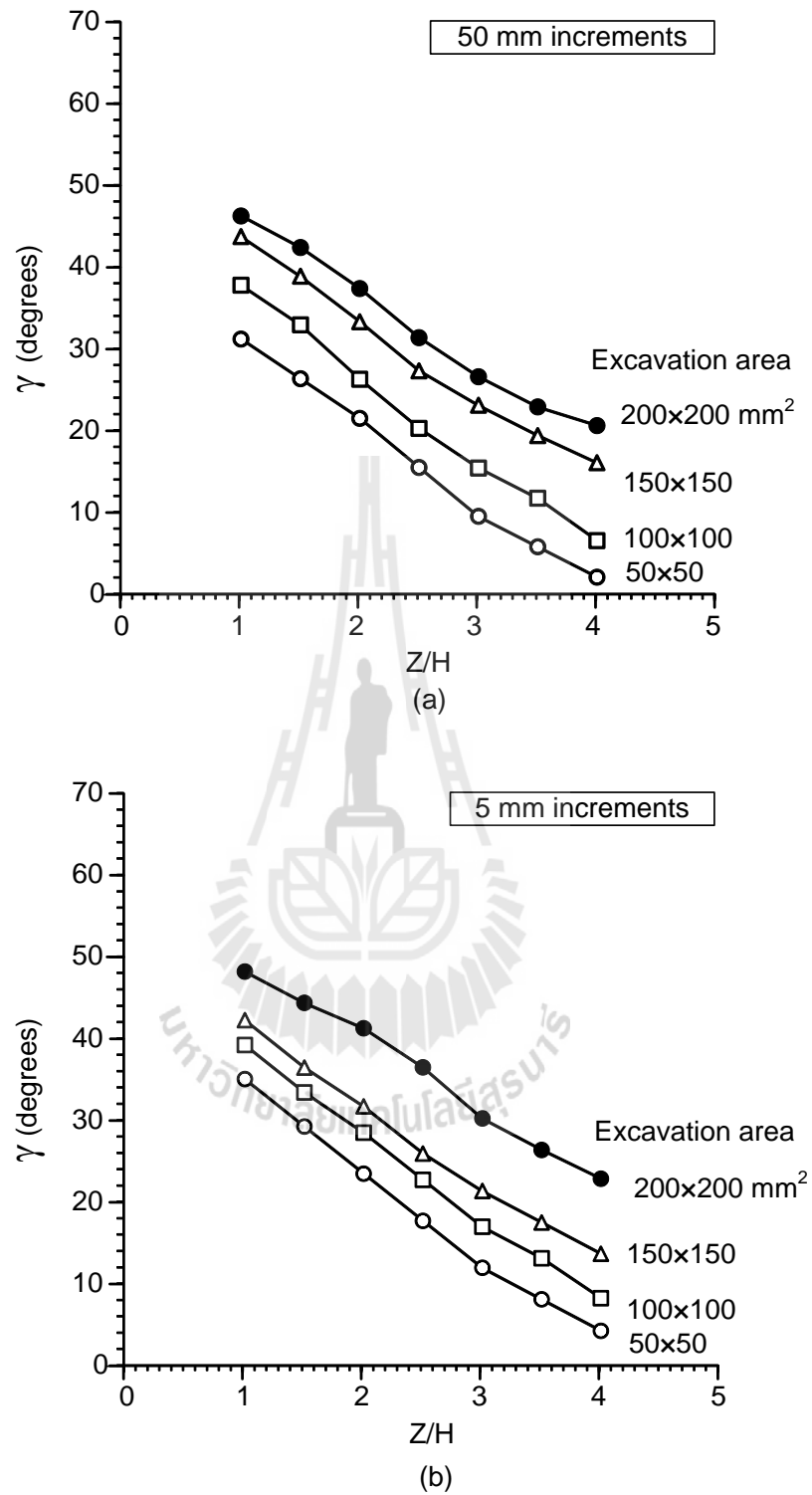


Figure 3.11 γ as a function of Z/H ratio under high excavation rate (a) and low excavation rate (b).

3.3.3 Overburden slope

The effect of overburden slope under various opening depths on the angle of draw and maximum subsidence is investigated. The opening depths are varied from 100 mm to 200 mm which is measured from the overburden surface to the center of opening roof (Figure 3.12). The angle of overburden slope (θ) are varied from 5, 10, 15 to 20 degrees. For all test series, the opening length and opening width are maintained constant at 250 mm and 50 mm, respectively. Figure 3.13 shows the subsidence profiles for different overburden slope angles. The measured angle of draw from this study is divided in to 2 angles: the angle of draw on up-slope (γ_{up}) and on down-slope (γ_{down}). The angle on the up-slope is always greater than on the down-slope. This is because under the super-critical condition, the mass of material on up-slope side is greater than that on the down-slope side.

Figure 3.14 shows the S_{max}/H ratio decreasing with increasing Z/H ratio under various overburden slope angles. The results show that the S_{max}/H ratio decreases with increasing slope angles from 0, 5, 10, 15 to 20 degrees. The angle of draw on up-slope increases with increasing slope angle and decreases with increasing slope angle (Figure 3.15). This is due to that the overburden thickness on up-slope is greater than that at the down-slope inducing particle flow into opening. The particles on the up-slope side can flow into opening easier and hence inducing larger angle of draw. The measurements of angle of draw and maximum subsidence when Z/H ratio equal 1 cannot made here. This is because the opening depth is insufficient ($Z < H$).

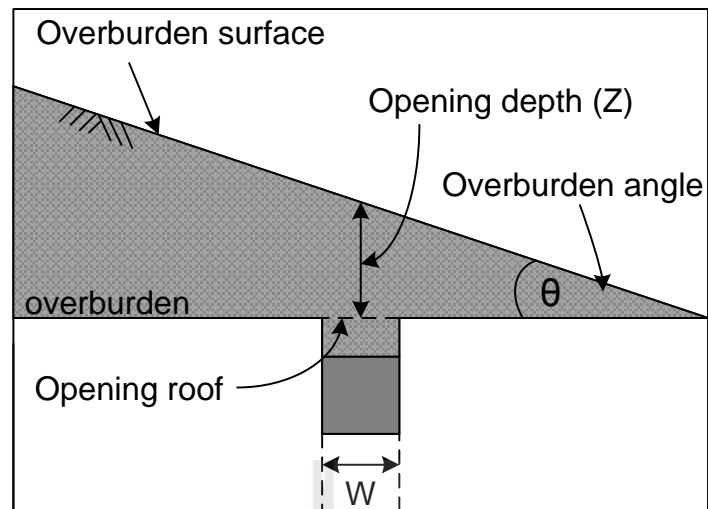
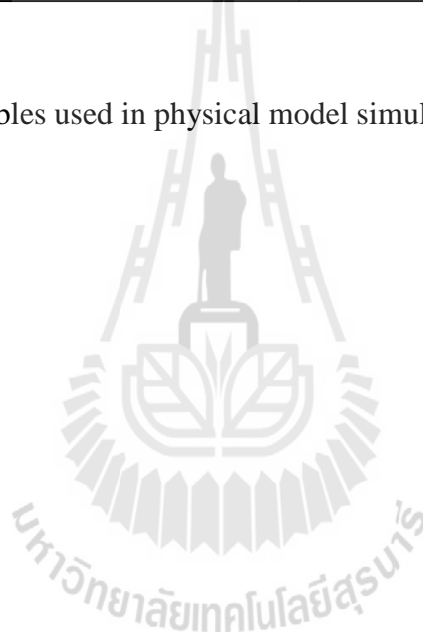


Figure 3.12 Variables used in physical model simulations of overburden slope.



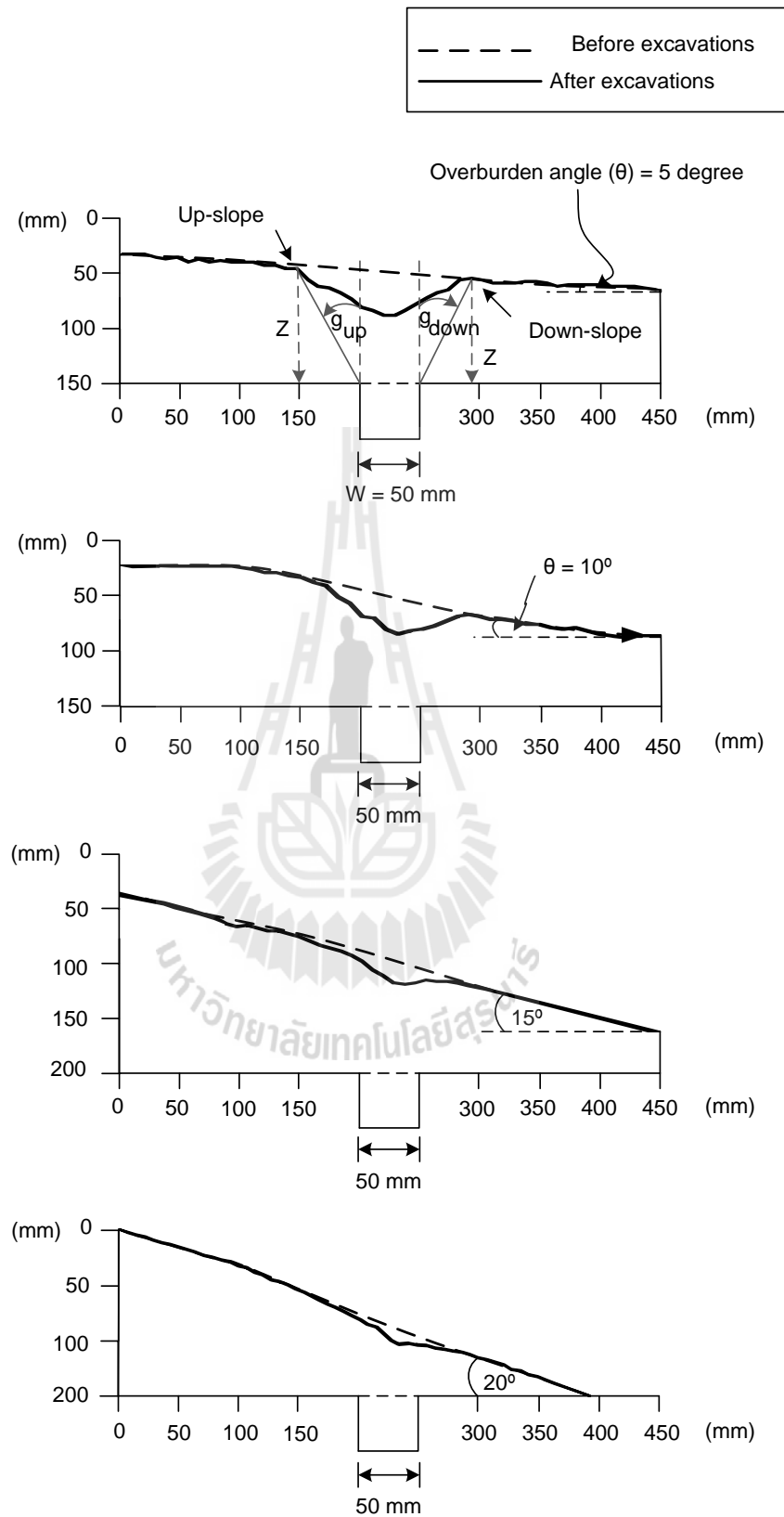


Figure 3.13 Subsidence profiles of surface subsidence under various surface slopes.

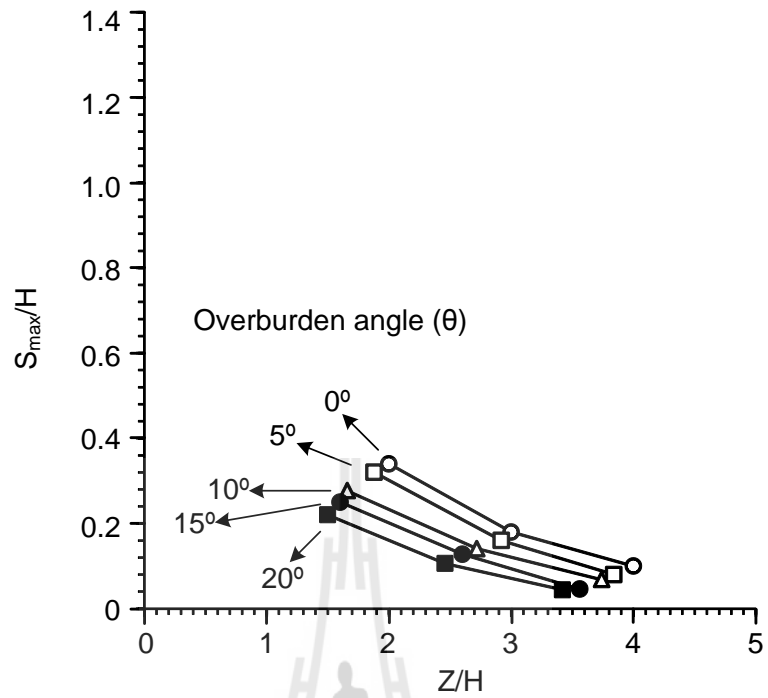


Figure 3.14 S_{max}/H ratio as a function of Z/H ratio for each ground surface slope.

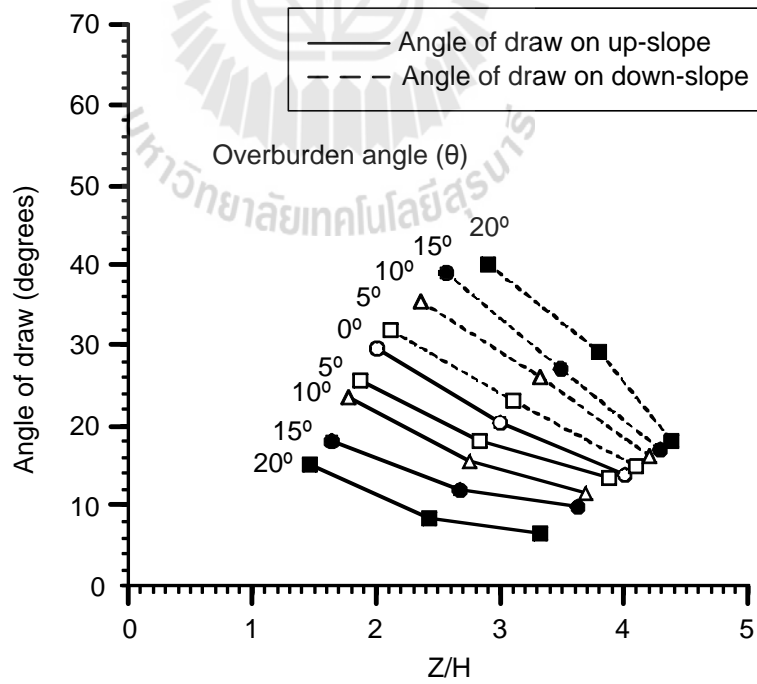


Figure 3.15 γ as a function of Z/H ratio under various slope face angles.

CHAPTER IV

COMPUTER SIMULATIONS

4.1 Introduction

This chapter describes the discrete element analyses performed by using Particle Flow Code in two dimensions (PFC^{2D}-Itasca, 2008) to simulate the subsidence under various excavation methods and surface slope angles under super-critical condition. The results obtained from the PFC^{2D} are compared with the physical model simulations.

4.2 Computer model simulations

The PFC^{2D} is used to understand granular material behavior and to solve real problems that involve complicated deformation of overburden under different excavation methods and overburden angle. The parameters used in the PFC^{2D} model are identical to those of the physical model tests. The particle radius is 1 mm, bulk density = 1,455 kN/m³, friction coefficient (ϕ) = 0.46, normal stiffness (K_n) = 44.54 MN/m, and shear stiffness (K_s) = 0.73 MN/m. The discrete element analyses are performed to compare the results with those of the physical models.

4.2.1 Mining Sequences

The command codes define the generation of the overburden model and the boundaries, as well as perform the extraction operations similar to those in the physical models. After the particles are at rest and the model equilibrium as predefine overburden thickness, the wall above the opening is deleted in respectively defined location (Figure 4.1) for simulating the mining sequences. The particles are continuously flowed in to the opening until the opening completely filled, and hence the surface subsidence is induced (Figure 4.2). Table 4.1 shows the test conditions for mining sequences case and its results. The results show that S_{\max}/H ratio tends to decrease with increasing Z/H ratio. The angle of draw slightly decreases when the Z/H ratio increases. The mining sequences affect to the most subsidence trough for shallow opening ($Z/H = 1$) and almost no effect to subsidence when $Z/H = 4$ (Figure 4.3). More subsidence is induce when the excavation start from the edge to the center of panel (case D)

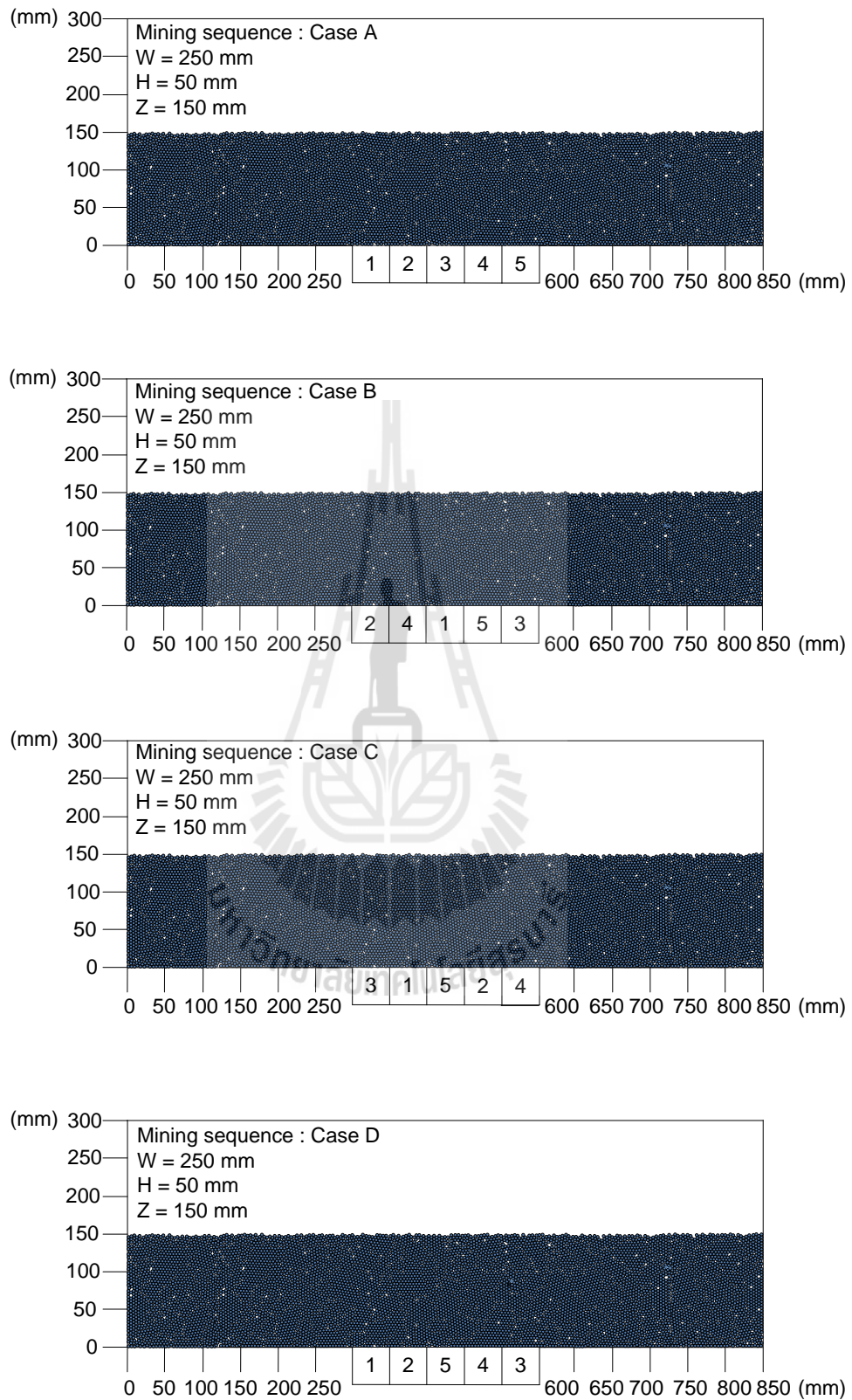


Figure 4.1 Surface subsidence before the opening simulation of mining sequences.

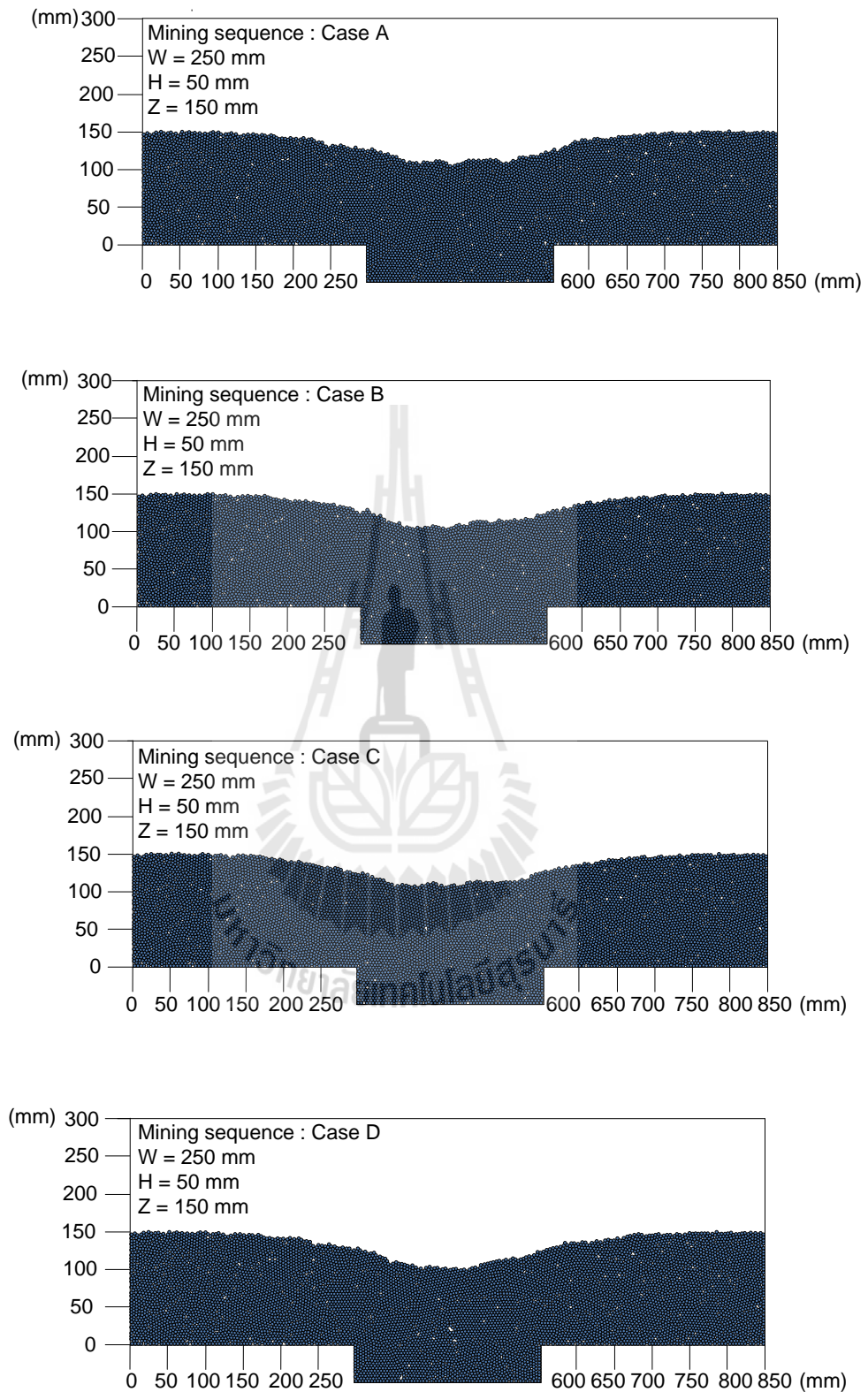


Figure 4.2 PFC^{2D} model simulations of surface subsidence after the opening are excavated.

Table 4.1 PFC^{2D} simulations results of mining sequences when constant H = 50 mm.

Parameter variable			Results	
Case	Z/H	W/H	γ (degrees)	S_{max}/H
Case A (12345)	1	5	60.4	1.07
	2		48.2	1.05
	3		38.4	1.02
	4		28.6	0.99
Case B (24135)	1		57.6	1.15
	2		45.3	1.11
	3		35.0	1.06
	4		28.5	1.03
Case C (31524)	1		52.8	1.23
	2		38.9	1.18
	3		33.4	1.13
	4		27.5	1.09
Case D (12543)	1		65.0	1.00
	2		52.0	1.00
	3		40.1	0.98
	4		28.0	0.95

- * Z = Opening depth Overburden thickness (mm)
W = Opening width (mm)
H = Opening height (mm)
 γ = Angle of draw (degree)
 S_{max} = Maximum subsidence (mm)

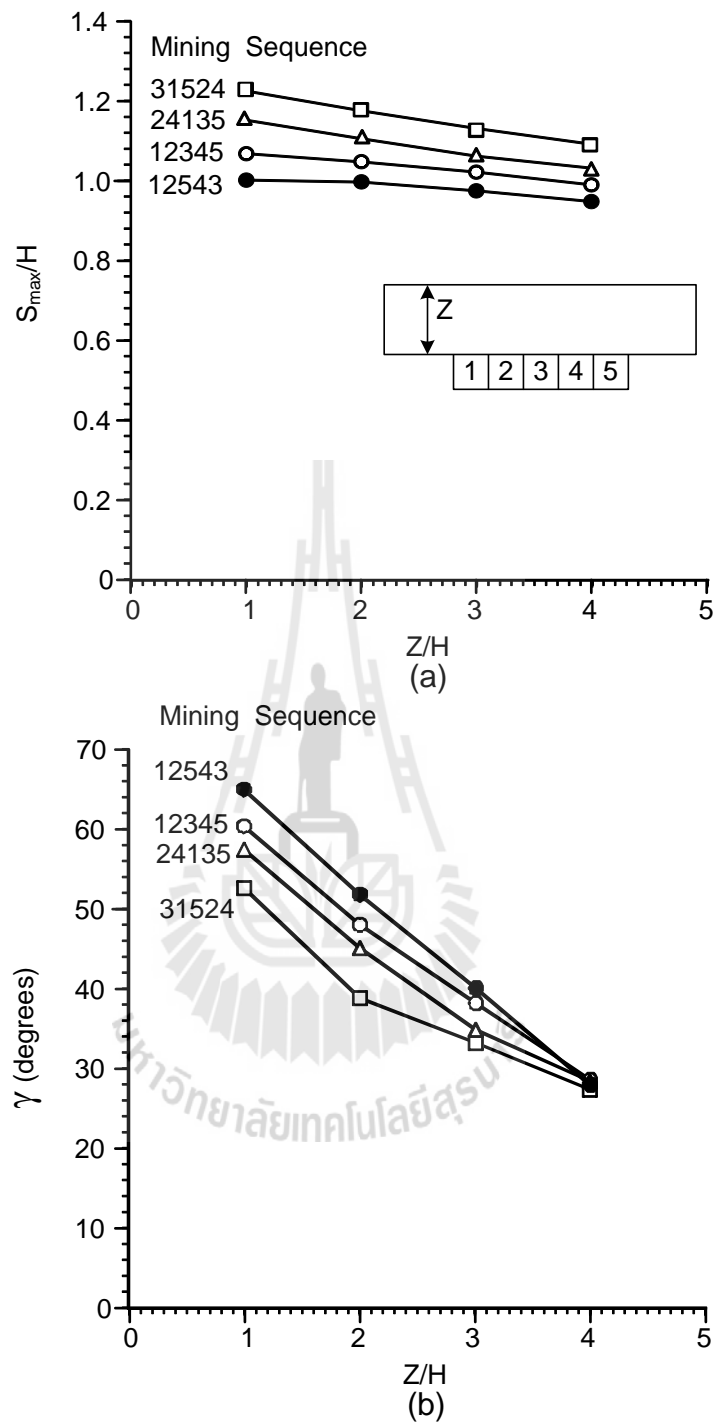


Figure 4.3 S_{\max}/H ratio as a function of Z/H ratio (a), and γ as a function of Z/H ratio (b).

4.2.2 Excavation Rates

To study the effect of excavation rate by using PFC^{2D} model, the simulations are divided into 2 cases; high excavation rate and low excavation rate. Figure 4.4 shows the example of PFC^{2D} model before simulation the opening. The opening height (H) is maintained constant at 50 mm, and width (W) and depth (Z) vary from 50, 100, 150 to 200 mm. For high excavation rate, after the particles are placed as predefined overburden thickness, the simulated roof of the opening is deleted. The particles are immediately flowed into opening floor at H = 50 mm. For low excavation rate, the opening roofs are generated every 5 mm of the 50 mm opening height (Figure 4.4 (b)). After the particles were at rest, the opening roofs are removed individually and hence the opening height increased every 5 mm. Figure 4.5 shows an example of PFC^{2D} model after simulation the opening. The summaries the simulation results of excavation rate in term of S_{max}/H and γ show in Table 4.2. The S_{max}/H ratio and γ decrease with increasing the Z/H ratio (Figures 4.6 and 4.7). The low excavation rate gives more S_{max} and γ values than the high excavation rate. This is due to the high excavation rate tends to induce inter-locking of granular particles in the overburden above the opening during flowing of particles.

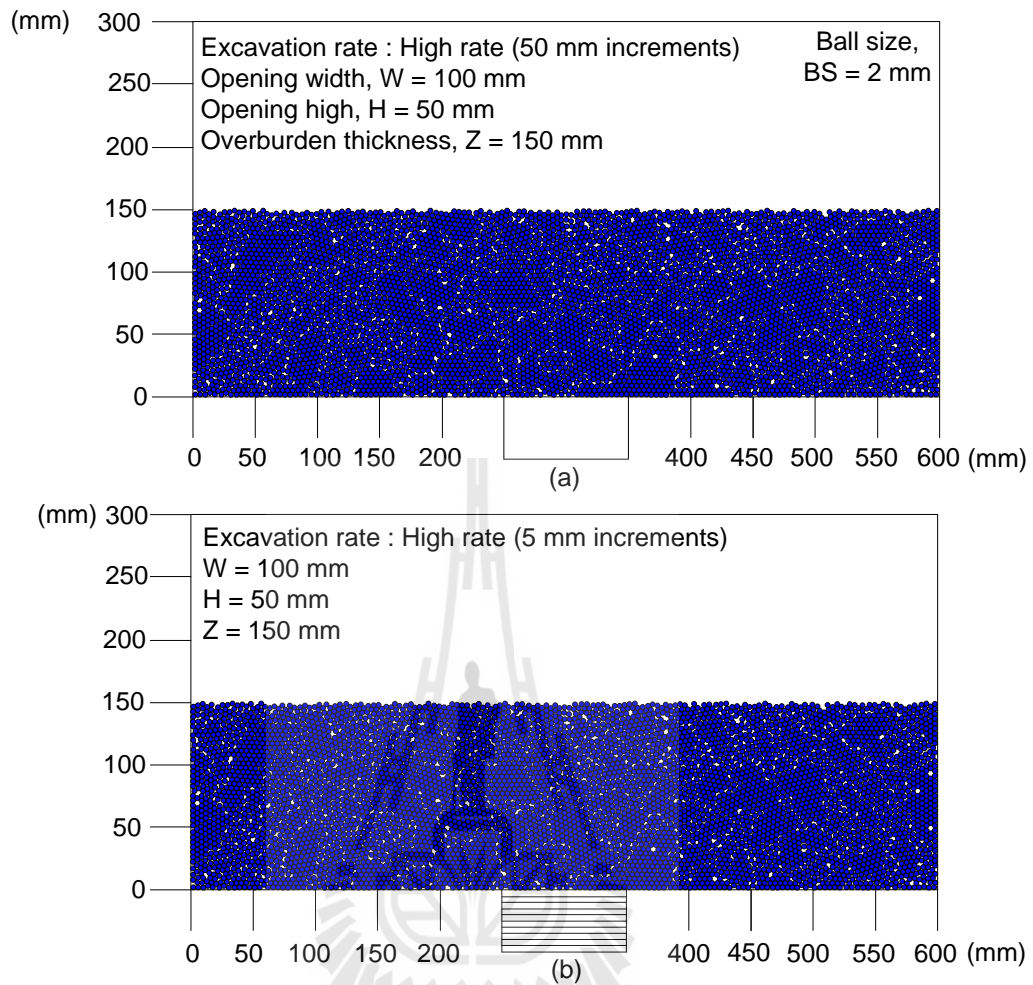


Figure 4.4 Surface subsidence before the opening simulation with predefined overburden thickness of high excavation rate (a) and low excavation rate (b).

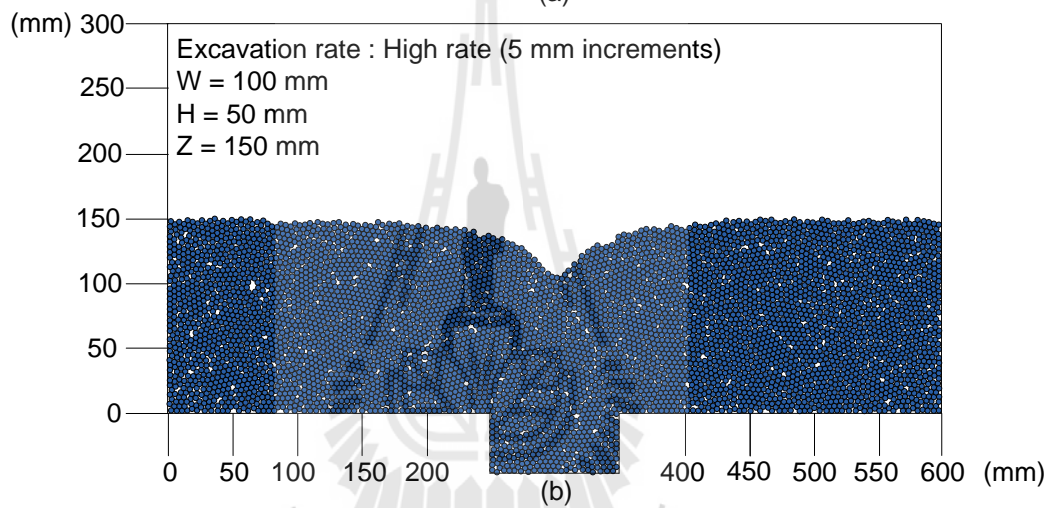
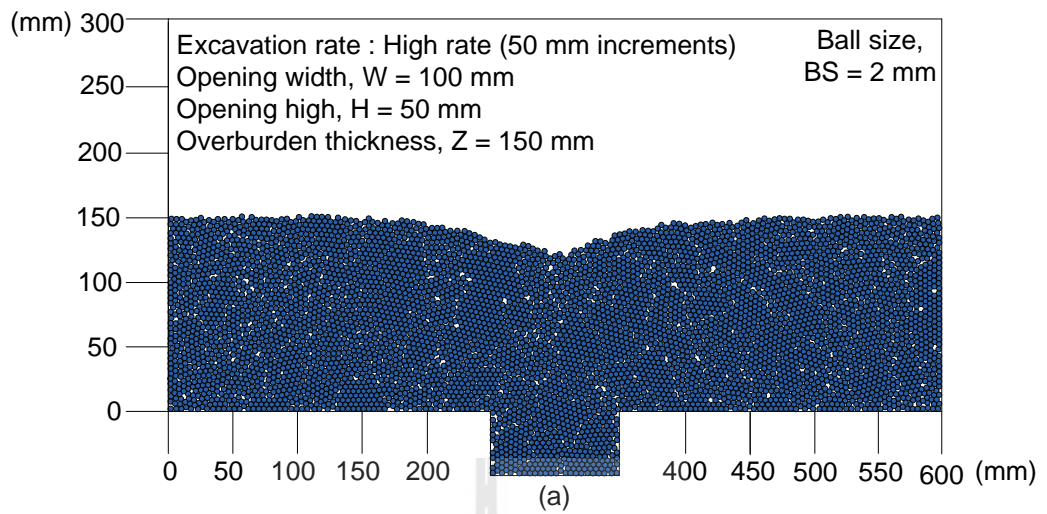


Figure 4.5 Surface subsidence of PFC^{2D} model after the opening simulation of high excavation rate (a) and low excavation rate (b).

Table 4.2 PFC^{2D} simulations results of excavation rates.

Parameter variable			Results	
Cases	Z/H	A (mm ²)	γ (degrees)	S _{max} /H
High excavation (50 mm increment)	1	50 × 50	32.9	0.57
		100 × 100	41.3	0.66
		150 × 150	46.9	0.74
		200 × 200	50.3	0.86
	2	50 × 50	23.1	0.55
		100 × 100	29.7	0.60
		150 × 150	36.4	0.69
		200 × 200	39.4	0.81
	3	50 × 50	11.0	0.46
		100 × 100	18.8	0.51
		150 × 150	25.1	0.58
		200 × 200	28.5	0.66
	4	50 × 50	3.5	0.31
		100 × 100	9.8	0.35
		150 × 150	16.0	0.39
		200 × 200	20.5	0.46
Low excavation (5 mm increment)	1	50 × 50	40.3	0.64
		100 × 100	42.4	0.88
		150 × 150	46.6	1.01
		200 × 200	50.6	1.11
	2	50 × 50	28.6	0.57
		100 × 100	31.5	0.81
		150 × 150	35.9	0.91
		200 × 200	40.5	0.99
	3	50 × 50	16.8	0.49
		100 × 100	19.7	0.64
		150 × 150	25.3	0.73
		200 × 200	32.3	0.79
	4	50 × 50	9.0	0.33
		100 × 100	12.8	0.47
		150 × 150	17.5	0.53
		200 × 200	24.8	0.62

* Z= Opening depth or Overburden thickness (mm)

A= Excavation area (mm²)

H= Opening height (mm)

γ = Angle of draw (degree)

S_{max} = Maximum subsidence (mm)

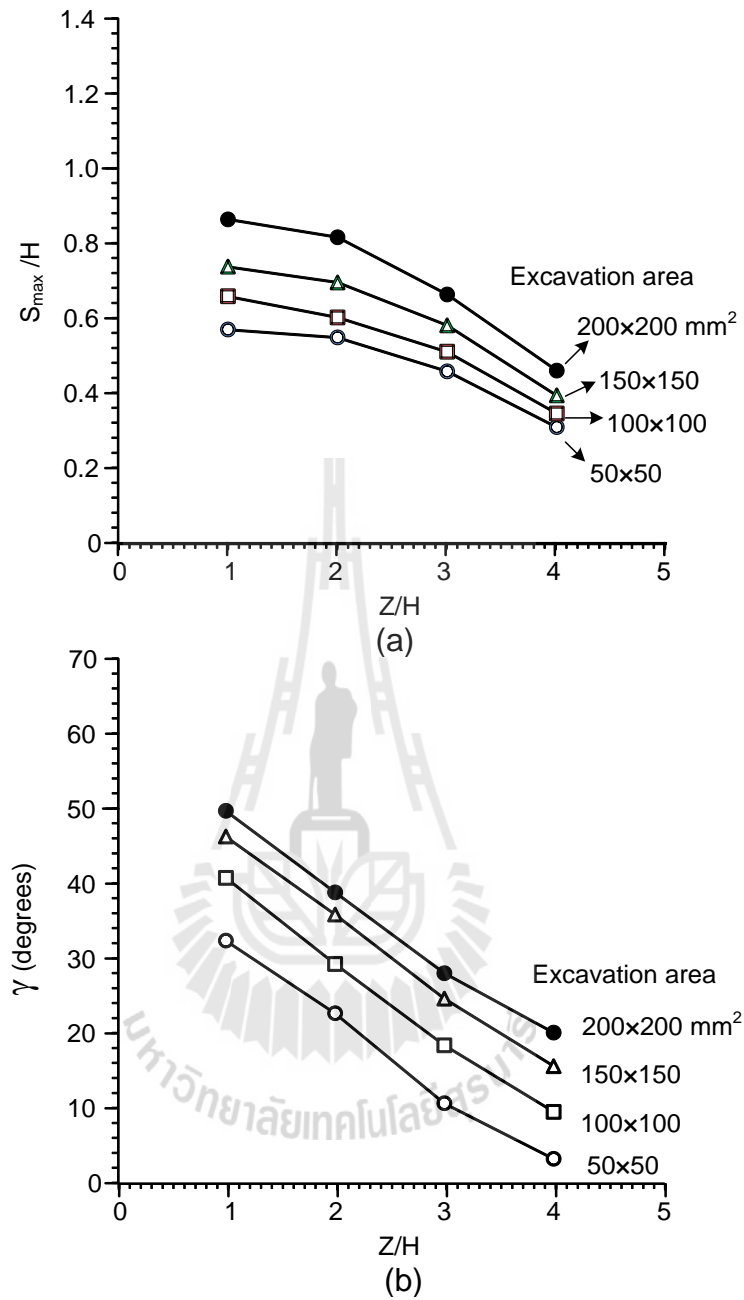


Figure 4.6 Maximum subsidence to height ratio (S_{max}/H) as a function of overburden thickness to height ratio (Z/H) (a) and angle of draw (γ) as a function of overburden thickness to height ratio (b) in case high excavation rate.

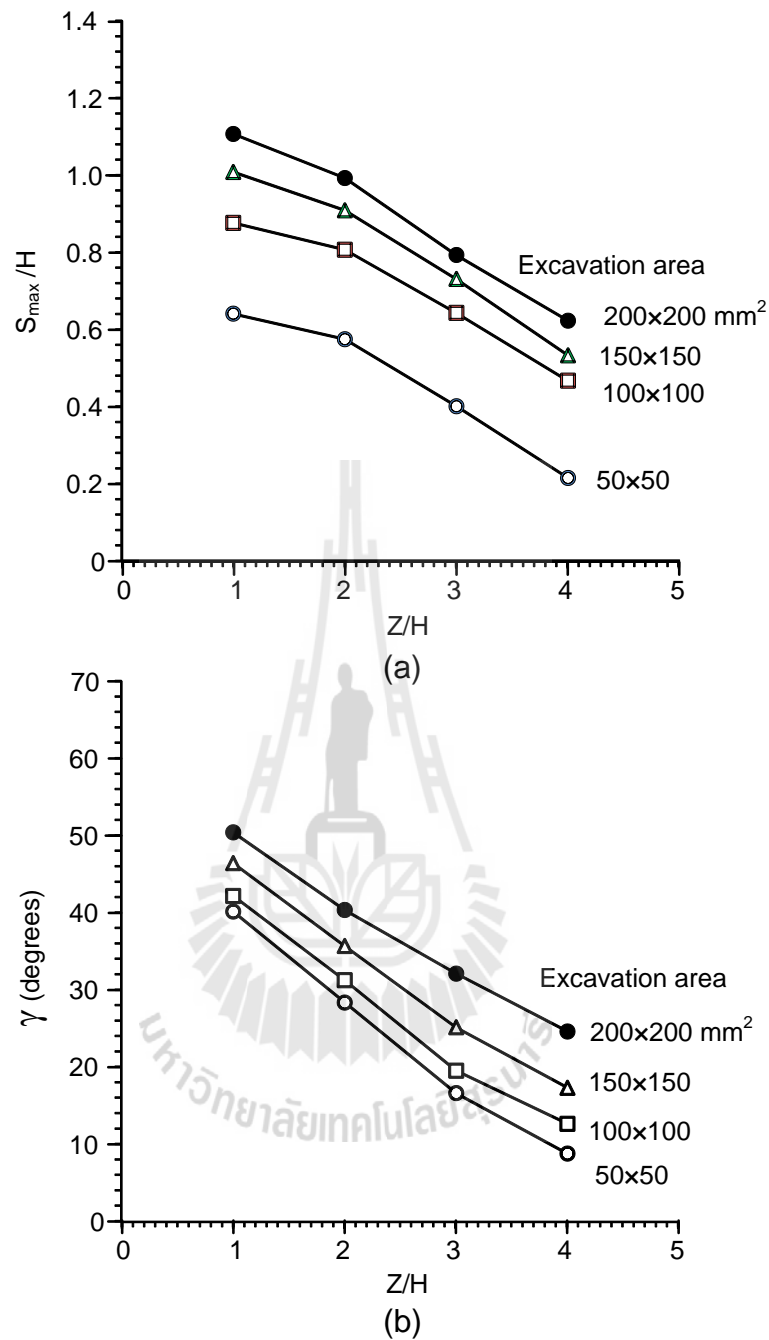
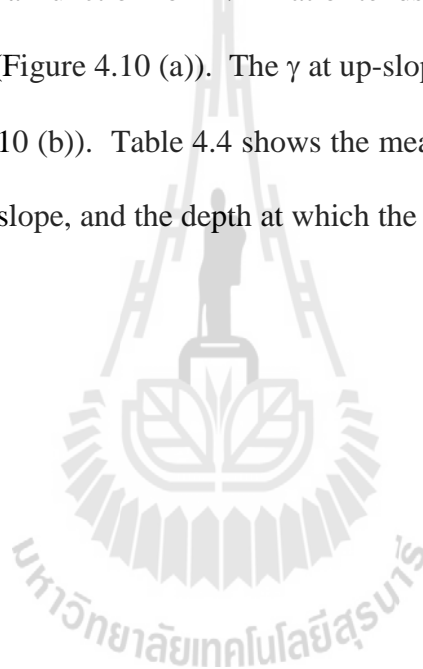


Figure 4.7 Maximum subsidence to height ratio (S_{max}) as a function of overburden thickness to height ratio (Z/H) (a) and angle of draw (γ) as a function of overburden thickness to height ratio (b) in case high excavation rate (5 mm increment).

4.2.3 Overburden slopes

The boundary conditions defined in the PFC^{2D} model, are similar to those in the physical models. The overburden angles are varied from 0, 5, 10, 15 to 20 degrees. Both opening width and height are 50 mm. The summary of test results is shown in Table 4.3. Figures 4.8 and 4.9 show the example of surface subsidence before and after the opening simulation with a predefined overburden slope angle. The S_{\max}/H ratio as a function of Z/H ratio tends to constant with increasing overburden thickness (Figure 4.10 (a)). The γ at up-slope gives the angle more than at down-slope (Figure 4.10 (b)). Table 4.4 shows the measurement of the angle of draw at up-slope and down-slope, and the depth at which the maximum subsidence occurs.



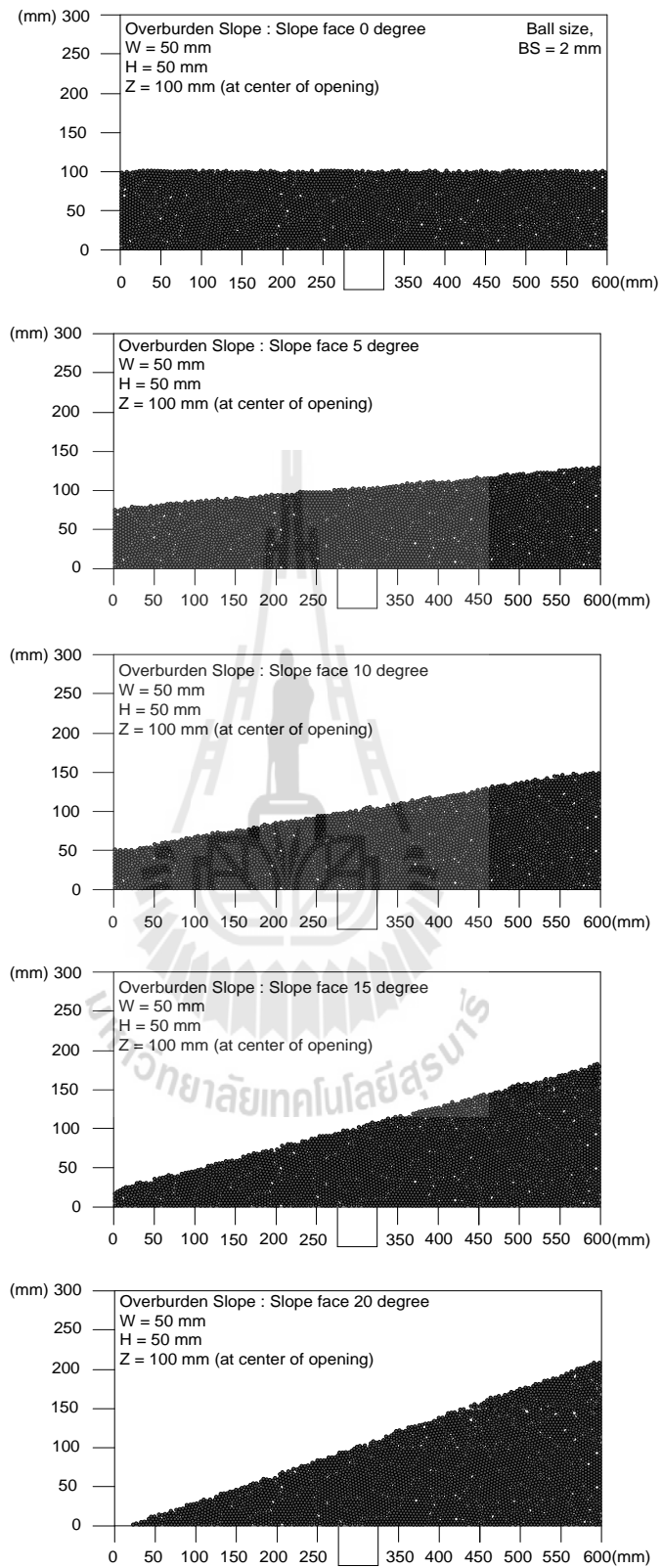


Figure 4.8 Examples of surface subsidence before the opening simulation.

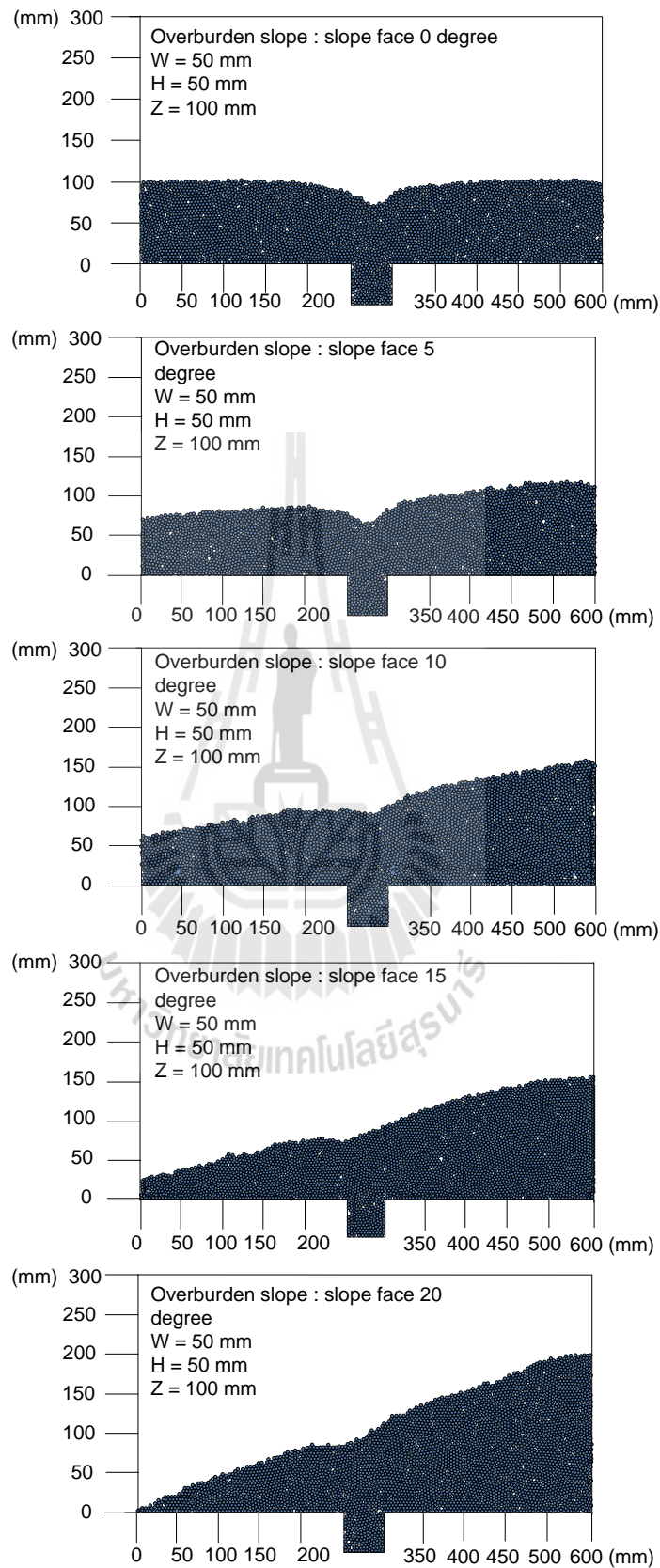


Figure 4.9 Examples of surface subsidence after the opening simulation.

Table 4.3 Results of overburden slope simulations.

Parameter variable			Results		
Slope angle (degrees)	Z (mm) at center of opening	W (mm)	γ (degrees)		S_{\max}/H
			Up-slope	Down-slope	
0°	100	50	20.1	20.1	0.46
	150		11.0	11.0	0.22
	200		3.5	3.5	0.07
5°	100		32.3	19.0	0.40
	150		18.6	10.0	0.20
	200		14.9	2.5	0.06
10°	100		38.0	18.0	0.32
	150		27.0	9.8	0.16
	200		20.2	2.4	0.05
15°	100		40.0	16.0	0.26
	150		31.2	8.0	0.14
	200		28.4	2.6	0.04
20°	100	42.0	12.3	0.20	
	150	34.5	6.0	0.12	
	200	30.0	1.7	0.02	

Table 4.4 Depth at angle of draw and maximum subsidence in overburden slope simulations.

Slope angle (degrees)	Z (mm) at center of opening	Depth of overburden (mm)		
		Up-slope	Down-slope	S_{\max}/H
0°	100	100	100	2.0
	150	150	150	3.0
	200	200	200	4.0
5°	100	109	97	2.1
	150	172	146	3.1
	200	204	194	4.1
10°	100	115	95	2.2
	150	170	135	3.4
	200	205	186	4.1
15°	100	120	90	2.4
	150	178	130	3.5
	200	217	175	4.2
20°	100	128	82	2.6
	150	180	122	3.6
	200	225	165	4.5

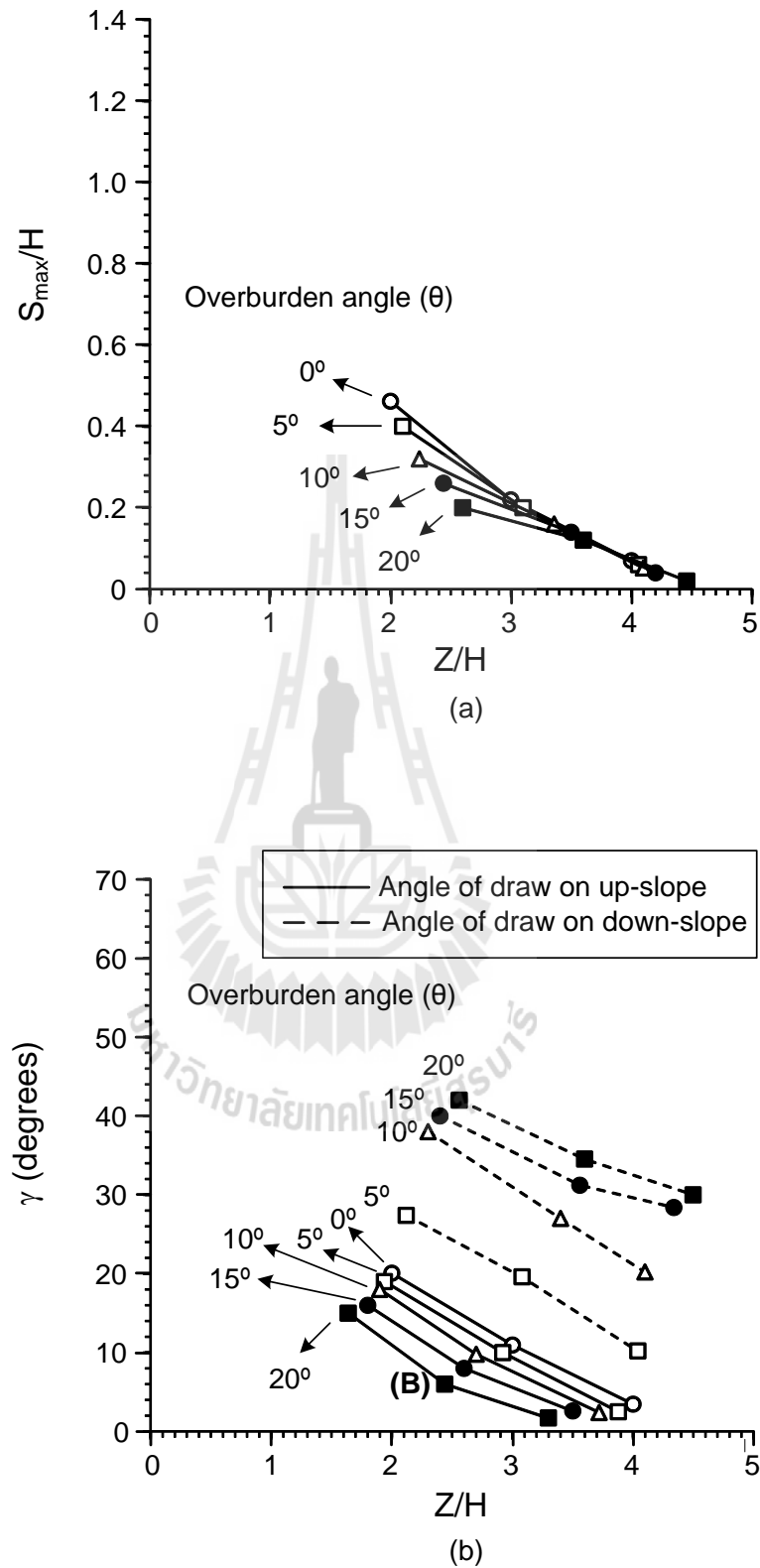


Figure 4.10 S_{\max}/H as a function of Z/H ratio (a) and γ as a function of Z/H ratio (b).

CHAPTER V

COMPARISON OF NUMERICAL AND PHYSICAL MODELS

5.1 Objectives

The objective of this chapter is to compare the physical model testing with the computer simulation (PFC^{2D} model) in terms of the maximum subsidence-to-height (S_{\max}/H) ratio and the angle of draw (γ).

5.2 Comparison of PFC^{2D} simulation and physical modeling

After several trials the angle of draw and maximum subsidence can be determined for each opening configuration under various excavation rates, mining sequences and overburden slopes.

The PFC^{2D} simulations results are compared with of observed from the physical models. Figures 5.1 and 5.2 show the comparison of the S_{\max}/H ratio and γ obtained from physical and PFC^{2D} models under variation of mining sequences. The PFC^{2D} simulations show the decreasing trends of the S_{\max}/H ratio and γ with overburden thicknesses which are similar to those observed from the test models. The physical model test gives the values of S_{\max}/H ratio and γ lower than those the PFC^{2D}

model probably because the particles of PFC^{2D} are circular particles models in the discrete element analyses are perfectly circular while the tested granular materials are not perfectly shaped.

Figures 5.3 and 5.4 shows the comparison the S_{\max}/H ratio and γ between PFC^{2D} and physical model under high excavation rate. For low excavation rate they are shown in Figures 5.5 and 5.6. The PFC^{2D} and physical simulations give value of S_{\max}/H ratio and γ slightly different for all cases. The values obtained from physical simulation are lower than the PFC^{2D} model. The comparisons of high excavation obtain from PFC^{2D} and physical model shows that the S_{\max}/H ratio and γ increase with increasing excavation area and with decreasing Z/H ratio. These are similar to the low excavation rate. This is probably due to the different angularities and frictional strengths of the particle. The particle are perfectly circular in PFC^{2D} model while in the physical model tests the shapes of particle are high sphericity and subangular.

In the case of overburden slope, the comparison between PFC^{2D} simulation and physical modeling of S_{\max}/H ratio as a function of Z/H ratio is shown in Figure 5.7. Figures 5.8 and 5.9 show the angle of draw on up-slope (γ_{up}) and down-slope (γ_{down}), respectively. The comparison of PFC^{2D} and physical model test shows the decreases of S_{\max}/H ratio and γ with increasing Z/H ratio. The S_{\max}/H ratio and γ_{up} of the physical model test results are lower than those of the computer modeling, whereas the γ_{down} of physical model is greater than that of the PFC^{2D} model. This is probably due to that the overburden thickness at down-slope is less than overburden thickness at up-slope and particles of PFC^{2D} and physical models are different.

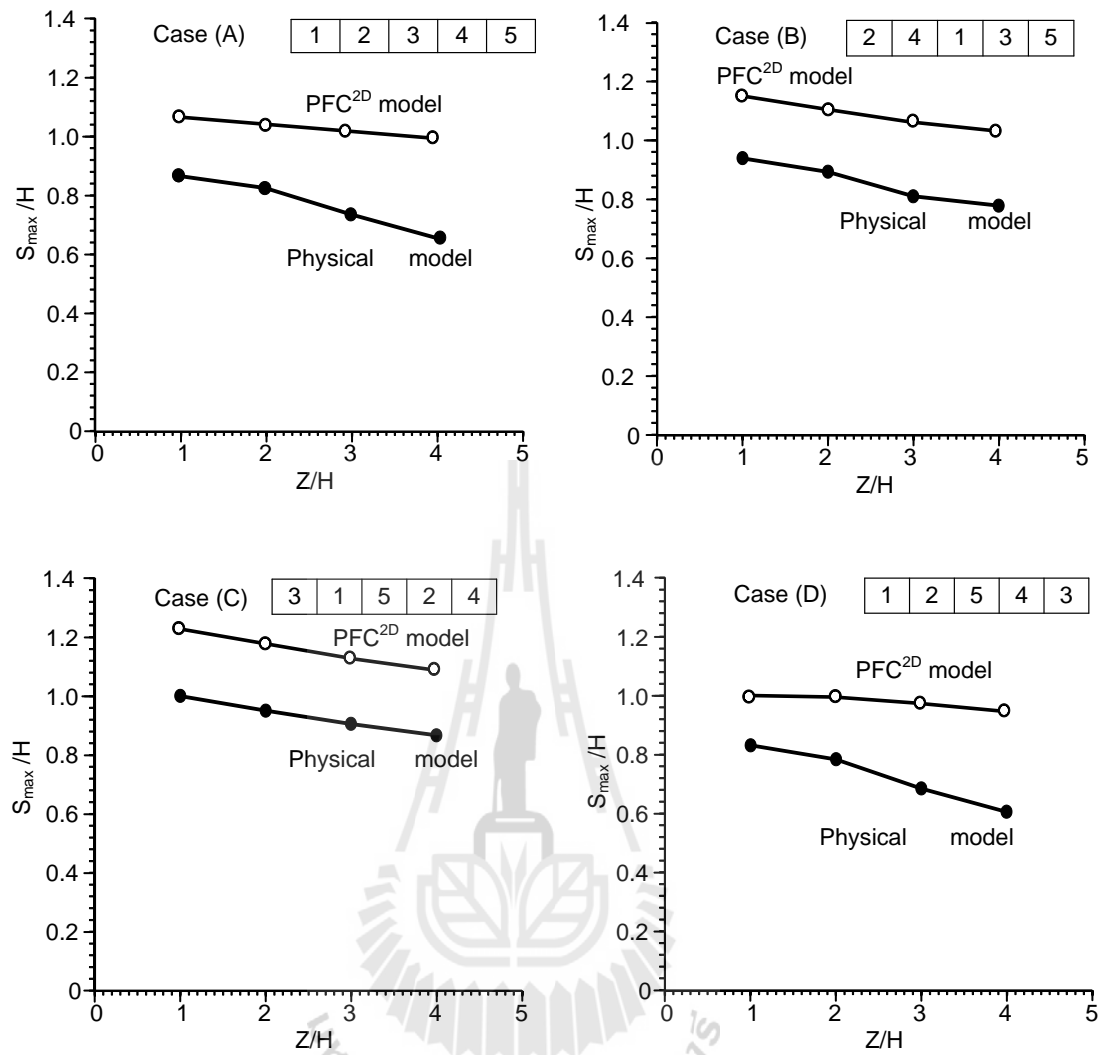


Figure 5.1 Comparison of mining sequences of S_{\max}/H ratio as a function of Z/H

ratio as a function of Z/H ratio of four mining sequence cases.

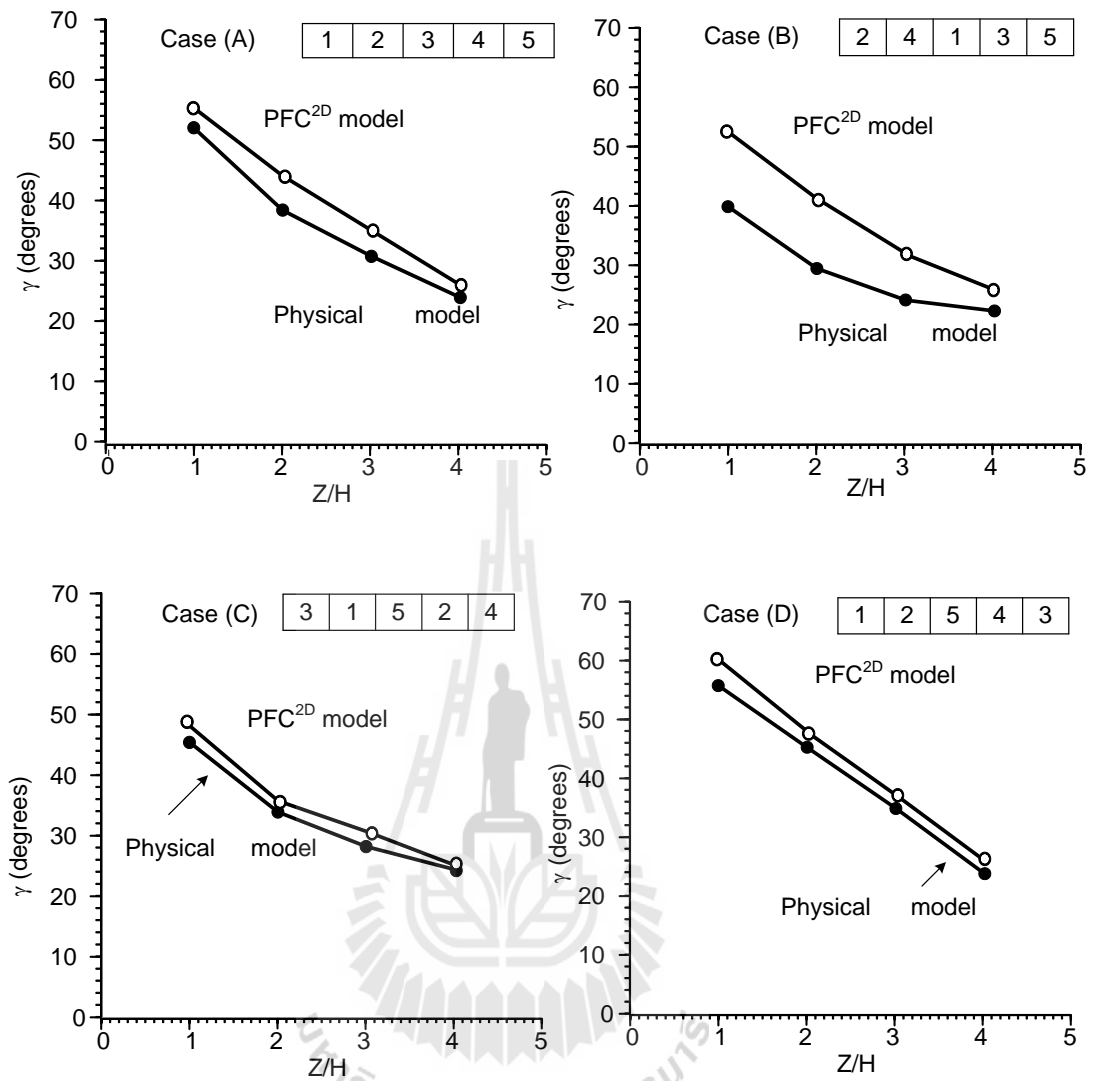


Figure 5.2 Comparisons of angle of draw (γ) as a function of Z/H ratio of mining sequence in four cases obtained from physical simulation and PFC^{2D} model simulation.

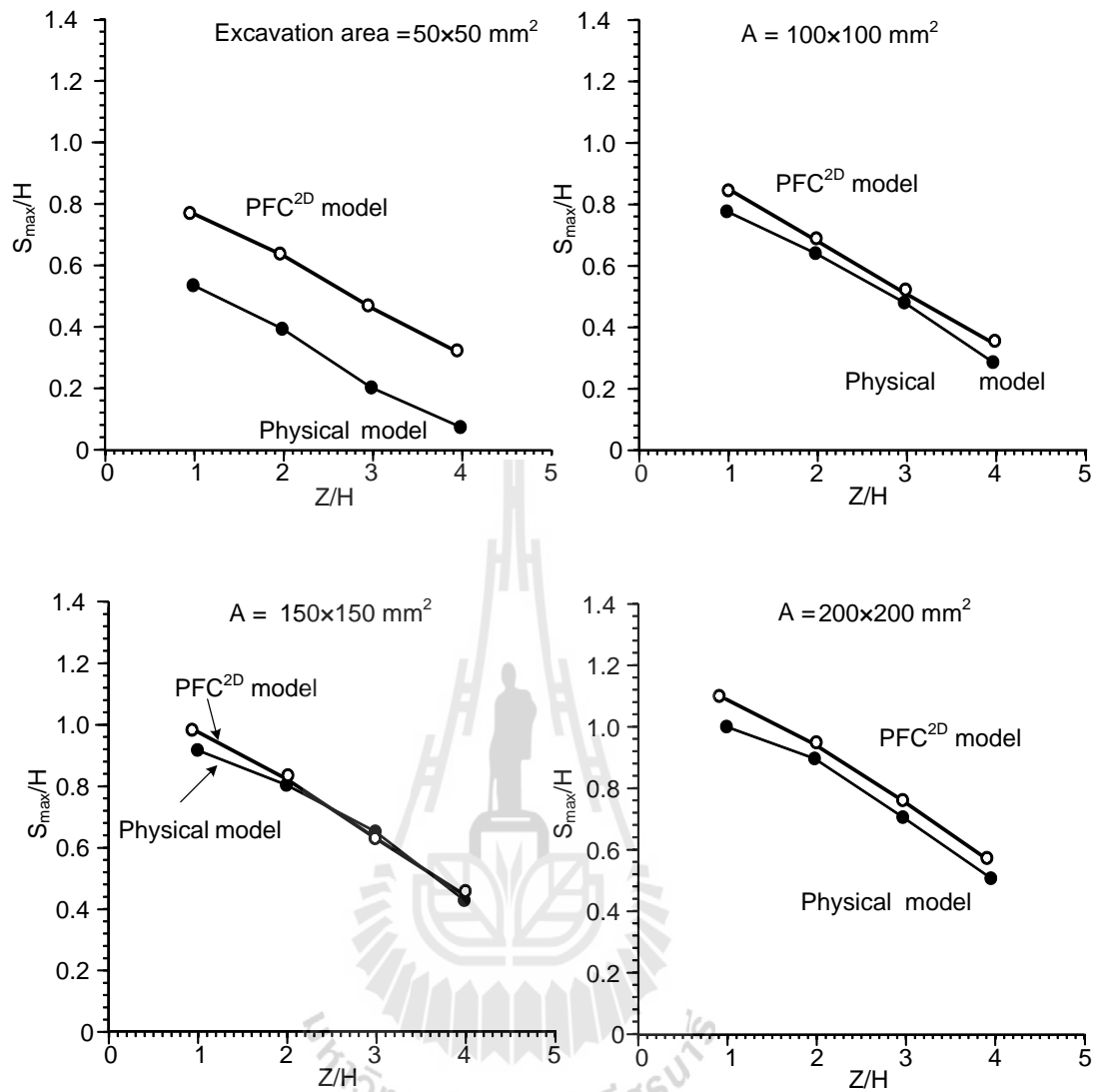


Figure 5.3 Comparisons of the maximum subsidence to height ratio (S_{\max}/H) of high excavation rates (50 mm increments) obtained from physical simulation and PFC^{2D} model simulation.

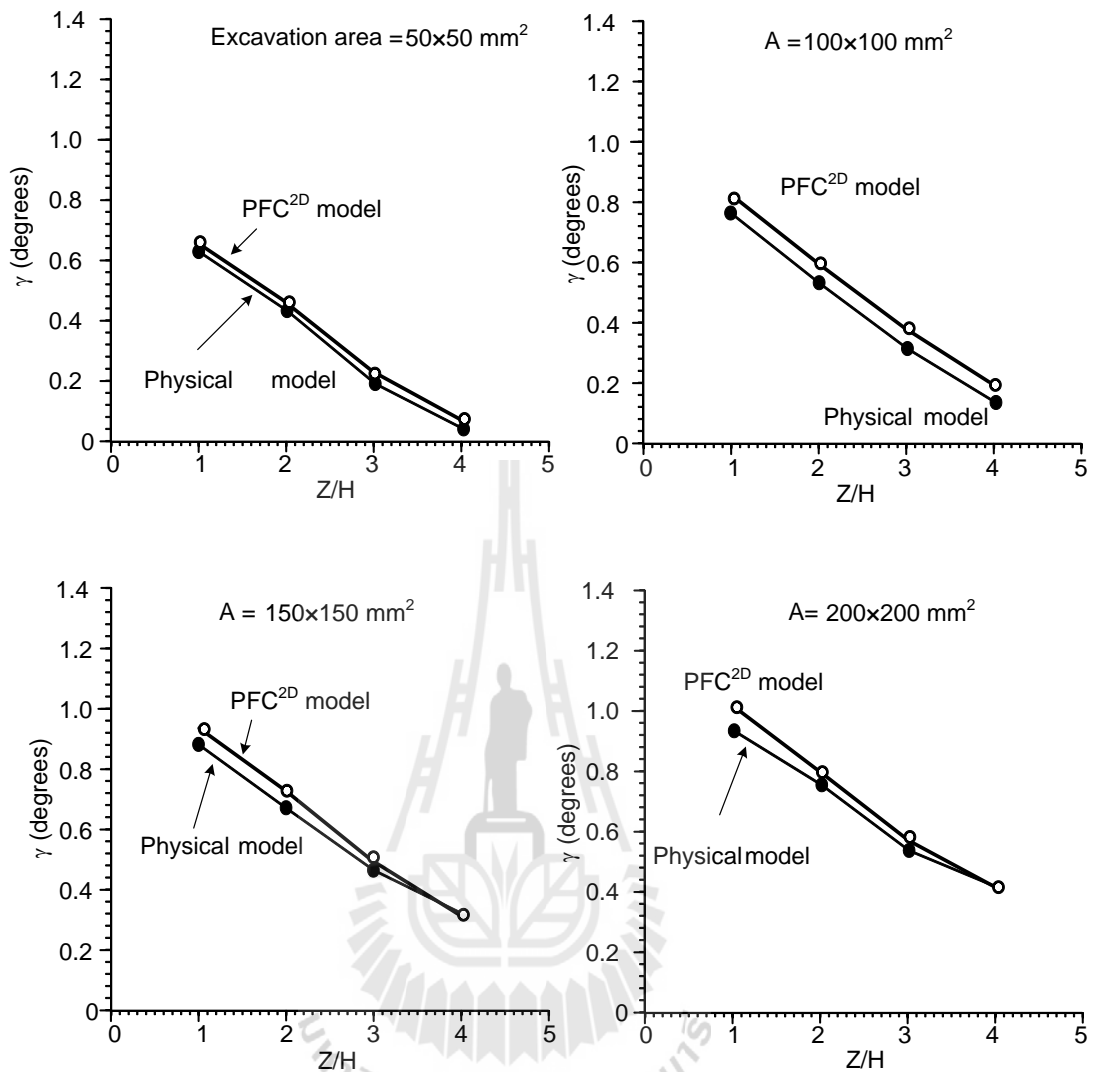


Figure 5.4 Comparisons of the angle of draw (γ) of high excavation rates obtained from PFC^{2D} and physical simulation.

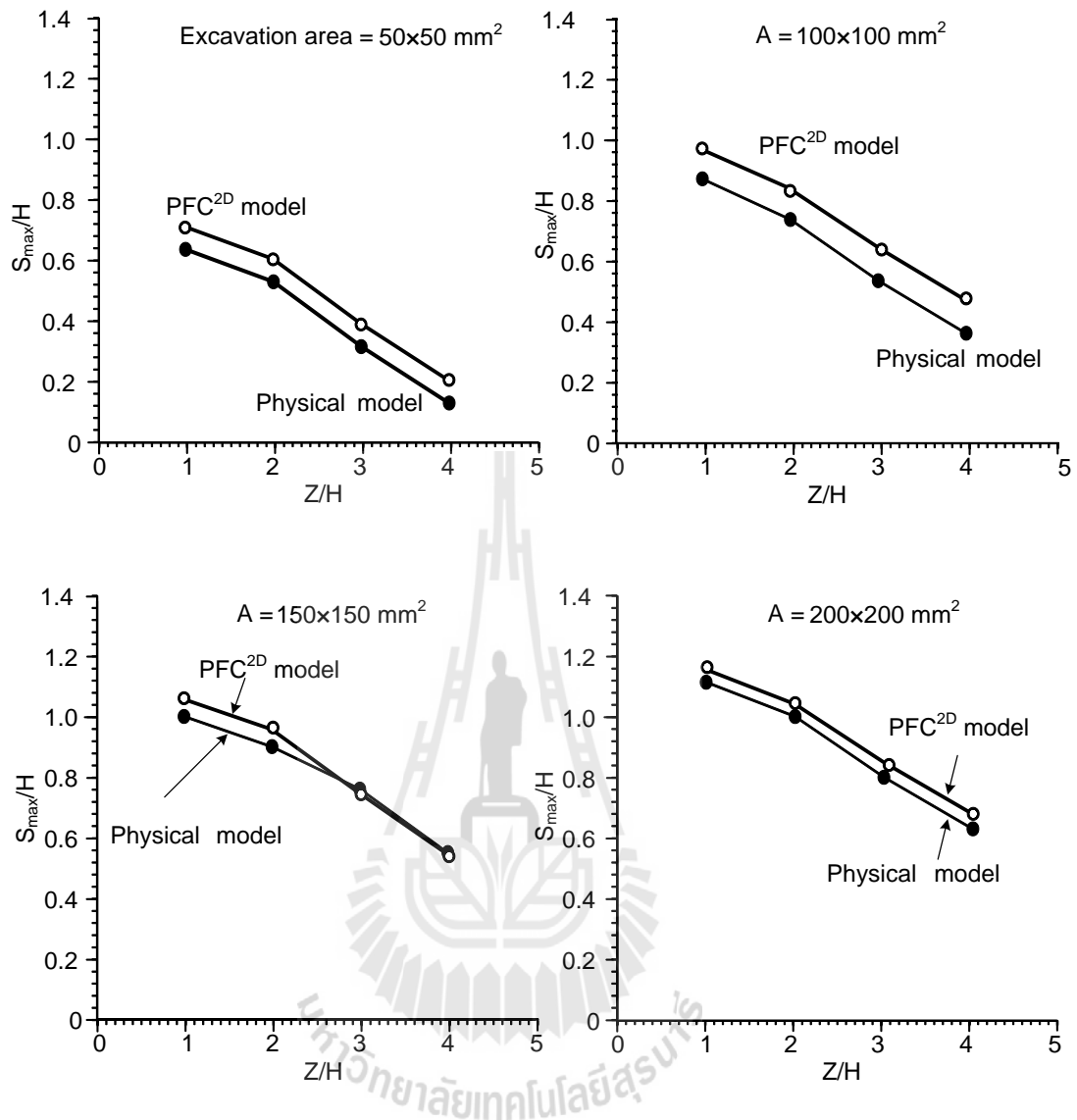


Figure 5.5 Comparisons of the maximum subsidence to height ratio (S_{\max}/H) of low excavation rates (5mm increments) obtained from physical simulation and PFC^{2D} model simulation.

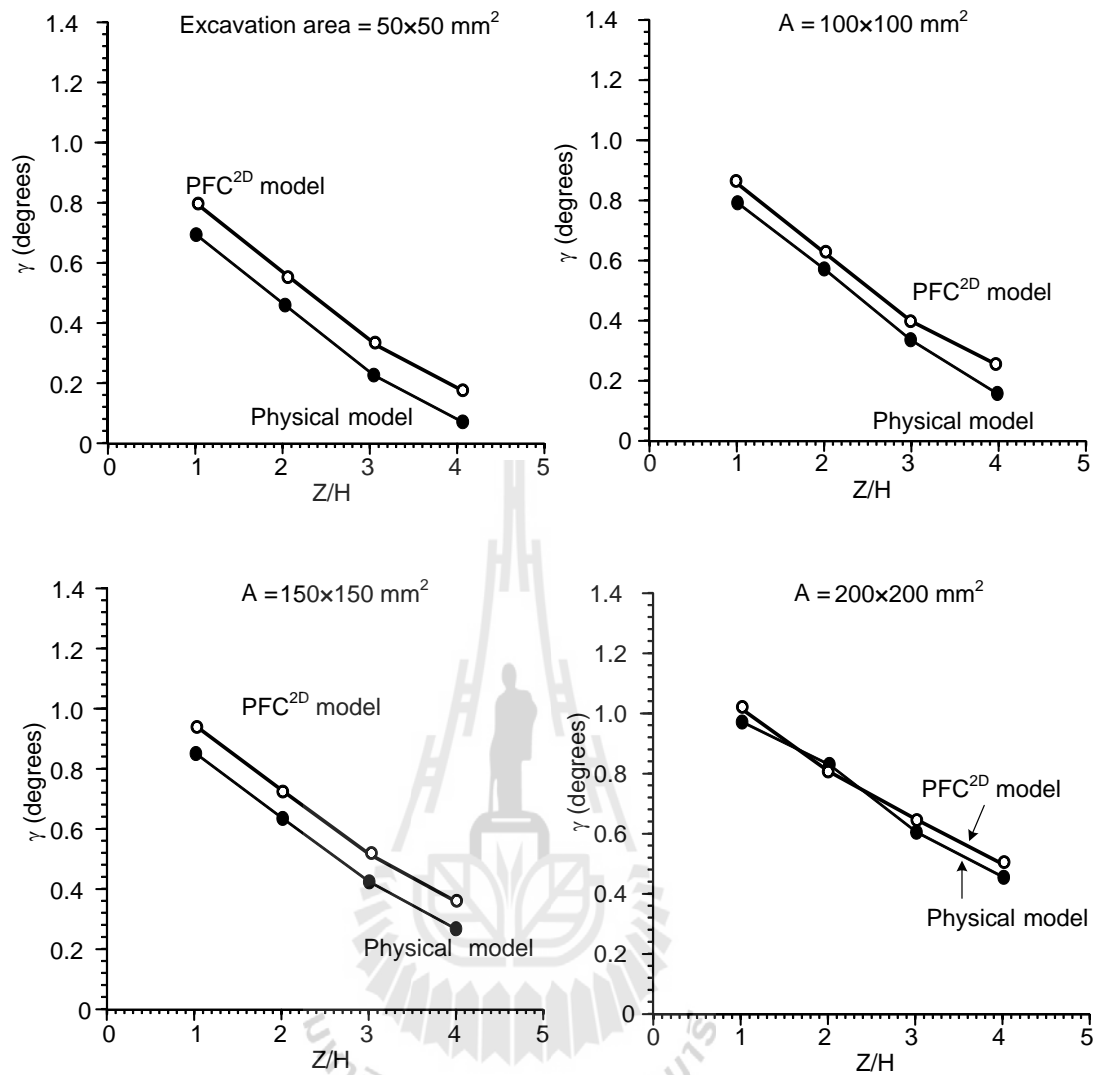


Figure 5.6 Comparisons of angle of draw (γ) of low excavation rates (5mm increments) obtained from physical simulation and PFC^{2D} model simulation.

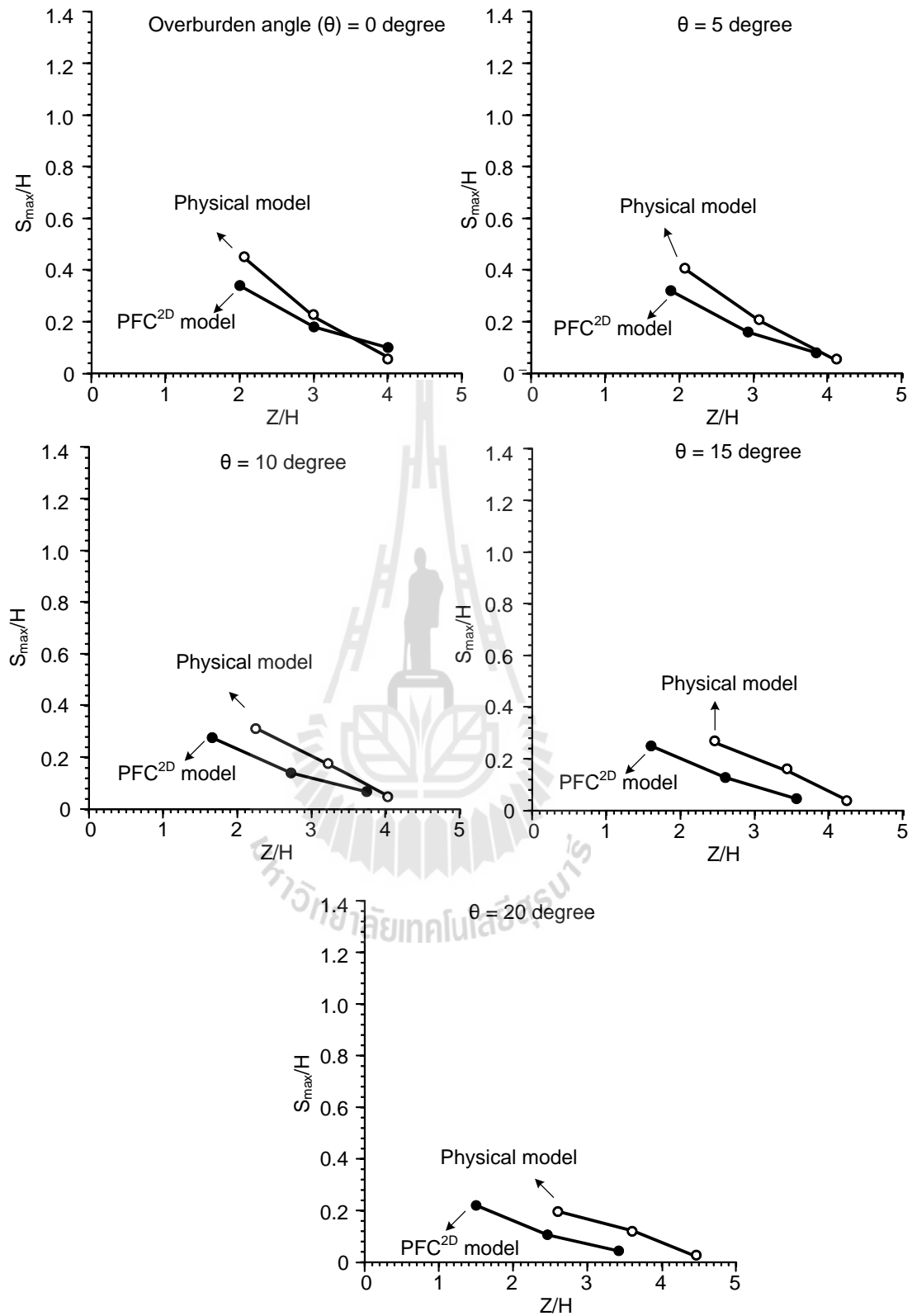


Figure 5.7 Comparisons of S_{\max}/H ratio of overburden slope obtained from physical simulation and PFC^{2D} model simulation.

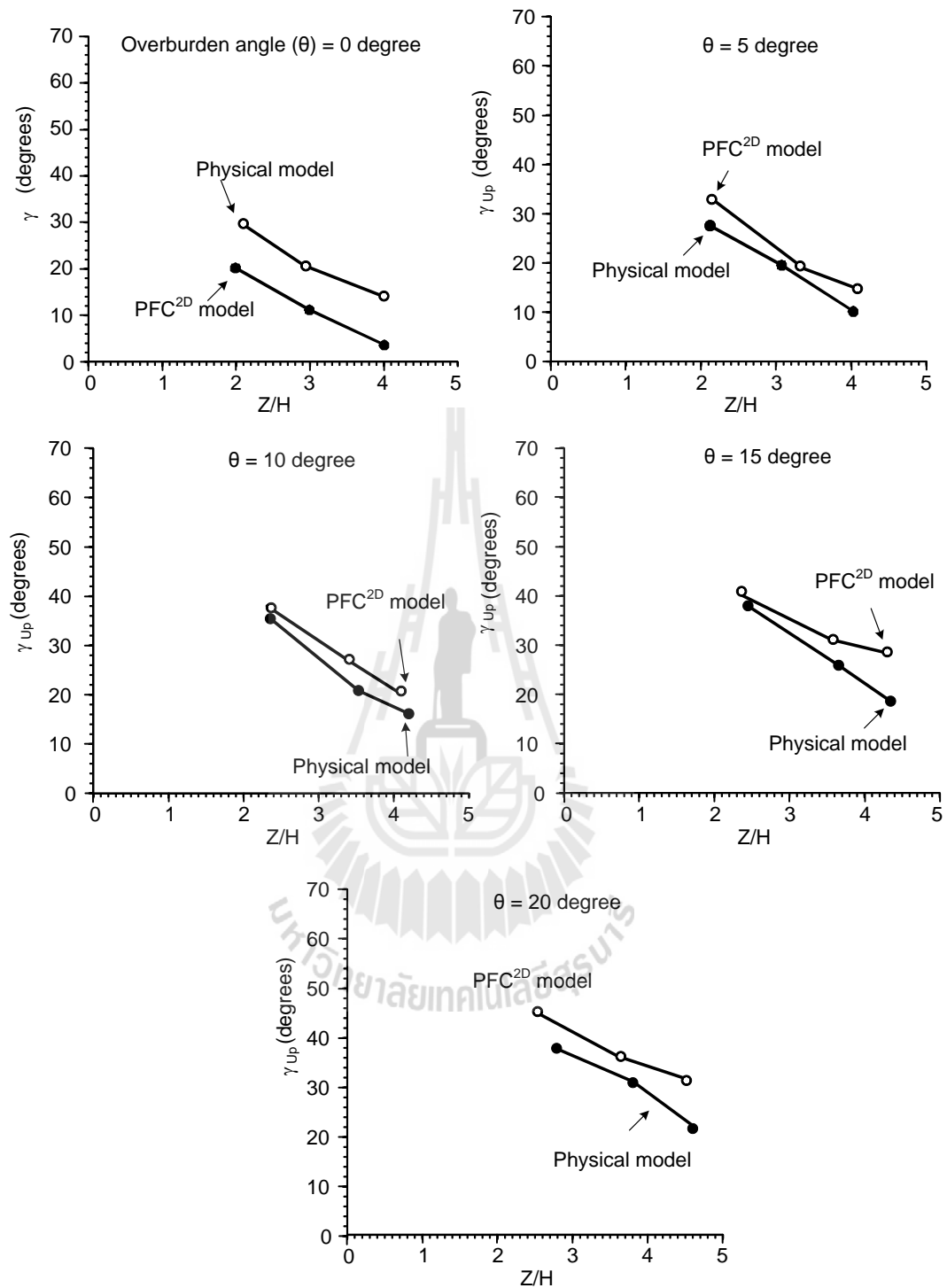


Figure 5.8 The comparisons γ on up-slope are obtained from physical simulation with PFC^{2D} model simulation of overburden slope.

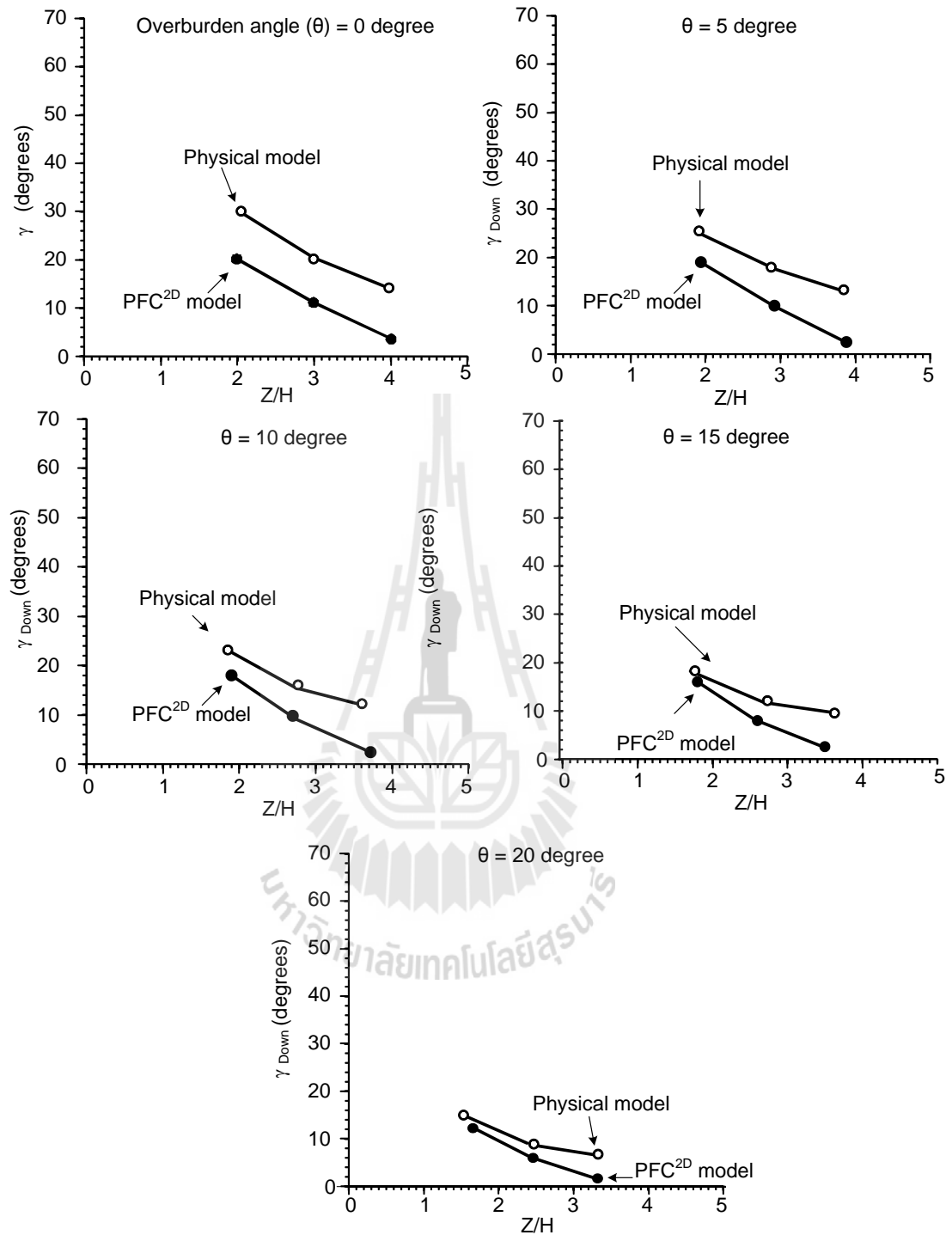


Figure 5.9 The comparisons obtained from physical simulation with PFC^{2D} model simulation of γ on down-slope of overburden slope.

CHAPTER V

COMPARISON OF NUMERICAL AND PHYSICAL MODELS

5.1 Objectives

The objective of this chapter is to compare the physical model testing with the computer simulation (PFC^{2D} model) in terms of the maximum subsidence-to-height (S_{\max}/H) ratio and the angle of draw (γ).

5.2 Comparison of PFC^{2D} simulation and physical modeling

After several trials the angle of draw and maximum subsidence can be determined for each opening configuration under various excavation rates, mining sequences and overburden slopes.

The PFC^{2D} simulations results are compared with of observed from the physical models. Figures 5.1 and 5.2 show the comparison of the S_{\max}/H ratio and γ obtained from physical and PFC^{2D} models under variation of mining sequences. The PFC^{2D} simulations show the decreasing trends of the S_{\max}/H ratio and γ with overburden thicknesses which are similar to those observed from the test models. The physical model test gives the values of S_{\max}/H ratio and γ lower than those the PFC^{2D}

model probably because the particles of PFC^{2D} are circular particles models in the discrete element analyses are perfectly circular while the tested granular materials are not perfectly shaped.

Figures 5.3 and 5.4 shows the comparison the S_{\max}/H ratio and γ between PFC^{2D} and physical model under high excavation rate. For low excavation rate they are shown in Figures 5.5 and 5.6. The PFC^{2D} and physical simulations give value of S_{\max}/H ratio and γ slightly different for all cases. The values obtained from physical simulation are lower than the PFC^{2D} model. The comparisons of high excavation obtain from PFC^{2D} and physical model shows that the S_{\max}/H ratio and γ increase with increasing excavation area and with decreasing Z/H ratio. These are similar to the low excavation rate. This is probably due to the different angularities and frictional strengths of the particle. The particle are perfectly circular in PFC^{2D} model while in the physical model tests the shapes of particle are high sphericity and subangular.

In the case of overburden slope, the comparison between PFC^{2D} simulation and physical modeling of S_{\max}/H ratio as a function of Z/H ratio is shown in Figure 5.7. Figures 5.8 and 5.9 show the angle of draw on up-slope (γ_{up}) and down-slope (γ_{down}), respectively. The comparison of PFC^{2D} and physical model test shows the decreases of S_{\max}/H ratio and γ with increasing Z/H ratio. The S_{\max}/H ratio and γ_{up} of the physical model test results are lower than those of the computer modeling, whereas the γ_{down} of physical model is greater than that of the PFC^{2D} model. This is probably due to that the overburden thickness at down-slope is less than overburden thickness at up-slope and particles of PFC^{2D} and physical models are different.

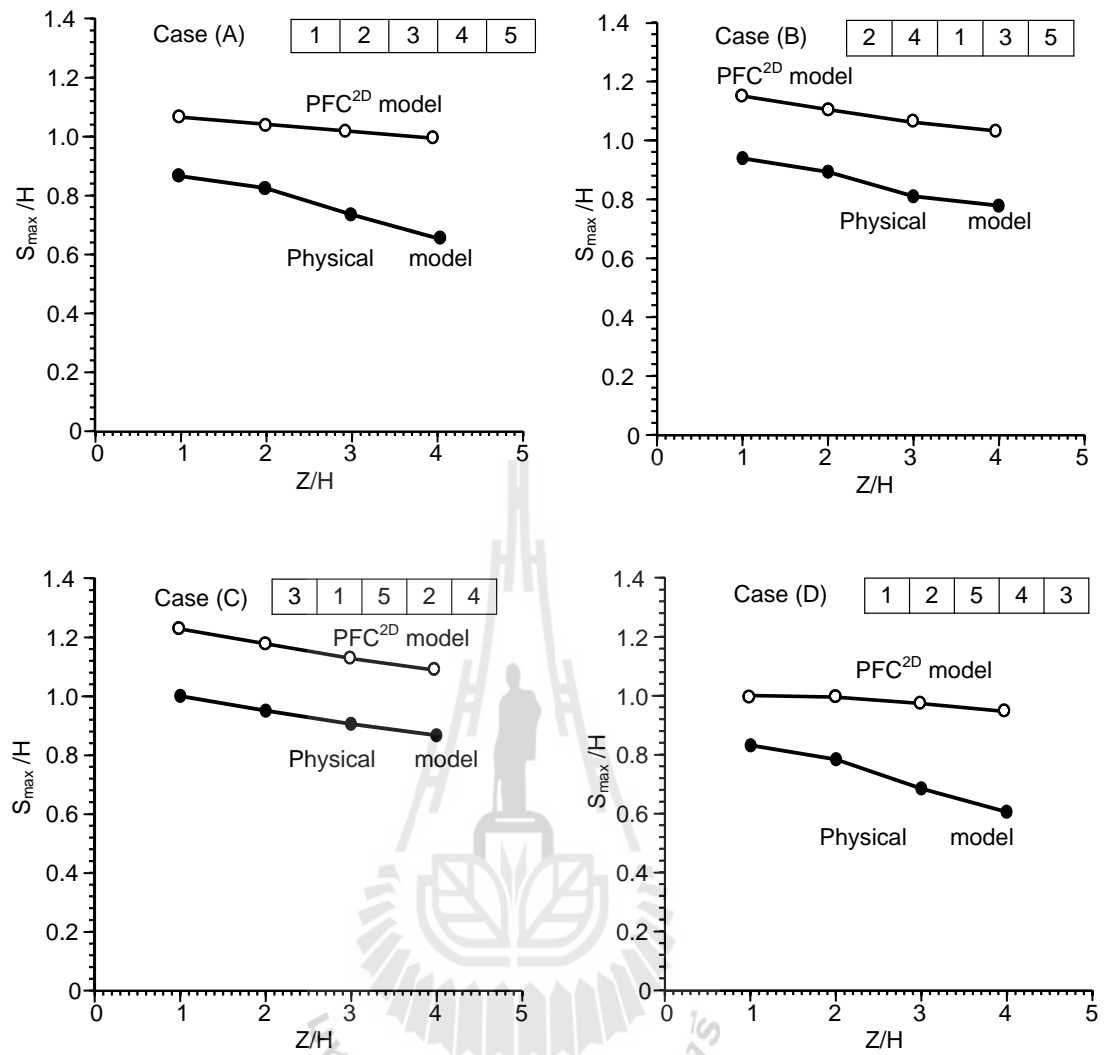


Figure 5.1 Comparison of mining sequences of S_{\max}/H ratio as a function of Z/H

ratio as a function of Z/H ratio of four mining sequence cases.

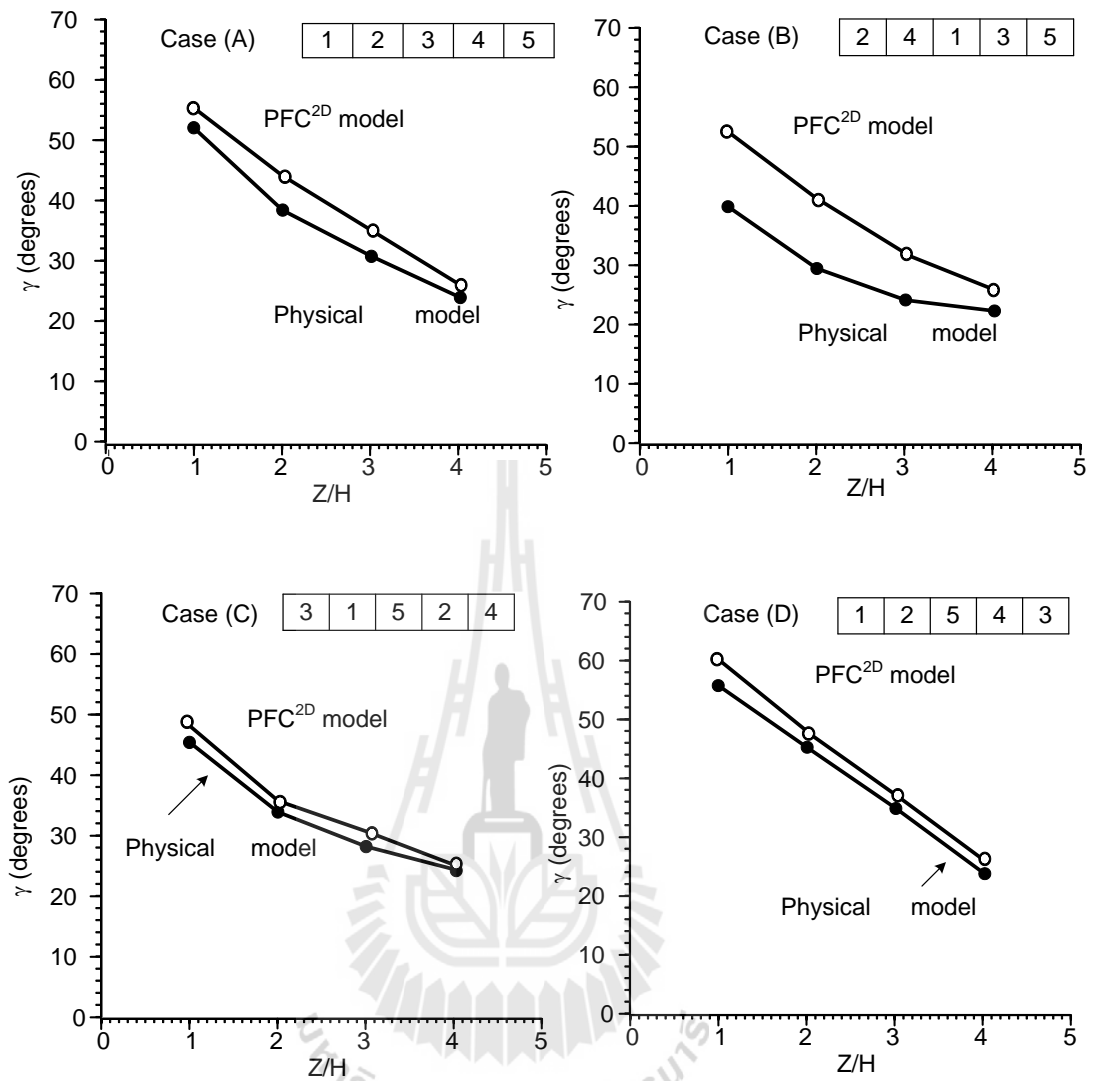


Figure 5.2 Comparisons of angle of draw (γ) as a function of Z/H ratio of mining sequence in four cases obtained from physical simulation and PFC^{2D} model simulation.

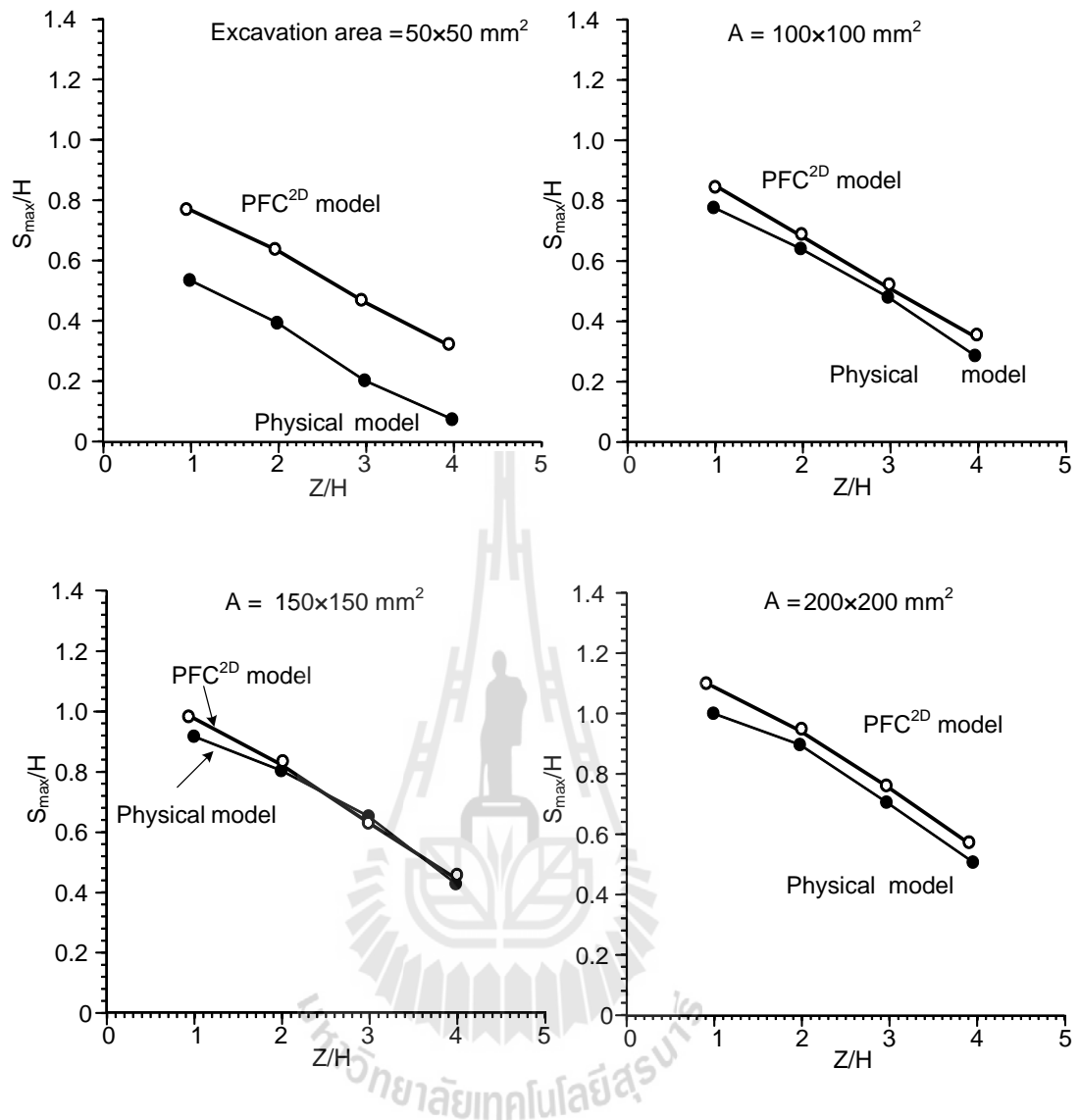


Figure 5.3 Comparisons of the maximum subsidence to height ratio (S_{\max}/H) of high excavation rates (50 mm increments) obtained from physical simulation and PFC^{2D} model simulation.

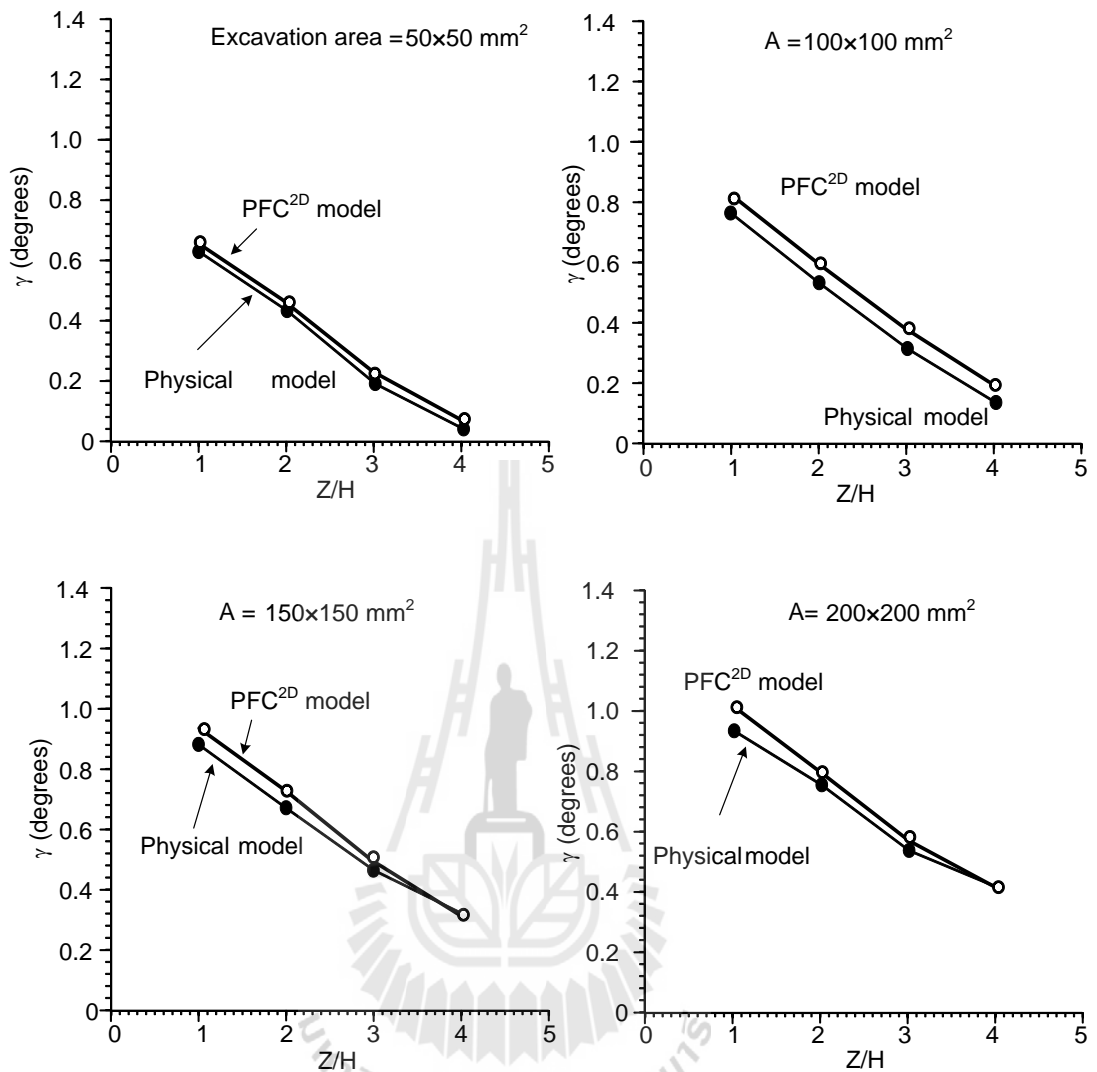


Figure 5.4 Comparisons of the angle of draw (γ) of high excavation rates obtained from PFC^{2D} and physical simulation.

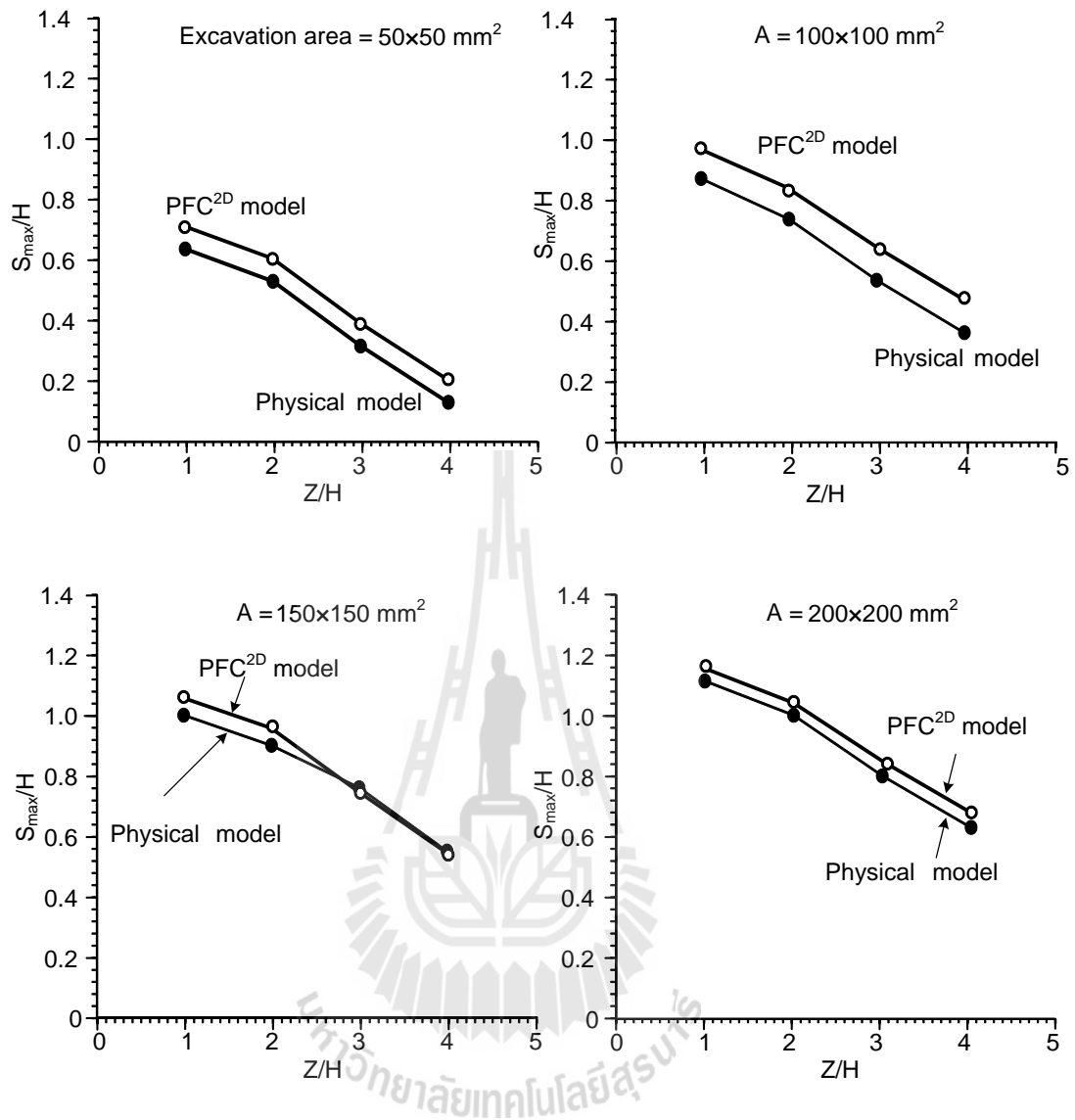


Figure 5.5 Comparisons of the maximum subsidence to height ratio (S_{\max}/H) of low excavation rates (5mm increments) obtained from physical simulation and PFC^{2D} model simulation.

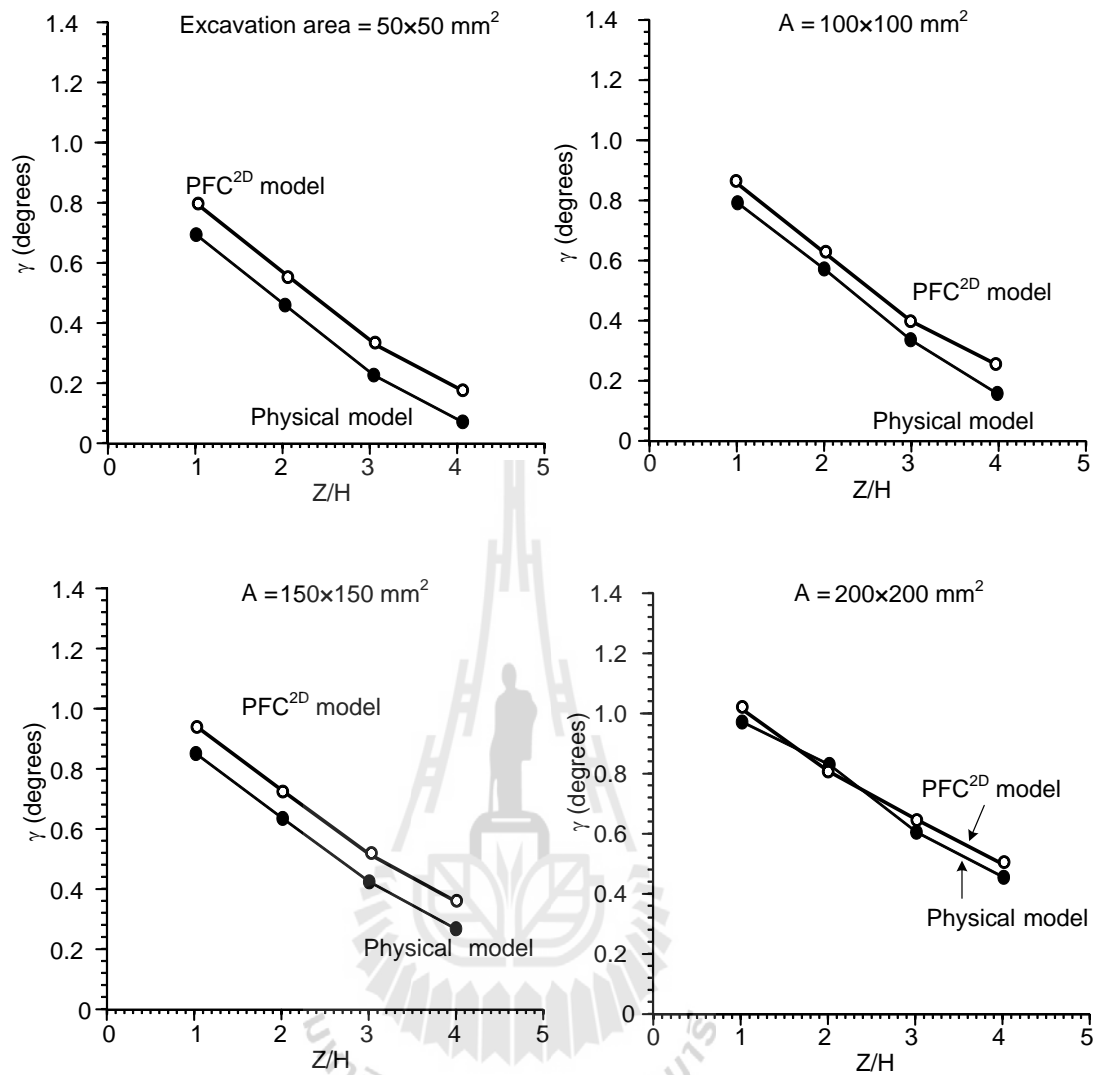


Figure 5.6 Comparisons of angle of draw (γ) of low excavation rates (5mm increments) obtained from physical simulation and PFC^{2D} model simulation.

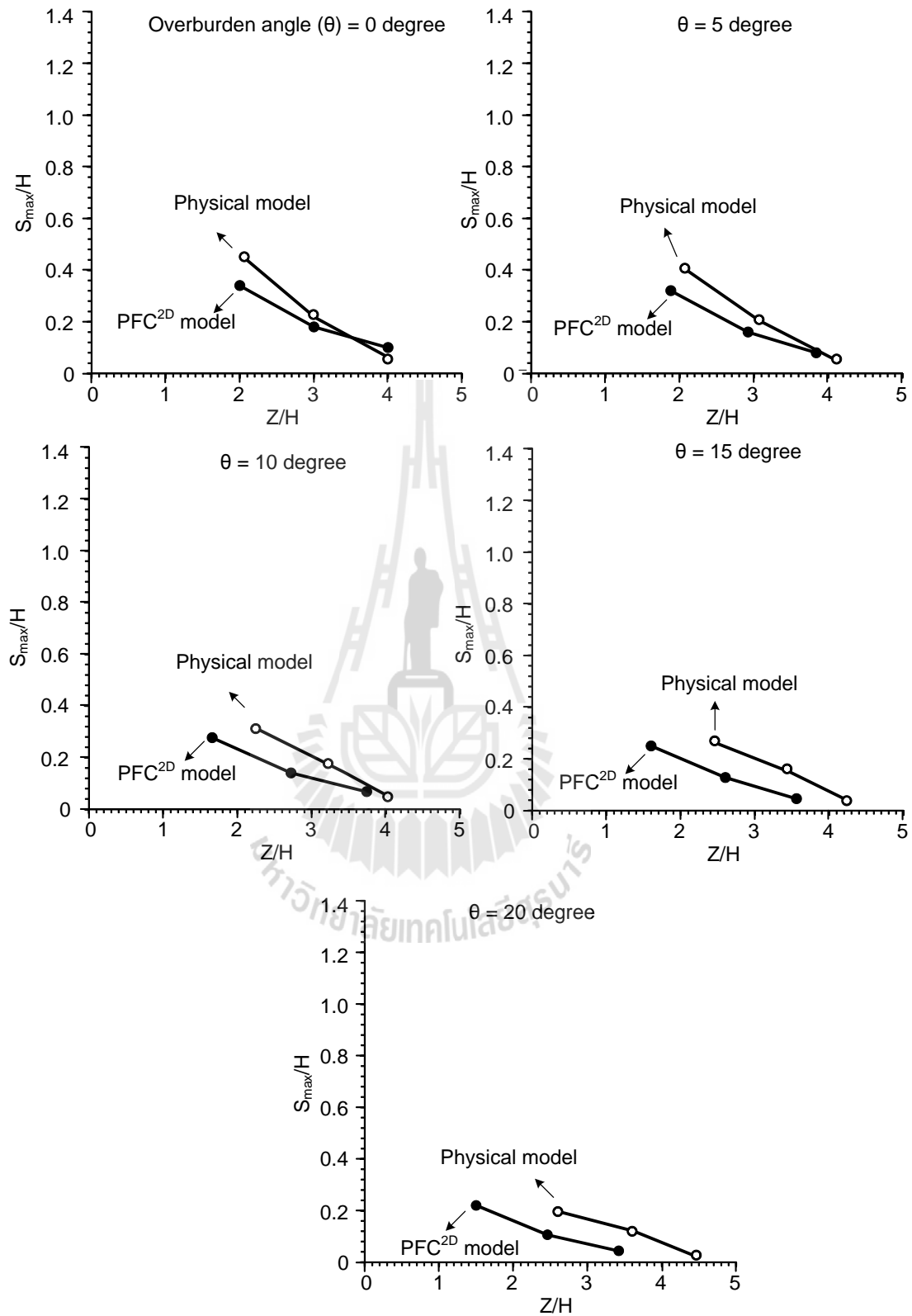


Figure 5.7 Comparisons of S_{\max}/H ratio of overburden slope obtained from physical simulation and PFC^{2D} model simulation.

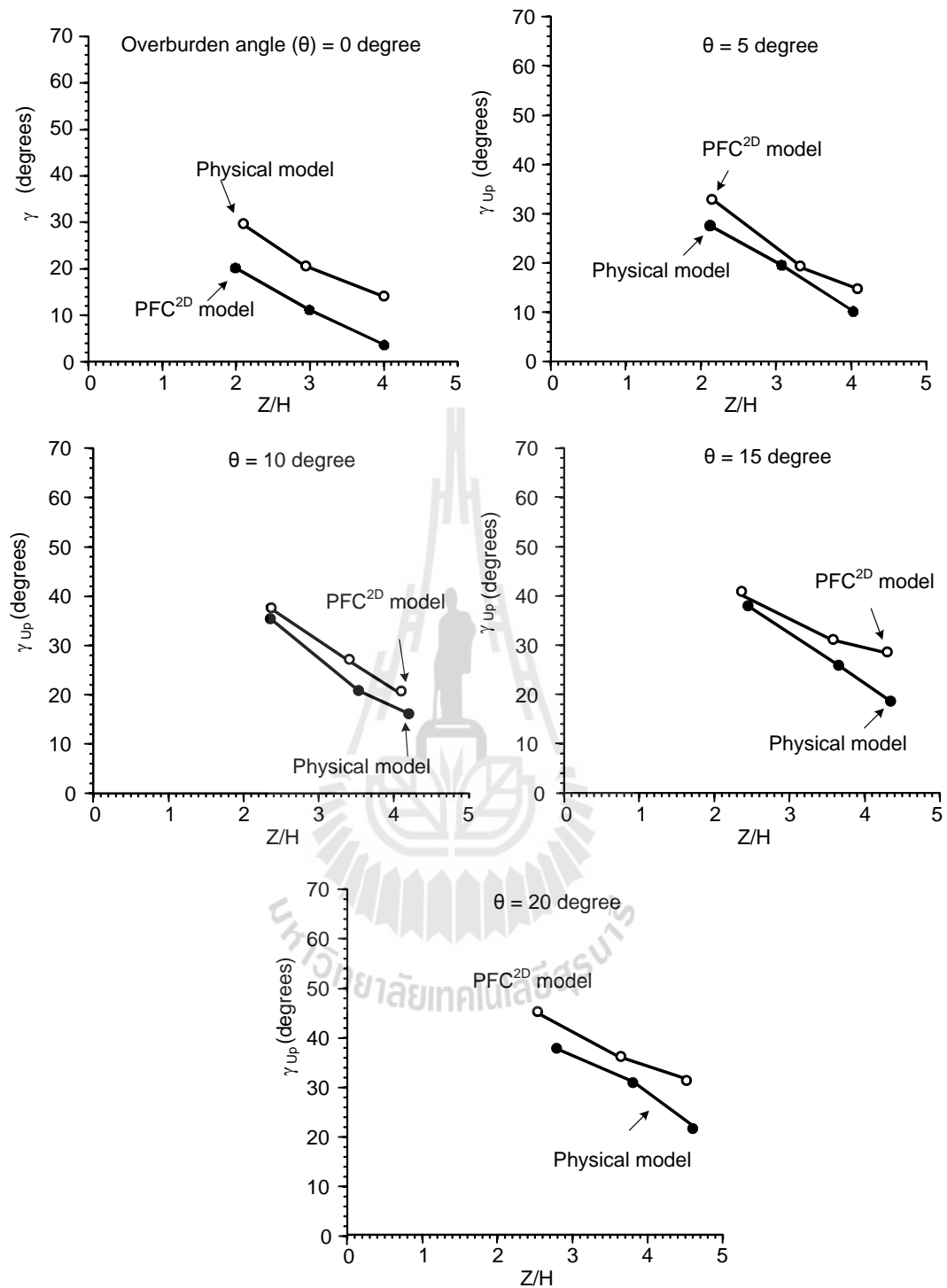


Figure 5.8 The comparisons γ on up-slope are obtained from physical simulation with PFC^{2D} model simulation of overburden slope.

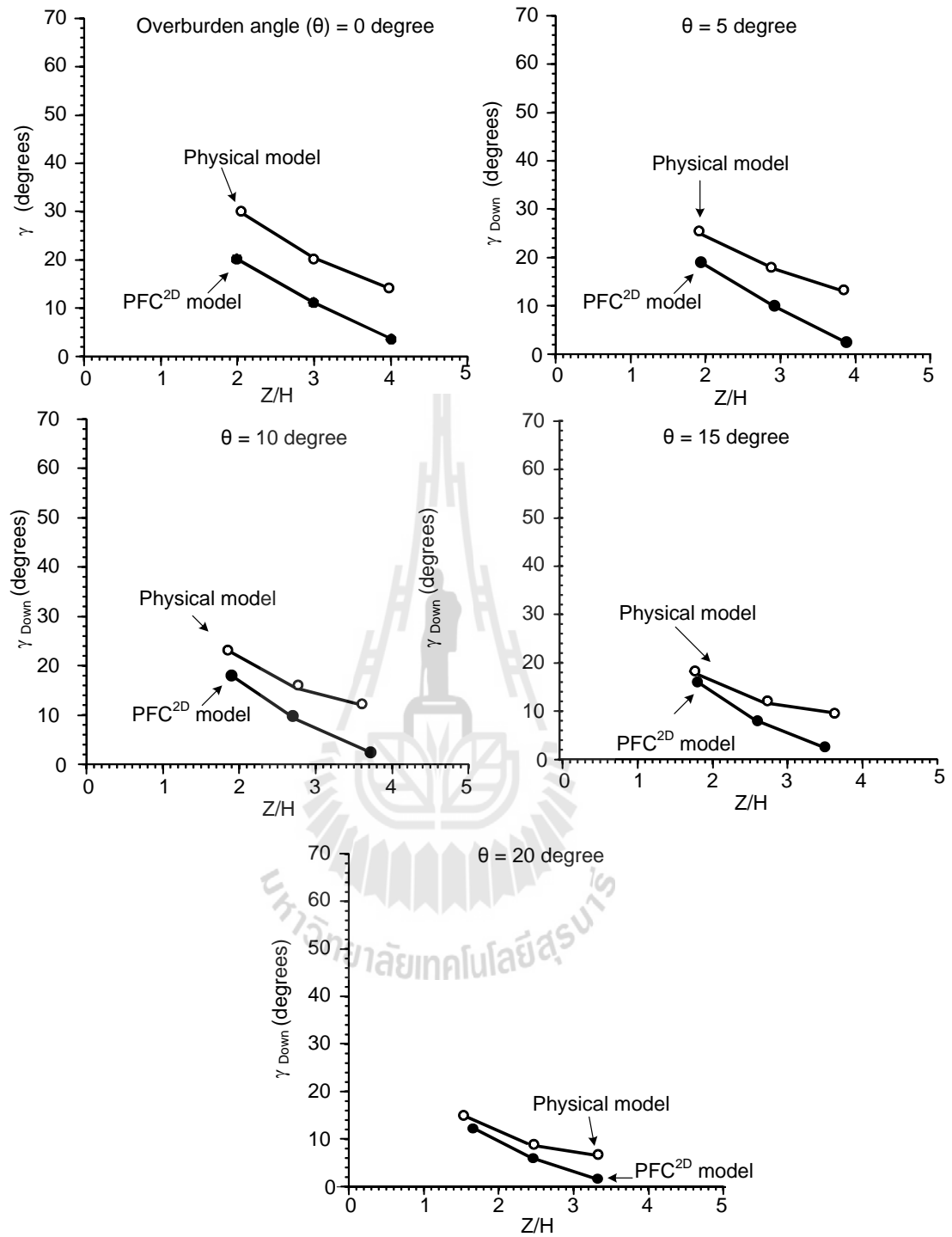


Figure 5.9 The comparisons obtained from physical simulation with PFC^{2D} model simulation of γ on down-slope of overburden slope.

CHAPTER VII

DISCUSSIONS AND CONCLUSIONS

7.1 Discussions

The aim of this study is to investigate the effects of mining sequence, excavation rate and overburden slope on the angle of draw and maximum surface subsidence induced in post-failure region under super-critical condition using scaled-down physical model. The test results are compared with the findings from the observations by other researchers.

The effect of opening depth is investigated here by varying Z/H ratio from 1, 2, 3 to 4. Under the same excavation area, increasing Z/H ratio can reduce the angle of draw and maximum subsidence. This is due to the subsidence created new voids created in the overburden above the opening which is agrees reasonably well with the related test results on the surface subsidence above and underground opening obtained by Thongprapha et al. (2015). For the studying of the effect of opening depth on the overburden slope, the measurement gives incorrect value of maximum subsidence and angle of draw when Z/H ratio = 1. This is because the opening depth on down-slope sides is insufficient ($Z < H$) (Shu and Bhattacharyya, 1992).

The effects of surface slope angle on the angle of draw are explicitly shown by subsidence profile obtained from physical models and numerical simulation. The angle of draw on up-slope sides increases and decreases on down-slope sides with increasing surface slope angle, which agrees with the experimental

results obtained by Zhang et al. (2011) and Liu et al. (2015). This is true for opening depth-to-height ratio more than 1 ($Z/H > 1$).

The particles size used in this study are relatively small. The effects of particle size on the settlement trough volume and settlement trough width are studied by Rankin, (1988) who found that the empirical equation for width of trough (i) is in good agreement for cohesionless material. Hence the larger particle size should be tested. This is because the shape and particle size of overburden affect the flowing of particles into the opening or panel. The small particle size can flow into the opening easily than larger particles. The trough volume is always less than the opening volume. The subsidence trough volume tends to decrease as the opening depth increases. This observation agrees well with Thongprapha et al. (2015) who study the surface subsidence above underground opening using gravel in order to exhibit a cohesionless frictional behavior of the overburden material.

The effect of overburden slope on angle of draw and maximum subsidence is investigated here. The results show that the particles on the up-slope sides can flow (collapse) into opening easier, and hence induces the larger angle of draw. The angle of draw on up-slope increases with increasing slope angle while the S_{\max}/H ratio decreasing with increasing Z/H ratio and slope angle. The values of S_{\max}/H ratio under various slope angles of the overburden are very similar. This is due to that the overburden thickness on up-slope is greater than that on the down- slope. This agrees with analytical calculation model by Yao et al. (1991), who studied the influence of overburden strength on limit subsidence characteristics. They indicate that the angle of draw is related to the overburden properties, depth and configurations of mine opening.

The empirical solution provided by Rankin (1998) fits well to the physical model results under high excavation rate, particularly for $Z/H = 4$. For the low excavation rate, the empirical solution fit well for the excavation area of 50×50 and $100 \times 100 \text{ mm}^2$ when Z/H ratio is 4. The empirical solution is not applicable to other mining sequences and different overburden slope conditions. The subsidence trough volume obtained from the physical models is higher than that obtained from the empirical calculations.

The subsidence trough volume tends to decrease as the Z/H ratio increases. These results agree well with the conclusion drawn by Thongprapha et al. (2015) that the subsidence trough volume decreases rapidly when the Z/W ratio increases beyond 3.

The excavation rate slightly affects the surface subsidence. The finding shows that the maximum subsidence increases with increasing excavation rate. The angle of draw decreases with increasing the excavation rate.

The remaining panel during excavation gives small curves of surface subsidence trough after the excavation completes. As opposed to the excavation from one side to the other, the subsidence trough is smoother. The excavation starting from the center of panel gives the lowest angle of draw and highest maximum subsidence for all depths. This is due to accumulation of particles at the center of opening. The excavation from the edge to center of panel shows the highest angle of draw and lowest surface subsidence. The results obtained here agree with Whittaker and Reddish (1989) and with other related studies by Liu et al. (2011), Huayang et al. (2010), Wold (1985) and Whittaker (1985) who study the effects of rock strata behavior in longwall mining.

7.2 Conclusions

All objectives and requirements of this study have been met. The results of the physical models testing, empirical calculations and computer simulations can be concluded as follows:

The physical model test results clearly indicate that the angle of draw and the maximum subsidence are controlled by the excavation method of underground openings and by overburden slope.

The lowest subsidence and highest angle of draw occurred when the sequences of mining excavation start from edge to the center of panel.

Under the same excavation area, the angle of draw and maximum subsidence are different with different excavation rates, the angle of draw and maximum subsidence is highest under low excavation rate and is lowest under high excavation rate.

Various overburden slope angles affect the angle of draw and maximum subsidence. The angle of draw on up-slope increases with increasing slope angle and the maximum subsidence decreases with increasing slope angle. This is because the particles on up-slope side can flow more easily than on the down-slope side.

The comparisons between physical model testing and computer simulations show that the measured values of angle of draw and maximum subsidence are greater than those obtained from the computer simulations. This is due to that the tested particles are not perfectly rounded and not uniform shape.

The subsidence value obtained from the empirical solution fits well to the measured profile obtained from the physical model for high excavation rate. For the

calculations under various mining sequence and overburden slope, the empirical solution does not fit the physical model results.

The measured subsidence trough volume from physical model indicates that the low excavation rate shows larger volume than the high excavation rate, under the same excavation area. Under different mining sequences, the excavation from the edge to the center of panel shows the lowest trough volume.

7.3 Recommendations for future studies

The uncertainties and adequacies of the study and results discussed above lead to the recommendations for future studies.

The overburden material with different sizes and gradations under various mining sequence, excavation rate and overburden slope should be tested to study their relations with the surface subsidence.

The effect of vertical and horizontal stressed under various mining sequences on subsidence trough should be studied for each overburden thickness.

The effect of groundwater on the induce subsidence-components should be tested.

The time-dependent analysis should be performed to assess the mechanisms governing the excavation rate effects.

Cohesive materials should be used to simulate the super-critical subsidence to understand the effects of overburden properties on the subsidence components.

REFERENCES

- Aracheeploha, S., Horkaew, P., and Fuenkajorn, K. (2009). Prediction of cavern configurations from subsidence data. In **Proceedings of the Second Thailand Symposium on Rock Mechanics** (pp. 116-176). Chonburi: Suranaree University of Technology.
- Attewell, P. B. (1978). Ground movements caused by tunnelling in soil. **Large ground movements and structures** (pp. 812-948). Pentech Press, London.
- Caudron, M., Emeriault, F., Kastner, R., and Al Heib, M. (2006). Sinkhole and soil-structure interaction: Development of an experimental model. In **Proceedings of International Conference on Physical Modeling in Geotechnics** (pp. 1261-1267). Hong-Kong.
- Clough, G.W. and Schmidt, B. (1981). Design and performance of excavations and tunnels in soft clay. **Soft Clay Engineering** (Chapter 8).
- Cording, E.J. and Hanmire, J.B. (1975). Displacements around soft ground tunnels. In **Proceedings of the Fifth Conference on Soil Mechanics Foundation Engineering** (pp. 571-633). Buenos Aires.
- Cui, X., Miao, X., Wang, J., Yang, S., Liu, H., Song Y., Liu, H. and Hu, X. (2000). Improved prediction of differential subsidence caused by underground mining. **International Journal of Rock Mechanics and Mining Sciences**. 37: 615-627.

- Fattah, M.Y., Shlash, K.S., and Salim, N.M. (2013). Prediction of settlement trough induced by tunneling in cohesive ground. **Acta Geotechnica**. 8: 167–179.
- Franzius, J.N. (2003). **Behavior of buildings due to tunnel induced subsidence**. Dr.Thesis, Civil and Environmental Engineering, Imperial College of Science, Technology and Medicine, University of London. pp.358.
- Ghabraie B., Ren G., Ghabraie, K., Xie Y. and Smith, J. (2014). Physical modeling of subsidence from sequential extraction of partially overlapping longwall panels and study of substrata movement characteristics. **International Journal of Coal Geology**. 80: 219-230.
- Hadjigeorgiou, J., Esmaili, K. and Grenon, M. (2009). Stability analysis of vertical excavations in hard rock by integrating a fracture system into a PFC model. **Tunnelling and Underground Space Technology**. 24: 296–308.
- Huayang, D., Xugang, L., Jiyan, L., Yixin, L., Yameng, Z., Weinan, D. and Yinfei, C. (2010). Model study of deformation induced by fully mechanized caving below a thick loess layer. **International Journal of Rock Mechanics and Mining Sciences**. 47: 1027–1033.
- Itasca. (2008a). **PFC^{2D}–Particle Flow Code in 2 Dimensions, Version 4.0**. User Manual, Itasca Consulting Group Inc., Minneapolis, MN, USA.
- Kim, S.H. (1996). **Model testing and analysis of interactions between tunnel in clay**. Ph.D. Thesis, University of Oxford. pp. 242.
- Kyu-Seok, W., Erik, E., Davide, E. and Doug, S. (2013). Empirical investigation and characterization of surface subsidence related to block cave mining. **International Journal of Rock Mechanics & Mining Sciences**. 61: 31–42.

- Li, Z. and Wang, J. (2011). Accident investigation of mine subsidence with application of particle flow code. **Procedia Engineering**. 26: 1698–1704.
- Liu, H., Deng, K., Lei, S. and Bian Z. (2015). Mechanism of formation of sliding ground fissure in loess hilly areas caused by underground mining. **International Journal of Mining Science and Technology**. 45: 553–558.
- Liu, Y., Zhou, F., Liu, L., Liu, C. and Hu, S. (2011). An experimental and numerical investigation on the deformation of overlying coal seams above double-seam extraction for controlling coal mine methane emissions. **International Journal of Coal Geology**. 87: 139 – 149.
- Mair, R. J., Taylor, R. N. and Bracegirdle, A. (1993). Subsurface settlement profiles above tunnels in clays. **Geotechnique**. 43(2): 315–320.
- Mcneary, R.L. and Barker, K.A. (1998). Numerical modeling of large-scale block cave physical models using PFC^{2D}. **Mining Engineering**. 50(2): 72-75.
- O'Reilly, M. P. and New, B. M. (1982). Settlements above tunnels in the united kingdom - their magnitude and prediction. **Tunnelling 82, The Institution of Mining and Metallurgy** (pp. 55–64). London.
- Park, D. and Li, J. (2004). Subsidence Simulation Using Laser Optical Triangulation Distance Measurement Devices. In **Gulf Rocks 2004, the Sixth North America Rock Mechanics Symposium (NARMS)** (pp. 6). Houston, Texas.
- Peck, R.B. (1969). Deep excavations and tunneling in soft ground. In **Proceedings of the Seventh international conference on soil mechanics and foundation engineering, State of the art volume** (pp. 225–290). Sociedad Mexicana de Mecánica de Suelos: Mexico.

- Rankin, W. (1988). Ground movements resulting from urban tunneling. In **Prediction and effects, Proceedings of the Twenty-third conference of the engineering group of the geological society** (pp. 79–92). London Geological Society.
- Reddish, D.J. (1989). The modeling of rock mass behavior over large excavations using non-linear finite element techniques. **Mining Engineering Department Magazine University of Nottingham**. 41: 93–102.
- Ren, G. and Li, J. (2008). A study of angle of draw in mining subsidence using numerical modeling techniques. **Electronic Journal of Geotechnical Engineering**. 13: 1-14.
- Schmidt, B. (1979). **Settlements and ground movements associated with tunnelling in soil**. Ph.D. thesis, University of Illinois.
- Schmidt, B. (1988). Discussion on: Sagaseta, c.: Analysis of undrained soil deformation due to ground loss. **Geotechnique**. 38(4): 647.
- Shu, D.M. and Bhattacharyya, A.K. (1992). Influence of the sloping of ground surface subsidence on mine subsidence. In **Eleventh International Conference on Ground Control in Mining** (pp. 475-482). The University of Wollongong, New South Wales.
- Singh, M.M. (1992). Mine subsidence. In H.L. Hartman (ed). **SME Mining Engineering Handbook** (pp. 938–971). Society for Mining Metallurgy and Exploration: Inc. Littleton, Colorado.
- Singh, R. P. and Yadav, R. N. (1995). Prediction of subsidence due to coal mining in Raniganj coalfield, West Bengal, India. **Engineering Geology**. 39: 103-111.

- Thongprapha, T. (2015). **Physical model simulation of 3-D subsidence induced by underground mines**. Ph.D. Thesis, Geotechnology, Suranaree university of technology. pp.88.
- Thongprapha, T., Fuenkajorn, K., and Daemen, J.J.K. (2015). Study of surface subsidence above an underground opening using a trap door apparatus. **Tunnelling and Underground Space Technology**. 46: 94–103.
- Whittaker, B. N. (1985). Ground fractures due to longwall mining subsidence. In **International Mine Water Association Proceedings** (pp.1057–1072). Spain.
- Whittaker, B. N. and Reddish, D. J. (1989). **Subsidence Occurrence, Prediction and Control** (Vol. 56). Amsterdam: Elsevier Science Publishers.
- Wold, M. B. (1985). Blocky physical model of longwall caving under strong roof conditions. In **Proceedings - Symposium on Rock Mechanics** (Vol. 2, pp.1007–1014). CSIRO, Div of Geomechanics, Australia.
- Yao, X.L., Whittaker, B.N., and Reddish, D.J. (1991). Influence of overburden mass behavioural properties on subsidence limit characteristics. **Mining Science and Technology**. 13: 167–173.
- Zhang, H., Liu, L. and Liu, H. (2011). Mountain ground movement prediction caused by mining based on BP-neural network. **Journal of Coal Science Engineering** (vol.17, pp.12–50). China.

BIOGRAPHY

Miss Naruemol Saoanunt was born in January 12, 1991 in Buriram province, Thailand. She received her Bachelor's Degree in Engineering (Geotechnology) from Suranaree University of Technology in 2014. For her post-graduate, she continued to study with a Master's degree in the Geological Engineering Program, Institute of Engineering, Suranaree University of Technology. During graduation, 2014-2016, she was a part time worker in position of research assistant at the Geomechanics Research Unit, Institute of Engineering, Suranaree University of Technology. She published technical paper related to rock mechanics, titled physical model simulations of super-critical subsidence as affected by mining sequence and excavation rate in the Proceeding of the 9th South East Asia Technical University Consortium (SEATUC) Symposium 2015, Suranaree University of Technology, Nakhon Ratchasima, Thailand.